Natural Resources Canada | Ressources naturelles Canada

GEOLOGICAL SURVEY OF CANADA
OPEN FILE 7754

Overview of field operations during a 2013 research expedition to the southern Beaufort Sea on the RV Araon

Y.K. Jin, M. Riedel, J.K. Hong, S.I. Nam, J.Y. Jung, S.Y. Ha, J.Y. Lee, G.Y. Kim, J. Yoo, H.S. Kim, G. Kim, K. Conway, G. Standen, M. Ulmi, and M. Schreker

2015

Canada

GEOLOGICAL SURVEY OF CANADA
OPEN FILE 7754

Overview of field operations during a 2013 research expedition to the southern Beaufort Sea on the RV Araon

Y.K. Jin[1], M. Riedel[2], J.K. Hong[1], S.I. Nam[1], J.Y. Jung[1], S.Y. Ha[1], J.Y. Lee[3], G.Y. Kim[1], J. Yoo[1], H.S. Kim[4], G. Kim[5], K. Conway[2], G. Standen[6], M. Ulmi[2], M. Schreker[1]

[1] Korea Polar Research Institute, 26 Songdomirae-ro, Yeonsu-gu Incheon, 406-840, Korea
[2] Natural Resources Canada, Geological Survey of Canada, 9860 West Saanich Road, Sidney, British Columbia
[3]KIGAM
[4] Korea Gas Corporation, 5th Floor, Korea Paperless Trade Centre, 688 Sampyeong-dong, Bundang-gu, Seongnam-si, Gyeinggi, Korea
[5]Gwangju Institute of Science and Technology, Gwangju, 500-712, Korea
[6] Geoforce Consultants Ltd., 1 Endeavour Drive, Bedford Institute of Oceanography, Dartmouth, Nova Scotia

2015

doi:10.4095/295856

This publication is available for free download through GEOSCAN (http://geoscan.nrcan.gc.ca/).

Recommended citation
Jin, Y.K., Riedel, M., Hong, J.K., Nam, S.I., Jung, J.Y., Ha, S.Y., Lee, J.Y., Kim, G.Y., Yoo, J., Kim, H.S., Kim, G., Conway, K., Standen, G., Ulmi, M., and Schreker, M., 2015. Overview of field operations during a 2013 research expedition to the southern Beaufort Sea on the RV Araon; Geological Survey of Canada, Open File 7754, p. 181. doi: 10.4095/295856

Table of Contents

Summary

Y. K. Jin, M. Riedel

Research experiments conducted and preliminary findings

The Expedition ARA04C is a multidisciplinary research program in the Beaufort Sea, carried out in collaboration between the Korea Polar Research Institute (KOPRI), Geological Survey of Canada (GSC), Department of Fisheries and Ocean (DFO), Monterey Bay Aquarium Research Institute (MBARI), and the Alfred Wegener Institute (AWI). The Expedition ARA04C on the IBRV Araon took place from September 6 to September 24, 2013 (Figure 0.1). Multiple research experiments were undertaken to study geological processes related to degrading permafrost, fluid flow and degassing, and associated geohazards, paleo-oceanography of the Beaufort shelf and slope region, as well as physical and chemical oceanography measurement of the Arctic Ocean linked with continuous atmospheric studies. The expedition focused on two main research areas: offshore Barrow, Alaska, from September 7 to September 9, 2013, and the Canadian Beaufort Sea from September 10 to September 24, 2013.

Multichannel seismic data, in conjunction with an ocean-bottom-seismometer (OBS) study were collected to support drilling proposals especially IODP pre-proposal #806 (Paull et al., 2012), and to verify distribution and internal structures of the offshore permafrost occurrences (Figure 0.2). The multi-channel seismic data were acquired on the outer continental shelf of the Canadian Beaufort Sea, totaling 14 lines with ~435 line-kilometers and ~4,500 shot gathers (Chapter 3). The combined multichannel seismic and OBS data will be processed post-expedition at KOPRI and the GSC, and will allow detailed velocity analyses to investigate the permafrost signature and help mapping zones of high-velocity sediments indicative of the presence of ice (Chapter 4). Individual shot gathers collected during the multichannel seismic program show clear refraction arrivals with velocities around 2000m/s in areas of expected permafrost occurrence, and shot gathers lacked such arrivals in zones where the permafrost was predicted to be absent. It is therefore expected that the OBS data, once processed, will also show clear refracted

arrivals for velocity analyses.

Continuous sub-bottom profiler (SBP) and multibeam data were collected along all ship tracks for detailed subsurface imaging of sediment structures and permafrost, as well as for core-site location verification (Chapter 5 and 6). During Expedition ARA04C, more than 3000 line-kilometers of SBP data were collected, co-located with multibeam and backscatter data. These data are an essential part of the study of sub-seafloor permafrost distribution and provide insights into sediment dynamics at critical boundaries, such as the shelf edge. Along the shelf edge, the occurrence of pingo-like features (PLFs) result in a rugged landscape with thousands of PLFs piercing through the otherwise laminated sediments. More than 30 crossings of this critical shelf-edge boundary were made during this expedition, which complement data acquired in 2012 with the Huntec system and 3.5 kHz data provided by ArcticNet as part of the regional multibeam map of the study area. High resolution data provided critical new insights in deep-water fluid expulsion zones. Key new data were acquired over the area of the "Gary Knolls", where PLF structures occur at the shelf edge in water depth of only 50 to 60 m. All SBP data from this expedition will be post-processed and analyzed for the presence of sub-seafloor permafrost, occurrence of the PLF structures and indications for fluid and gas migration. Multibeam and backscatter data were collected along all ship tracks, adding to the database of existing information gathered through previous expeditions to the study region.

Heat flow measurements were undertaken at eight stations (Figure 0.3) to study the thermal structure of fluid expulsion features, as well as degrading permafrost along a slope-shelf transect in the eastern Mackenzie Trough (Chapter 7). The data provide critical constraints on the distribution of sub-seafloor permafrost as well as the gas hydrate stability zone around fluid expulsion features. A very important finding is the observation made at the mud volcano in 420 m water depth, where seafloor temperatures are the highest in all observed stations, indicating active mud volcanism.

Geological sampling using gravity coring and multi-coring tools was performed at strategic sites to support two research objectives. The first objective was to provide key data towards ongoing international research linked to IODP pre-proposals #753 (O'Regan et al., 2010) and #806 (Paull et al., 2012). The second objective was to collect core to

define key seismo-stratigraphic horizons critical to the understanding of geohazards in the region (Chapter 8). In total, 21 gravity cores and 12 multi-cores were taken (Figure 0.4, Table 8.3). All cores were scanned with a multi-sensor core-logger to measure physical properties (Chapter 9). Most sediment analyses on the cores will be performed post-expedition at KOPRI, GSC, and laboratories of other University-based collaborators in Canada and Germany. Onboard, sub-samples were taken from all shallow multi-cores and selected gravity cores. On selected cores from the Canadian Beaufort study region pore-waters were extracted using rhizones. These samples will be analyzed post-expedition at MBARI.

Water sampling and Conductivity-Temperature-Depth (CTD) profiling was undertaken at most core sites to study physical and chemical properties of the seawater (Figure 0.5). These station-measurements were complemented by continuous water-property and atmospheric measurements when the Araon was underway. Most samples taken will be analyzed post-expedition at KOPRI for DIC/TA, nutrients, DOC, and POC. The pH of seawater, underway data of pCO_2, CH_4, and N_2O, as well as a variety of subsequent calculations is required for accurate estimates in the above listed parameters. Methane was also measured with a methane sensor attached to the CTD tool and at the mud volcano in 420 m water depth, methane concentrations of more than 100-times ocean background were seen. The methane plume was also acoustically imaged with the echo sounder systems on board the IBRV Araon. Further details on the water sampling and atmospheric measurements are given in Chapter 10 and 11.

References

Paull, C.K., Dallimore, S.R., Collett, T.S., Jin, Y.K., Mienert, J., Mangelsdorf, K., Riedel, M., 2012. Drilling to investigate methane release and geologic processes associated with warming permafrost and gas hydrate deposits beneath the Beaufort Sea Shelf. IODP Pre-Proposal 806, available online at http://iodp.org/

O'Regan, M., de Vernal, A., Hill, P., Hillaire-Marcel, C., Jakobsson, M., Moran, K., Rochon, A., St-Onge, G., 2010. Late quaternary paleoceanography and glacial dynamics in the Beaufort Sea, IODP pre-proposal #753, available online at http://iodp.org/.

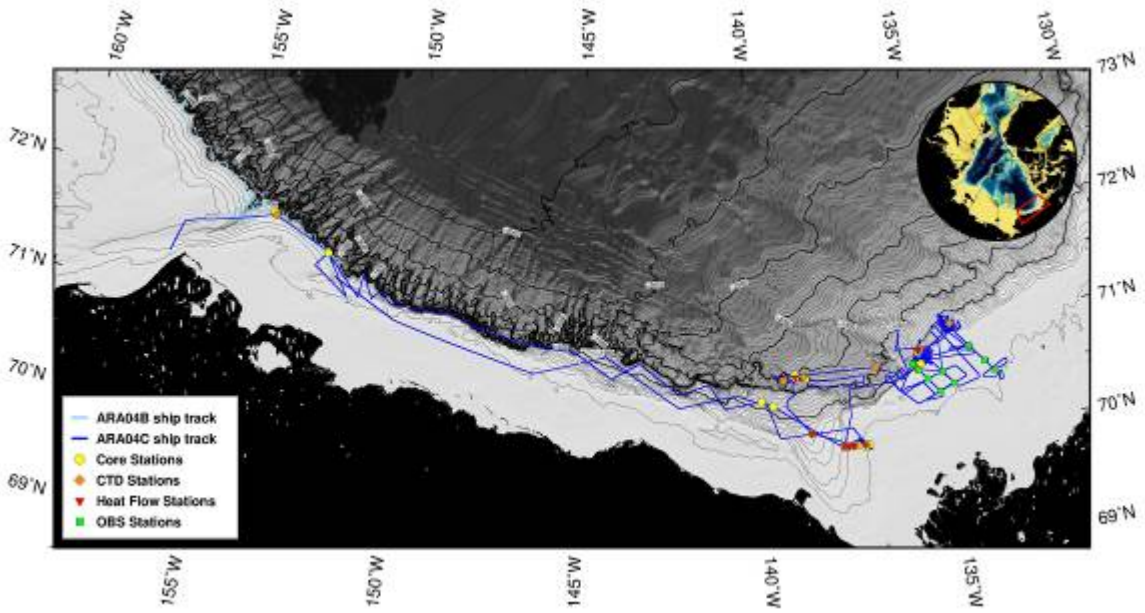

Figure 0.1 Overview map of the ship track for Expedition ARA04C. The expedition is split into two parts: September 6 - 9, 2013 in Alaskan waters off Barrow, and September 10 - 24 in Canadian waters off the Mackenzie Delta shelf and slope region.

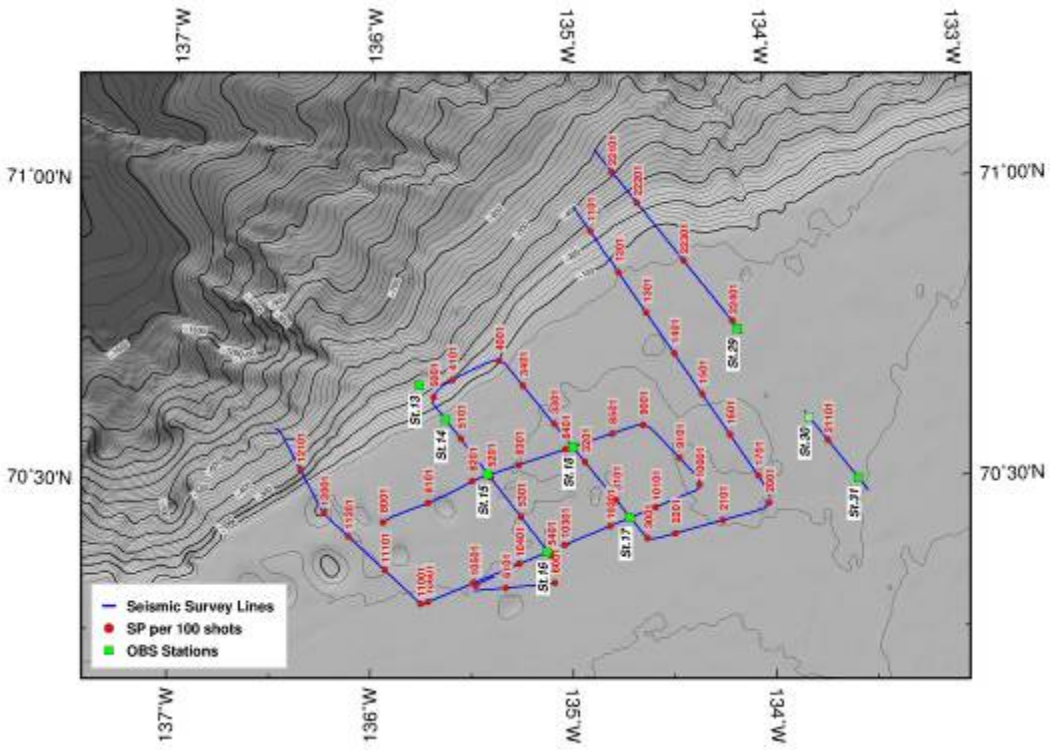

Figure 0.2 Map showing seismic survey lines with OBS stations, and consecutive shot-point labels.

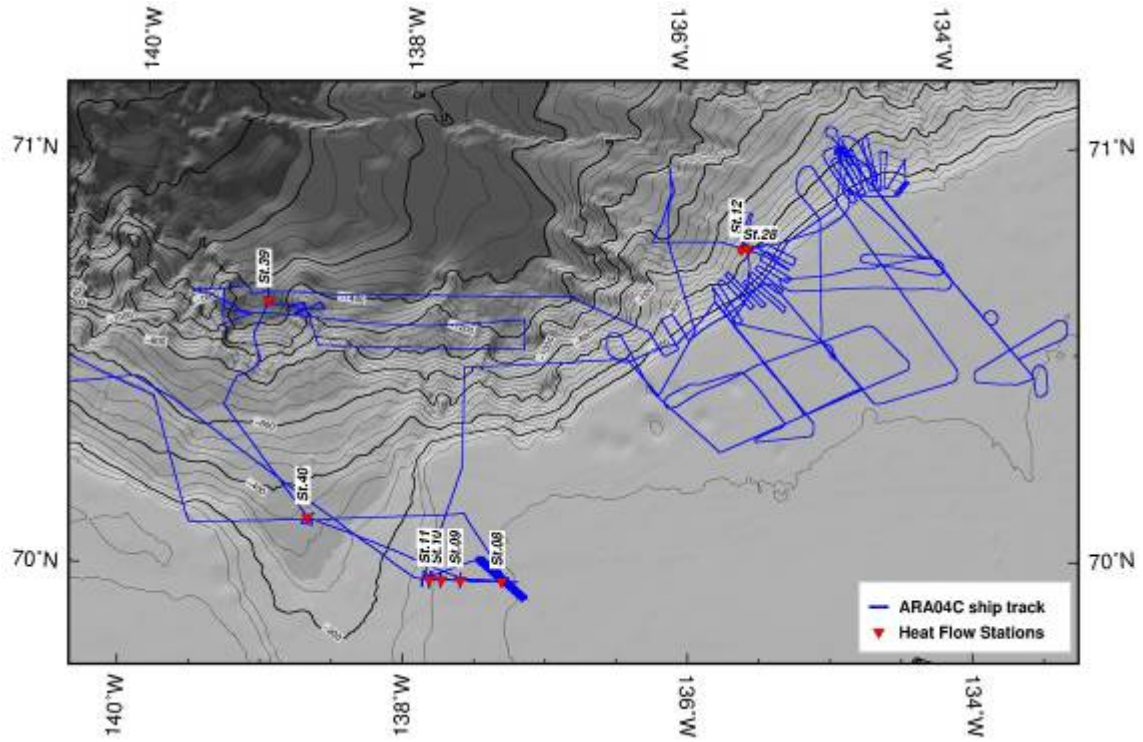

Figure 0.3 Map showing all Heat Flow stations occupied during Expedition ARA04C.

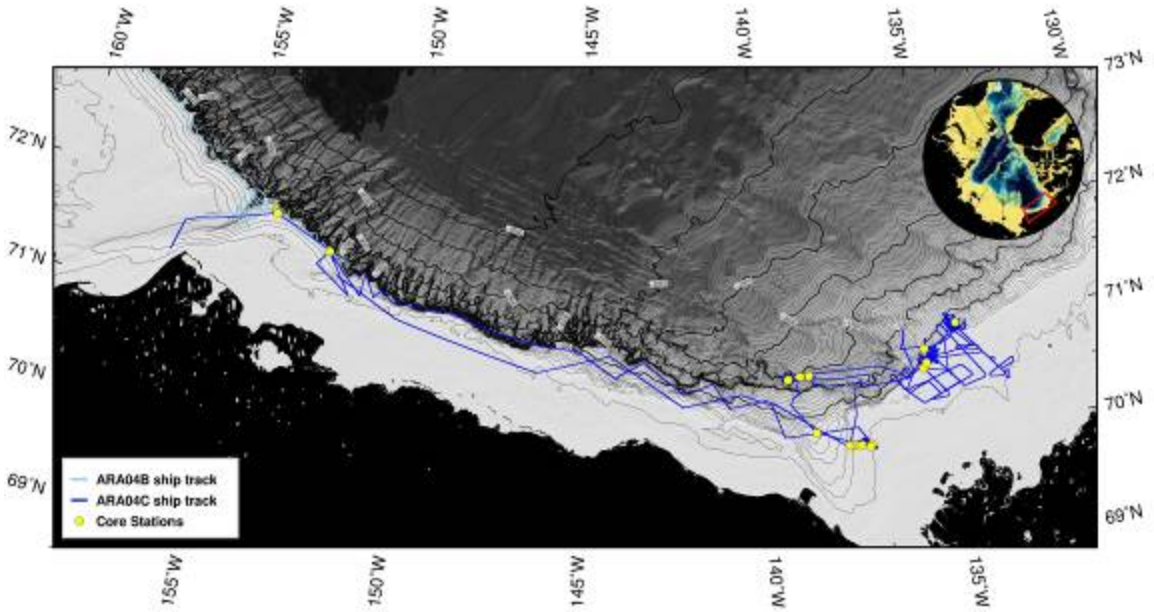

Figure 0.4a Map showing distribution of all core stations occupied during Expedition ARA04C.

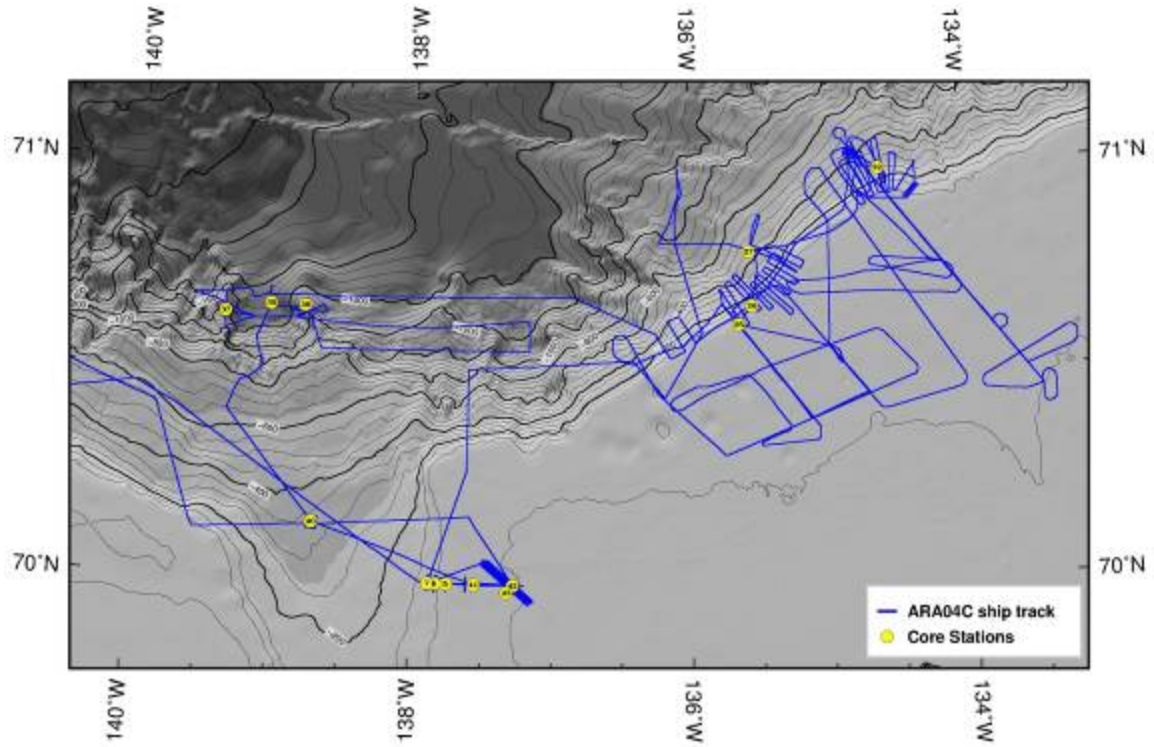

Figure 0.4b Map showing distribution of all core stations occupied in the Canadian Beaufort Sea only, during Expedition ARA04C.

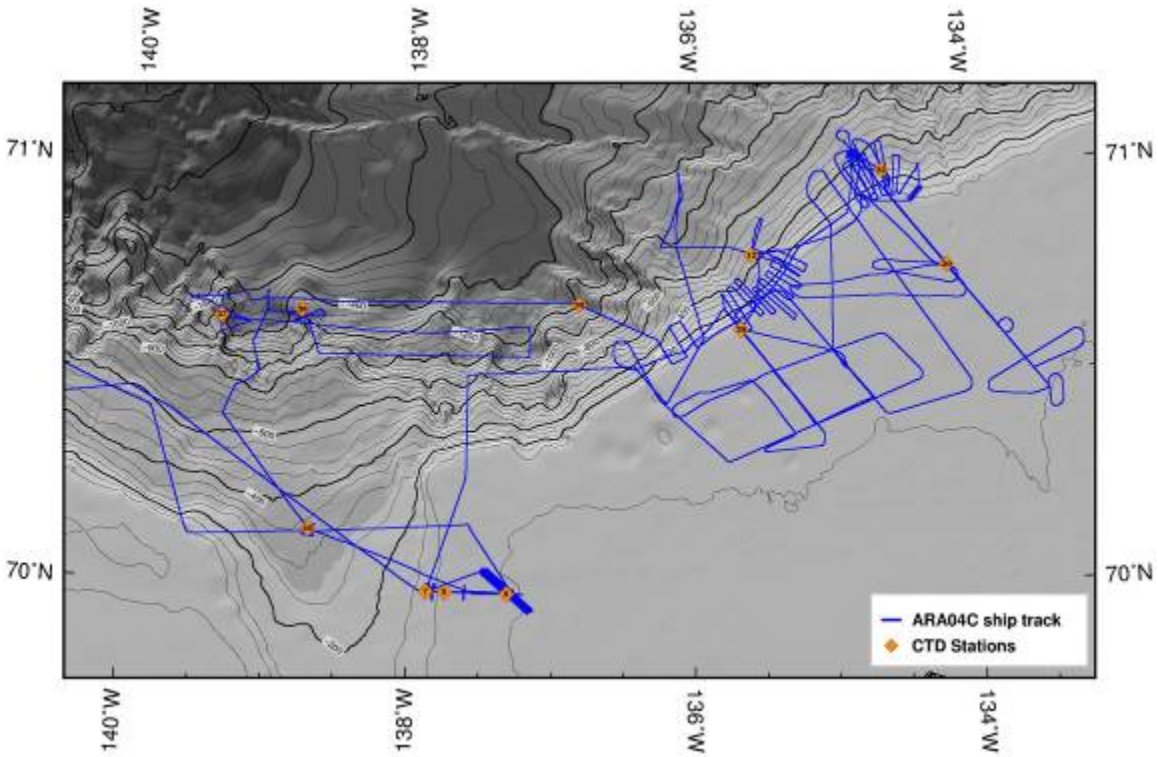

Figure 0.5 Map showing all CTD stations visited during Expedition ARA04C.

Chapter 1 Introduction

Y. K.Jin, M. Riedel

1.1 Rationale and Scientific Motivation

As described in the IODP pre-proposal 806 by Paull et al. (2012), Arctic continental shelf areas that are less than 100 m deep make up more than 3.2 million square kilometres, or approximately 30% of the area of the Arctic Ocean (Figure 1.1). Throughout the past two million years these shallow water settings have experienced a varied and dynamic geologic history. During periods of low sea level, many of the current marine shelf areas were not covered with water and were exposed to mean annual air temperatures that were -20ºC or colder (Brigham and Miller, 1983). These cold temperatures caused the formation of thick permafrost and established pressure and temperature conditions favourable for the formation of permafrost-associated gas hydrate. In contrast, sea level rise during interglacial periods resulted in marine transgression that inundated coastal areas with relatively warm seawater that ultimately will yield the complete degradation of offshore permafrost and gas hydrate. Because of the slow diffusion of heat, it will, however, take thousands of years to fully melt the subsurface permafrost and dissociate the gas hydrate deposits.

The repeated changes between permafrost and gas hydrate formation during terrestrial exposure, and warming/degradation during marine transgression has had substantial impact on the geology of Arctic shelves. Large quantities of methane are trapped within the permafrost and gas hydrate deposits (Collett and Dallimore, 2002). Ongoing warming due to the present transgression is destabilizing these deposits, creating the potential for gas migration and release into the ocean and atmosphere (e.g. Hughes-Clark, 2009; Shakhova et al., 2010; Blasco et al., 2010; 2013). Unique geologic and hydro-geologic processes are also likely to occur as a consequence of such water and gas release. Paull et al. (2007) have suggested that large conical features on the Beaufort shelf termed “pingo-like features” (PLFs) may be due to methane-generated overpressure in subsurface sediments causing sediment extrusion. Similar processes may cause methane

releases associated with geomorphic features at that shelf edge transition including PLFs, pockmarks and landslides (Paull et al., 2011).

The Arctic shelf also contains vast offshore hydrocarbon resources, and new phases of exploration and development are expected in the near future. Given that the geologic processes described above can pose a significant hazard (Hovland, 2010), there is impetus to quantify the hazard and ultimately its risks in this setting. Finally, climate warming is expected to be of greater magnitude and to occur more rapidly in the Arctic. Arctic shelves will experience continued warming and changes in hydrologic inputs, possibly accelerating methane release and altering geologic processes (Anisimov et al., 2007).

1.2 History of KOPRI-GSC collaboration

The expedition ARA04C is part of a long-term collaborative study conducted by the Geological Survey of Canada (GSC), Department of Fisheries and Ocean (DFO), Korea Polar Research Institute (KOPRI), Monterey Bay Aquarium Research Institute (MBARI), Alfred Wegener Institute (AWI), and the MARUM Institute, University of Bremen, focusing on the Arctic Ocean, specifically the Beaufort Sea. The work conducted during this expedition is enabled through a Memorandum of Understanding (MoU) and Specific Project Annex, signed by KOPRI and the GSC in February 2010. In the MoU and Project Annex, both parties expressed their interest to carry out joint work in the Arctic, with a special emphasis on marine geohazards and issues of global methane release and its potential contribution to climate change.

Through a series of meetings between 2009 and 2011 the science teams from the GSC (lead by Scott Dallimore) and KOPRI (lead by Young K. Jin), developed a proposal for funding of the Araon expedition, following a RFP call by the Korean funding agency.

The proposal was accepted by December 2012 enabling a formal collaboration between the institutes. Additionally, the IODP pre proposal 806 (Paull et al., 2012) was submitted and forms, together with the IODP pre-proposal 753 by O`Reagan et al (2010), the backbone of the science motivation of the Araon expedition ARA04C.

The program permitting began in March 2012, when all six communities in the Inuvialuit Settlement Area visited for consultation with the Hunter and Trapper

Committees (HTCs) as well as with the public. A team of two GSC scientists visited Inuvik, Aklavik, Tuktoyaktuk, Sachs Harbour, Paulatuk, and Ulukhaktok. In the fall of 2012, the project description was submitted to the Inuvialuit Environmental Screening Committee (EISC) and the program was approved by March 2013. Additional permits for the vessel operation in Canadian Arctic waters were secured over the spring-summer period of 2013.

Prior to the Araon Expedition ARA04C, two expeditions in 2010 and 2012 with the Canadian Coast Guard Ship (CCGS) Sir Wilfrid Laurier were carried out, studying the shelf edge region and fluid-expulsion features in various water depths. Piston- and gravity cores were taken for regional stratigraphic and geochemical pore water analyses. MBARI designed, built, and operated a custom ROV for use in 2010 and 2012 for seafloor video imagery and gas sampling. Results from these two expeditions, together with the regional geological framework completed through ArcticNet and previous GSC studies (especially detailed multibeam mapping), form the foundation of the work carried out during the Araon Expedition ARA04C.

Expedition ARA04C will be complemented by a 16-day science expedition onboard the CCGS Laurier from September 25 to October 10, 2013. The primary tasks for this expedition include: AUV and ROV seafloor mapping, piston and gravity coring, pore water collection for geochemical analyses, measurements of heat flow, cone-penetrometer deployments, and mooring work.

1.3 Objectives for Expedition ARA04C

A two-ship scientific research expedition to the southern Beaufort Sea in the Arctic Ocean was carried out September 10th to October 10th, 2013 using the KOPRI research icebreaker Araon and the CCGS Sir Wilfrid Laurier. The multidisciplinary science program will include geological, geophysical, and oceanographic investigations of the continental shelf and slope. The research will improve the understanding of geohazards in this setting by assessing the regional geology, the stability of decomposing permafrost and gas hydrate, mechanisms for surficial gas/fluid migration and active geologic processes.

Priorities for the Araon Expedition ARA04C included multi-channel seismic surveys and detailed bathymetric mapping to evaluate the interactions and linkages between oceanography and geologic processes in the outer shelf and slope area with the hope to collect sufficient site-survey data for the IODP proposal 806 and 753. The Araon also has several unique sediment coring instruments and a state of the art ship-board laboratory for studying cores. Priorities for the CCGS Sir Wilfrid Laurier expedition are detailed mapping of seafloor expulsion features, shelf edge pingo-like features, and land-slide morphologies. Piston and gravity cores, combined with heat-flow measurements and cone-penetrometer deployments will complement the work.

1.3.1 Multichannel Seismic Survey

The unique opportunity to use the Araon's permanently installed multichannel seismic system provides the means to collect site survey data in support of IODP proposal 806 and 753. The site-survey data are required to define drill site locations for safe operations and to ensure, science goals are met. Therefore, the seismic lines must be acquired in a systematic grid-pattern of perpendicular lines crossing the shelf edge and lines parallel to the shelf edge. Prior to the Expedition ARA04C, the science team met several times to discuss the requirements for the seismic survey and to optimize the survey design. Discussions included industry partners who provided unique insights to the area through their analyses of their 3D seismic data sets acquired in deep-water areas of the Beaufort Sea (Pokak 3D, Ajurak 3D, Chevron 3D). Industry well locations with

high quality well logs, which allow for the determination of the base of permafrost as well as stratigraphic information, were used as tie-points for the main IODP transects.

In total, five transects were defined (color-coded for simplicity) and are shown in Figure 1.3 with respect to the main bathymetric features and permafrost distribution in the study area. In order of priority, the transects are: "red", "yellow" "blue", "cyan", and "white". Around each of these transects a set of parallel and perpendicular lines would suffice for the IODP site survey data.

1.3.2 Ocean Bottom Seismometer Survey

In addition to the multichannel seismic survey, a set of Ocean Bottom Seismometers (OBS) was used to define the velocity structure of the permafrost setting along the above mentioned transects. The OBS were strategically deployed along the transects and a set of crossing airgun lines was acquired over each OBS, so that velocity information can be acquired in two directions. The permafrost distribution shown in Figure 1.3 is based on work by the GSC using refracted arrivals from high-velocity material in the subsurface (Pullan et al., 1987). By using OBSs, we hope to be able to verify the distribution of permafrost, and obtain a more detailed vertical (1D) velocity structure beneath each OBS station. We also plan to acquire shear-wave velocity data from the two horizontal geophone components, which will be a unique data set in the offshore Beaufort Sea.

1.3.3 Sub-Bottom Profiler Survey and Seismo-Stratigraphic Horizons

High resolution sub-bottom profiler data have been acquired during previous expeditions in the study area, mostly from the 3.5 kHz profiler installed on the CCSG Amundsen. However, data acquisition was often not optimized for imaging of the subsurface structures, as many profiles acquired on the Amundsen were focused on multibeam data acquisition and line-orientation was not optimal for cross-shelf transects. During the CCGS Laurier expedition in 2012, a unique set of sub-bottom profiler data was collected using a Huntec system.

The 3.5 kHz and Huntec data from previous cruises were used to define several seismo-stratigraphic units describing the sediment depositional environments and form

the base of the new data acquisition with the Araon during Expedition ARA04C (Figure 1.4).

(a) Deep water laminated stratigraphy: Undeformed "Orange" unit representing the youngest deposit in deeper-water (> 250 m), overlying where present the "Yellow" unit, which is a characteristic set of high amplitude parallel reflections with deformation structures;

(b) Underlying massive unit 1: The "Cyan" unit, mostly acoustically transparent showing signs of creep-deformation, resulting in extensional deformation style in the "Yellow" unit, resembling the nature of normal faulting. The "Cyan" unit is believed to also form the material of the pingo-like features, which are intrusions into and piercing through the "yellow" unit;

(c) Deepest imaged horizon: The "Red" unit is seen in parts as bottom reflection from the "Cyan" unit. This reflection is also imaged in the 3D industry seismic data and may host glacial plough-marks (grooves, or ice-scours) from previous glaciations.

The sub-bottom profiler system onboard the Araon was used to collect new data with the aim to acquire key-transects over features of interest as follows:

- Shelf edge with pingo-like features
- Deep-water fluid expulsion features
- Imaging of the "cyan" unit, transitions from deep to water shallow water
- Onset of "orange" unit and extent of deformation in "yellow" unit
- Structure of the top of "red" unit (deepest imaged unit) to compare with 3D data
- Eastern slope region of Mackenzie Trough
- Gary Knolls area with pingo-like features

1.3.4 Multibeam Mapping and Backscatter

Although multibeam data has been acquired over most of the study region, some gaps still remain. Areas of special interest for new multibeam mapping are the area of the eastern Mackenzie Trough region, especially the zone of Gary Knolls, as well as the deep-water Mackenzie Trough region over the Chevron lease block. Limited backscatter data have been collect (e.g. over the deep-water expulsion features), the Araon's system

will collect new, valuable backscatter data for interpretation of the seafloor structures and sediment strength.

1.3.5 Heat Flow Analyses

The detailed thermal structure of the study area is unknown and relies mostly on historical well-log data, from which depth of permafrost was inferred. A few historical heat-flow data exist, but data coverage is spares, and not focused on the deep-water expulsion zones. Thermal modeling carried out along a regional transect through key industry wells, provides some base for the boundary of pinch-out of offshore permafrost, and marine gas hydrate zones (ref). To aid in detailed gas hydrate phase boundary definition, especially at the deep-water expulsion zones, a heat-flow analysis project was carried out during the Araon Expedition ARA04C and will be complemented by work on the CCGS Laurier Expedition. During Expedition ARA04C, a 4 m long Ewing-type probe was used for thermal gradient definition, and during the CCGS Laurier Expedition outriggers with temperature probes attached to the gravity core will be used to measure temperature with depth. Thermal conductivity of the sediment can be defined from the data obtained with the Ewing-type probe (see Chapter 7) but selected measurements of thermal conductivity on sediment cores will also be carried out. Targets for the Expedition ARA04C were the transect on the eastern Mackenzie Trough, as well as deep-water expulsion features.

1.3.6 Coring and Sediment Analyses

The wide-diameter gravity corer onboard the Araon was used to target some strategic sediment stratigraphic horizons. The multi-corer system was used at some of the locations to sample the top 50 - 100 cm of sediment for high resolution paleo-climate studies using various micro-fossils, physical property analyses with the multi-sensor core logger, bulk-sediment analyses, pore-water extraction for detailed sulfate and chlorinity measurements to define the sulfate-methane transition zone, as well as biomarker analyses. All cores obtained were scanned onboard with a multi-sensor core-logger for physical properties. The gravity and multi-corer system was used during airgun maintenance and/or ice-related downtimes for airgun operation.

1.3.6.1 Eastern Mackenzie Trough

Along the Huntec line acquired in 2012, six coring targets were defined from deep-water, laminated sediments to the shallow outcropping massive and acoustically transparent unit, forming the Gary Knolls area.

1.3.6.2 Chevron Block

Within the area of the Chevron Block, deep-water Mackenzie Trough region, two core locations were proposed supporting IODP proposal 753 by O'Reagan et al. (2010). In addition, six different core site locations were proposed by Chevron for gravity coring that could be obtained by either the Araon or Laurier expeditions.

1.3.6.3 Fluid Expulsion features

The fluid expulsion feature at 420m water depth was targeted for coring to obtain samples for gas analyses) and to possibly core gas hydrate samples. This feature is also a prime target for the heat-flow analyses.

1.3.6.4 "Cyan" Unit outcrop and PLFs

The "Cyan" Unit is a key sediment interval, likely responsible for deformation seen on the slope region of the study zone and the formation of pingo-like features (PLFs). Most of the unit are buried underneath thick laminated sediments ("Yellow", and "Orange" Units) but few outcrops or near-seafloor occurrences exist. Prior to the expedition, several potential coring sites to get samples from the "Cyan" Unit were defined. Also, coring the PLFs is a priority to compare the sediments from the "Cyan" Unit to the PLF.

1.3.6.5 "Orange" Unit

The youngest stratigraphic horizon identified prior to the Expedition ARA04C is the "Orange" Unit overlying the "Yellow" Unit, capping the deformation caused by the underlying "Cyan Unit". Dating this unit will help understand the sedimentation history of the margin and onset of deformation.

1.3.7 Gravity Survey

The Araon is equipped with a Micro-g Lacoste gravimeter (air-sea marine system). Gravity data are automatically collected and corrected for ship-motion and other effects. Data for the entire expedition will be used by the Canadian Geodetic Survey to update their gravity database in the Mackenzie Trough and Beaufort Sea region.

1.3.8 Water-Column Oceanographic Studies

Using the Conductivity-Temperature-Depth (CTD) tool, continuous water-property profiles of pressure (depth), temperature, salinity, oxygen, fluorescence, and methane content were obtained. The water sampling rosette was used to collect several water samples for other chemical water-property analyses at locations of opportunity to characterize the sea water and ocean-stratification in the Beaufort Sea. Data obtained from the studies will be integrated in the KOPRI global ocean-property database. The CTD data will also be used to calculate the sound speed profile at the OBS locations, which is required for accurate ray-tracing as part of the subsurface velocity inversion process.

1.3.9 Underway Sea Water and Atmospheric Studies

While the Araon is underway or during seismic/SBP data collection, continuous water and atmospheric samples are taken for detailed chemical analyses, including pCO_2, N_2O, and CH_4. These data are collected continuously together with regular weather information such as wind direction and speed, humidity, temperature, pressure.

References

Anisimov, O.A., Vaughan, D.G., Callaghan, T.V., Furgal, C., Marchant, H., Prowse, T.D., Vilhjálmsson, H., Walsh, J.E., 2007. Polar regions (Arctic and Antarctic). Climate Change 2007: Impacts, Adaptation and Vulnerability. Contribution of Working Group II to the Fourth Assessment Report of the Intergovernmental Panel on Climate Change, M.L. Parry, O.F. Canziani, J.P. Palutikof, P.J. van der Linden and C.E. Hanson, Eds., Cambridge University Press, Cambridge, p. 653-685.

Blasco, K.A., Blasco, S.M., Bennett, R., MacLean, B., Rainey, W.A., and Davies, E.H., 2010. Seabed geologic features and processes and their relationship with fluid seeps and the benthic environment in the Northwest Passage, Geological Survey of Canada, Open File Report, 6438, pp. 110.

Blasco, S., Bennett. R., Brent, T., Burton, M., Campbell, P., Carr, E., Covill, R., Dallimore, S., Davies, E., Hughes-Clarke, J., Issler, D., Leonard, L, MacKillop, K, Mazzotti, S, Patton, E., Rogers, G., Shearer, J., White, M., 2013. Geological Survey of Canada Open File Report, p. 306.

Brigham, J.K., Miller, G.H., 1983. Paleo-temperature estimates of the Alaskan Arctic Coastal Plain during the last 125,000 years, Proceedings of the 4th International Conference on Permafrost, Fairbanks, Alaska, p. 80-85.

Collett, T.S., Dallimore, S.R., 2002. Detailed analysis of gas hydrate induced drilling and production hazards. Proceedings of the 4th International Conference on Gas Hydrates, Yokahama, Japan, p. 47-52.

Paull, C.K., Dallimore, S.R., Collett, T.S., Jin, Y.K., Mienert, J., Mangelsdorf, K., Riedel, M., 2012. Drilling to investigate methane release and geologic processes associated with warming permafrost and gas hydrate deposits beneath the Beaufort Sea Shelf. IODP Pre-Proposal 806, available online at http://iodp.org/

Hovland, M., Backman, J., Coakley, C., Collett, T., Darby, D., Foucher, J.P., Francis, T., Mikhail, Gelfgat, M., Gorshkovsky, A., Jokat, W., Kaminski, M. , Kristoffersen, Y., Takahashi, K., Thiede, J., Wiley,C., and Zachos, J., 2011. The High-Arctic Drilling Challenge: Excerpts from the Final Report of the Arctic's Role in Global Change Program Planning Group (APPG) JOIDES Journal, v. 27, p. 7-20.

Hughes Clarke, J., 2009. Identification of Active Gas Seeps on the Beaufort Continental Margin: New Multibeam Water Column Imaging Capability of the CCGS Amundsen. Proceedings of Arcticnet Annual Scientific Meeting, Victoria, B.C. Canada, p. 49-59.

Paull, C.K., Ussler, W., Dallimore, S.R,. Blasco, S.M., Lorenson, T.D., Melling, H., Medioli B.E,, Nixon, F.M., McLaughlin F.A., 2007. Origin of pingo-like features on the Beaufort Sea shelf and their possible relationship to decomposing methane gas hydrates Geophysical Research Letters, v. 34, no. 1, doi:10.1029/2006GL02797.

Paull, C. K., Dallimore, S.R., Hughes-Clarke, J., Blasco, S.M., Lundsten, E., Ussler, W. III, Graves, D., Sherman, A., Conway, K., Melling, H., Vagle, S., Collett, T.S., 2011. Proceedings of the 7th International Conference on Gas Hydrates, Edinburg, Scotland, July 2011.

Shakhova, N., Semiletov, I., Salyuk, A., Yusupov, V., Kosmach, D., Gustafsson, O., 2010. Extensive Methane Venting to the Atmosphere from Sediments of the East Siberian Arctic Shelf.Science,v. 327 no. 5970, p. 1246-1250.

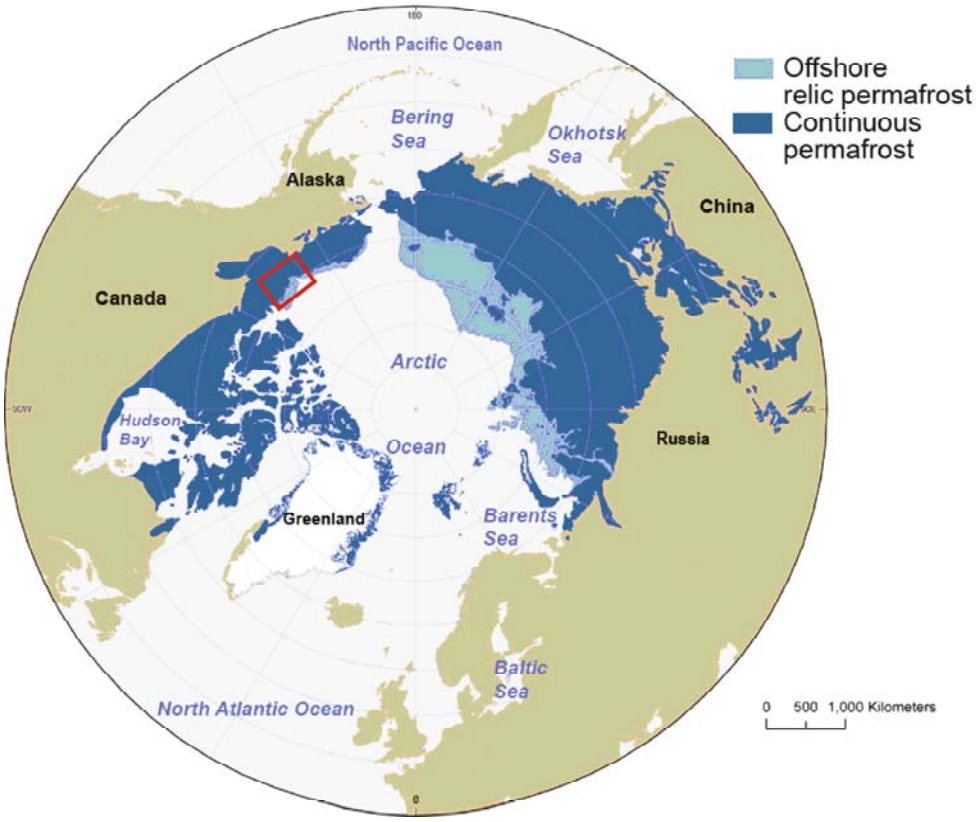

Figure 1.1 Polar projection of northern hemisphere, showing distribution of continuous permafrost on land and relic offshore permafrost beneath shelf areas of the Arctic Ocean. The red inset box shows the research area of this Expedition ARA04C with the Araon in the Beaufort Sea, detailed further in Figure 1.2 (from IODP pre-proposal 806, by Paull et al., 2012).

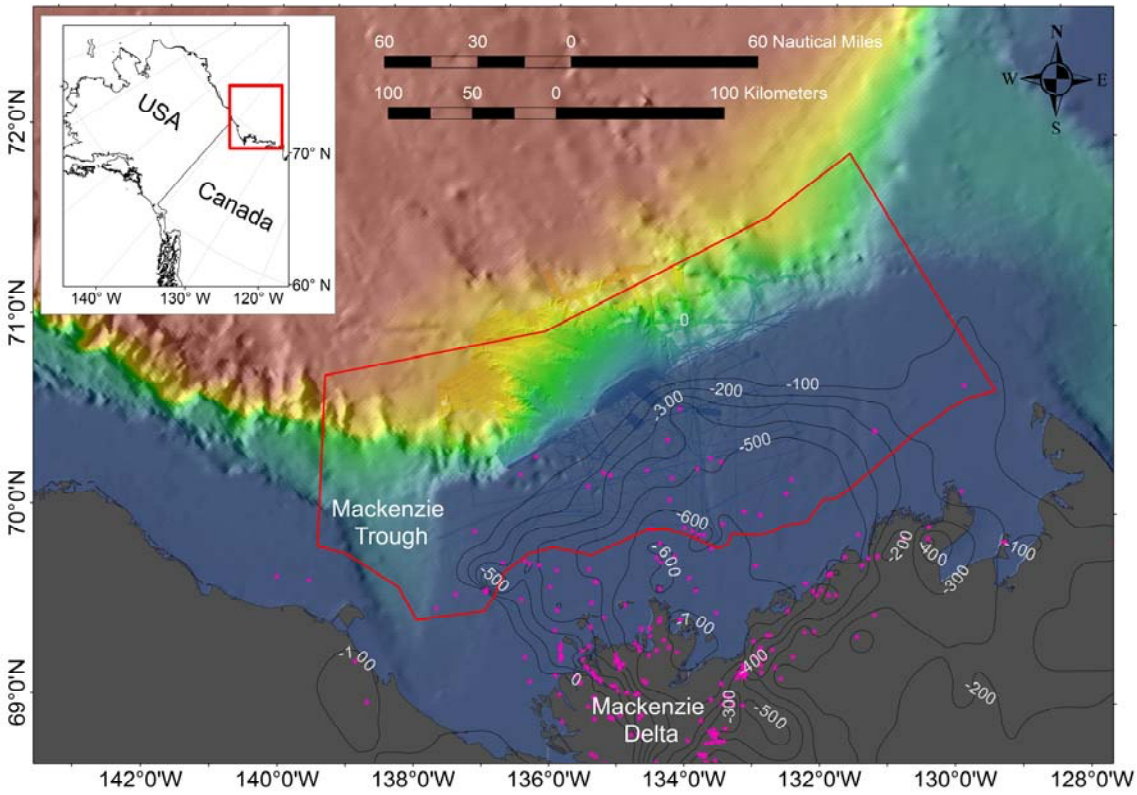

Figure 1.2 Location map of Beaufort Shelf study area showing location of industry wells (purple stars) and contour-lines of the depth (in m) to the base of permafrost. The figure also shows a portion of the outer shelf where detailed multi-beam data allow consideration of the detailed morphology of the shelf/slope transition area. The study permit area is outlined by the red line.

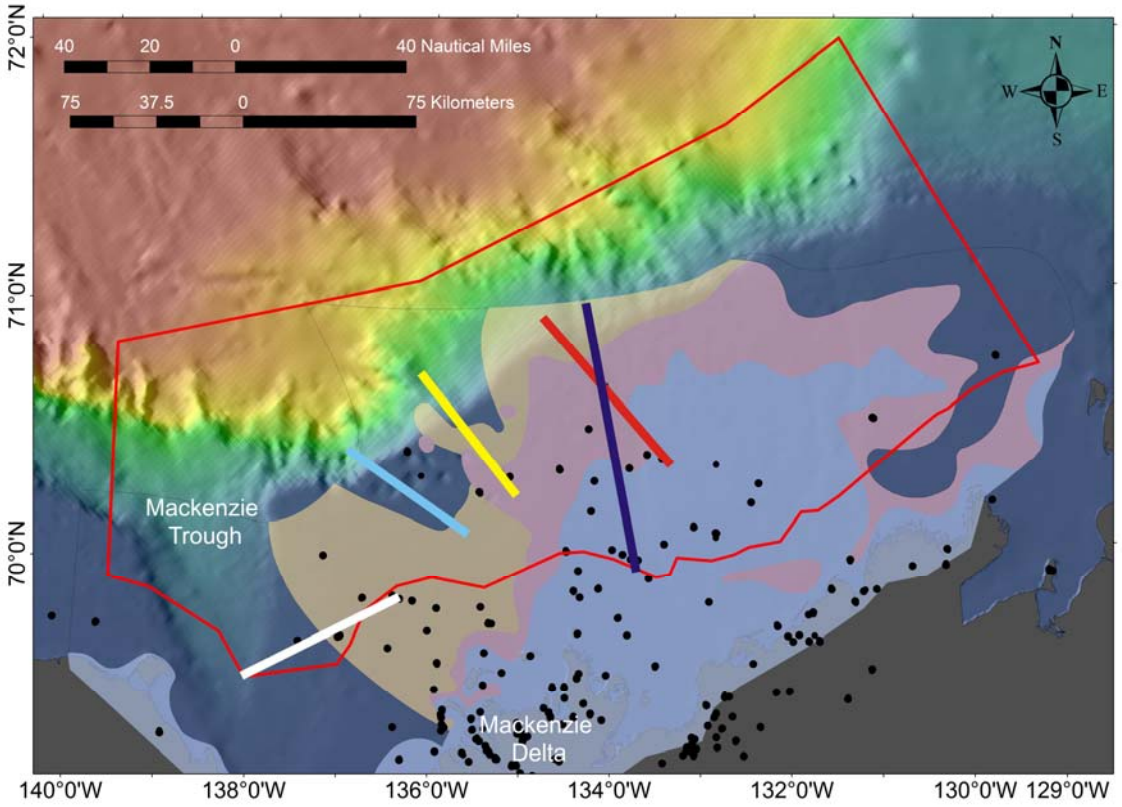

Figure 1.3 Location map of five main transects selected for regional characterization of permafrost distribution based on selected industry well sites. In order of priority, the transects are: "red", "yellow" "deep-blue", "cyan", and "white". Color-shaded regions are zones of different ice-content in sediments, based on work by Pullan et al., 1987. (blue" continuous ice-bonded sediments, pink: discontinuous ice-bonding, orange: no or low ice content).

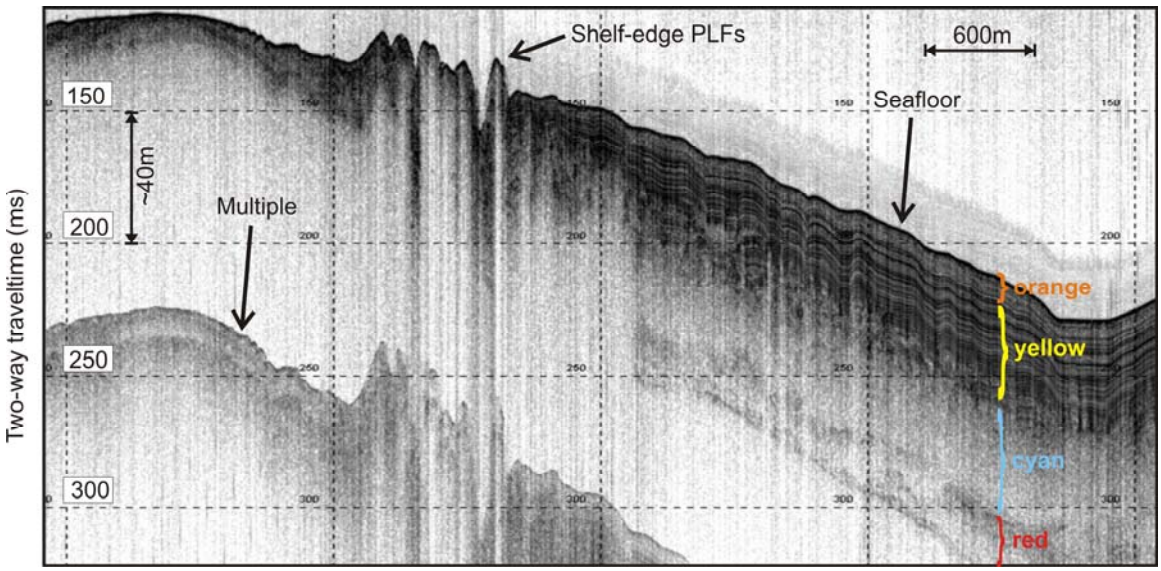

Figure 1.4 Example of seismo-stratigraphic units defined from 3.5 kHz sub-bottom profiler data acquired during Expedition ARA04C (line ARA04C_cl_007).

Chapter 2 Regional geological setting and permafrost regime in the Canadian Beaufort Sea

M. Riedel, Y. K. Jin

2.1 The Beaufort Shelf/Slope

The Beaufort Sea -Mackenzie shelf and slope is one of the best documented Arctic coastal areas in the world as it has benefited from more than forty years of scientific research. Substantive engineering activities were initiated during a phase of intensive offshore hydrocarbon exploration in the 1970s and 80s. Gas hydrate research at the Mallik site (Dallimore and Collett, 1995; Dallimore et al., 2005) clearly documented gas hydrate occurrences and serves as a terrestrial analogue with which to compare the shelf environment. The Mackenzie Delta region is generally characterized by greater than 10 km of upper Cretaceous to Cenozoic aged sediments, comprised primarily of folded and faulted deltaic complexes. The geological and geotechnical properties of shallow shelf sediments are heavily influenced by the glacial and inter-glacial history and permafrost formation. The margin has been studied by GSC scientists since the 1970s and resulted in a wealth of background information available for this study (e.g. Pelletier, 1988; Hill et al, 1992, 1993; Blasco et al., 1990, 1998). Permafrost, or sediments that are below 0°C, is widespread beneath of the Beaufort Shelf (Pelletier, 1988) having formed during periods of lower sea level when portions of the shelf currently in less in than ~100 m water depth were an emergent coastal plain exposed to very cold surface temperatures. An important consideration for evaluating the geo hazard is the presence or absence of ice-bonding. Ice-bonding substantially strengthens both compressive and shear strength of the sediment while reducing its porosity and permeability. Normal consolidation of ice-bonded permafrost can be substantially impeded due to the increase in strength of the ice-bonded sediments, and thus intervals that are under-consolidated can be created. Another unique consideration in terms of offshore permafrost is the temporal aspect of its response to ongoing marine transgression. The inundation of the shelf with relatively warm marine and estuarine waters has imposed a step change from mean annual

temperatures as low as -20ºC during terrestrial exposure, to present bottom water temperatures that are near -1ºC. Despite the fact that deeper parts of the shelf have been submerged for more than 7000 years, the submerged offshore permafrost is still responding to this thermal change because of slow rates of heat diffusion and latent heat associated with thawing (Paull et al., 2011; 2007; Taylor et al., 1996). Similarly, where permafrost pinches out at the edge of the shelf there may be conditions where pressurized fluids migrate vertically and horizontally. Such conditions could substantially influence pore pressures in shelf edge and slope sediments, making them particularly susceptible to liquefaction and slope failure. Critical to the understanding of these processes is an improved knowledge of the timing and rate of deposition, subaerial exposure and transgression of the permafrost-affected sediments. Because permafrost degradation is ongoing, it is also important to evaluate the effects of ocean temperature variability, including potential warming of bottom water, on the geothermal regime controlling the degradation.

2.2 Geothermal Setting

The scientific underpinning for Expedition ARA04C is based on a comprehensive understanding of the geothermal environment of the shelf and the contrasting setting associated with the continental slope. Using an archive of industry acquired data, researchers have estimated both permafrost and gas hydrate occurrence beneath the southern Beaufort shelf in the vicinity of the Tuktoyaktuk Peninsula (Figure 2.1). The ice-bonded permafrost interval varies from 400 to 700 m thickness (Judge, 1982; Smith and Judge, 1983) with an associated base of gas hydrate stability between 650 and 1300 m (Weaver and Stewart, 1982; Majorowicz and Hannigan, 2000). Geothermal modeling has been conducted to evaluate the lateral changes in the geothermal setting of the transgressed Beaufort shelf, worldwide sea level trends during the last 125,000 (insert ref). The model predicts that a thick and relatively continuous body of permafrost at near isothermal conditions at -2°C, continues from the coast to approximately 60 m water depth (~80 km offshore). These modeling efforts indicate that the thermal structure changes little across most of the shelf. However, rapid lateral change occurs in the zone associated with water depths between 90-110 m near the shelf edge. From 60 m water

depth the permafrost body rapidly thins, until it pinches out completely at about 100 m water depth. The gas hydrate stability field is controlled by the thermal regime established by this permafrost body. Intra-permafrost gas hydrate (Figure. 2.2), where gas hydrate co-exists with pore ice within the sediment matrix (Dallimore and Collett, 1995), may occur from approximately 250 m depth to the base of permafrost. The result is that the terrestrial permafrost and gas hydrate zones, which extend across the shelf, pinch out at ~100 m water depths.

The present day hydrographic conditions in the Beaufort Sea are remarkable, the coldest portion of the water column (mean annual temperature of -1.6°C) occurs at or above ~160 m water depths, while the maximum water temperatures occur at a depth of 300 m (mean annual temperature of ~1°C (insert ref). These thermal conditions have profound implications for both the distribution of permafrost and gas hydrate at the shelf edge and upper slope (Fig. 2.2). In addition to the extent of the permafrost and gas hydrate stability field, an important consideration for understanding the geothermal regime is the evolution of the porous media environment over time (Figure 2.3). The gradual warming of the permafrost interval results in thawing at the both top and bottom of the permafrost. The permafrost may also warm to near isothermal conditions that are controlled by latent heat effects associated with phase changes. Because permafrost can contain substantial amounts of unfrozen water, even at negative temperatures, the gradual warming of the permafrost seaward can change sediment strength and permeability characteristics. Complete thawing of permafrost can also cause sudden loss of sediment strength due to release of pore water leading to over-pressure (Ruffel et al., 1988). The gas hydrate stability field also experiences rather substantial change as a consequence of transgression. The top of the intra-permafrost interval, where gas hydrate and pore ice can co-exist (Dallimore and Collett, 1995), will shift downwards, whereas the base of the sub-permafrost gas hydrate stability will shift upward. As is the case with thawing of ice-bonded permafrost, dissociation of gas hydrate can result in liberation of pore water and loss of sediment strength. A substantive additional consequence of gas hydrate dissociation is the potential liberation of large quantities of free gas which can generate substantial overpressure (Weaver and Stewart, 1982). If the reacting sediments are within a closed system, the overpressure can be maintained for long periods of time. However, if

there are permeability conduits, overpressure can also induce water and gas migration within the sediment. Given that ice-bonded permafrost and hydrate-bearing sediments generally have low permeability, one likely preferred pathway would be laterally towards the shelf edge where permafrost and gas hydrate fields are predicted to pinch out (Figure 2.2). Another possibility is that pore water and free gas migrate vertically through breakthroughs in the permafrost.

2.3 Surficial Features Indicative of Degrading Permafrost or Gas Hydrate

Evidence of possible degradation of transgressed permafrost or gas hydrate include occurrences of shallow gas or overpressure in subsurface sediments, unique geologic structures indicating sediment and/or fluid expulsion from depth, and sea bed gas release (Figure 2.4). Indications of shallow gas on the Beaufort Shelf have been inferred from shallow reflection seismic surveys that show some intervals with acoustic blanking and or bright spots (O'Connor, 1980). In other areas of the Beaufort Sea, seismic signatures indicative of possible gas chimneys have been identified (Blasco et al., 2011). Shallow gas and overpressure have also been observed within the permafrost and permafrost gas hydrate interval during the course of hydrocarbon exploration drilling (Weaver and Stewart, 1982). More recently, high-resolution seabed mapping undertaken by industry in collaboration with the ArcticNet program has allowed detailed characterization of the morphology of the outer shelf area. A remarkable number of surficial geologic features suggesting seabed gas release and sediment dynamics occur in the vicinity of the outer shelf and upper slope (Blasco et al., 2011; Hughes-Clark., 2009; Nixon and Grozic, 2007; Paull et al., 2007; 2011). Surficial features, which are associated with seabed gas release, include the widespread occurrence of large conical hills called pingo-like features (PLFs) in the mid- and outer shelf (Figure 2.5), and large-scale landslide features (Figure 2.6) in the shelf-slope transitional area. Deepwater conical structures on the Beaufort slope thought to be associated with possible sea floor outcroppings of gas hydrate have also been described (Figure 2.7).

References

Blasco, K.A., Blasco, S.M., Bennett, R., MacLean, B., Rainey, W.A., Davies, E.H., 2010. Seabed geologic features and processes and their relationship with fluid seeps and the benthic environment in the Northwest Passage, Geological Survey of Canada, Open File Report, 6438, pp. 110.

Blasco, S. M., Shearer, J. M., Myers, R., 1998. Seabed scouring by sea-ice: scouring process and impact rates, Canadian Beaufort Shelf. In: Proceedings of Ice Scour and Arctic Marine Pipelines Workshop, 13th International Symposium on Okhotsk Sea and Sea-Ice, pp 53-58.

Blasco, S.M., Fortin, G., Hill, P.R., O'Connor, M.J., Brigham-grette, J.K., 1990. The Late Neogene and Quaternary stratigraphy of the Canadian Beaufort Continental Shelf. In: Grantz, A., Johnson, L., Sweeney, J.F., (eds.) The Arctic Ocean region: Boulder, Colorado, Geological Society of America, The Geology of North America series, Volume L, Chapter 28, p. 491-502.

Blasco, S., Bennett, R., Brent, T., Burton, M., Campbell, P., Carr, E., Covill, R., Dallimore, S., Davies, E., Hughes-Clarke, J., Issler, D., Leonard, L., MacKillop, K., Mazzotti, S., Patton, E., Rogers, G., Shearer, J., White, M., 2013. 2010 State of Knowledge: Beaufort Sea Seabed Geohazards Associated with Offshore Hydrocarbon Development; Geological Survey of Canada, Open File 6989, 340 p. doi:10.4095/292616

Dallimore, S.R., Collett, T.S., 1995. Intrapermafrost gas hydrates from a deep core in the Mackenzie Delta, Northwest Territories, Canada, Geology, v. 23, p. 527-530.

Dallimore, S.R. and Collett (eds.) 2005. Scientific Results from Mallik 2002 Gas Hydrate Production Research Well Program, Mackenzie Delta, Northwest Territories, Canada. Geological Survey of Canada, Bulletin 585: Printed Volume with papers as PDF files on a CD-ROM and data on a DVD disk.

Hill, P.R., Blasco, S.M., Harper, J.R., Fissel, D.B., 1992. Sedimentation on the Canadian Beaufort Shelf, Continental Shelf Research, 11, 821-842.

Hill, P.R., Héquette, A., Ruz, M.-H., 1993. Revised Holocene sea level curve for the Canadian Beaufort Shelf. Canadian Journal of Earth Sciences, 30, 103-108.

Hughes Clarke, J., 2009. Identification of Active Gas Seeps on the Beaufort Continental Margin: New Multibeam Water Column Imaging Capability of the CCGS Amundsen. Proceedings of Arcticnet Annual Scientific Meeting, Victoria, B.C. Canada, p. 49-59.

Judge, A.S., 1982. Natural gas hydrates in Canada, *in* French, H.M., ed. Proceedings, Fourth Canadian Permafrost Conference: Ottawa, National Research Council of Canada, p. 320-328.

Majorowiz, J.A., Hannigan, P.K., 2000. Stability Zone of Natural Gas Hydrates in a Permafrost-Bearing Region of the Beaufort–Mackenzie Basin: Study of a Feasible Energy Source, Natural Resources Research, v. 9, no. 1, p. 3-25.

Nixon, M.F., Grozic, J.L.H., 2007. Submarine slope failure due to gas hydrate dissociation: a preliminary quantification. Canadian Geotechnical Journal, March 2007, p. 314-325.

O'Connor, M.J., 1980. Development of a proposed model to account for the surficial geology of the southern Beaufort Sea, Geological Survey of Canada Open File Report, p. 128.

Paull, C.K., Ussler, W., Dallimore, S.R,. Blasco, S.M., Lorenson, T.D., Melling, H., Medioli, B.E., Nixon, F.M., McLaughlin, F.A., 2007. Origin of pingo-like features on the Beaufort Sea shelf and their possible relationship to decomposing methane gas hydrates Geophysical Research Letters, v. 34, no. 1, doi:10.1029/2006GL02797.

Paull, C.K., Dallimore, S.R., Hughes-Clarke, J., Blasco, S.M,. Lundsten, E., Ussler, W. III, Graves, D., Sherman, A., Conway, K., Melling, H., Vagle, S., Collett, T.S., 2011. Proceedings of the 7th International Conference on Gas Hydrates, Edinburg, Scotland, July 2011.

Pelletier, B. R., editor, 1988. Marine science atlas of the Beaufort Sea: geology and geophysics. Geological Survey of Canada, Miscellaneous Report 40.

Ruffel, J.P, Murphy, T.R., Graham, C., 1988. Planning and execution of a 500m corehole through permafrost, Proceedings of the Fifth Canadian Permafrost Conference, Quebec, National Research Council of Canada, p. 271-282.

Smith, S.L., Judge, A.S., 1993. Gas hydrate database for Canadian Arctic and selected East Coast wells. Geological Survey Canada. Open File Report, 2746, 120 p.

Taylor, A.E., Dallimore, S.R., Outcalt, S.I., 1996. Late Quaternary history of the Mackenzie-Beaufort region, Arctic Canada, from modelling of permafrost temperatures. 1. The onshore-offshore transition. Canadian Journal of Earth Sciences, v. 33, p. 52-61.

Taylor, A.E., Dallimore, S.R., Hill, P.R., Issler, D.R., Blasco, S., Wright F., 2013. Numerical model of the geothermal regime on the Beaufort Shelf, Arctic Canada since the Last Interglacial, Journal of Geophysical Research, Earth Surface, Vol. 118(4), 2365-2379.

Weaver, J.S., Stewart, J.M., 1982. *In situ* hydrates under the Beaufort Sea Shelf, *in* French H.M., ed., Proceedings, Fourth Canadian Permafrost Conference: Ottawa, National Research Council of Canada, p. 312-319.

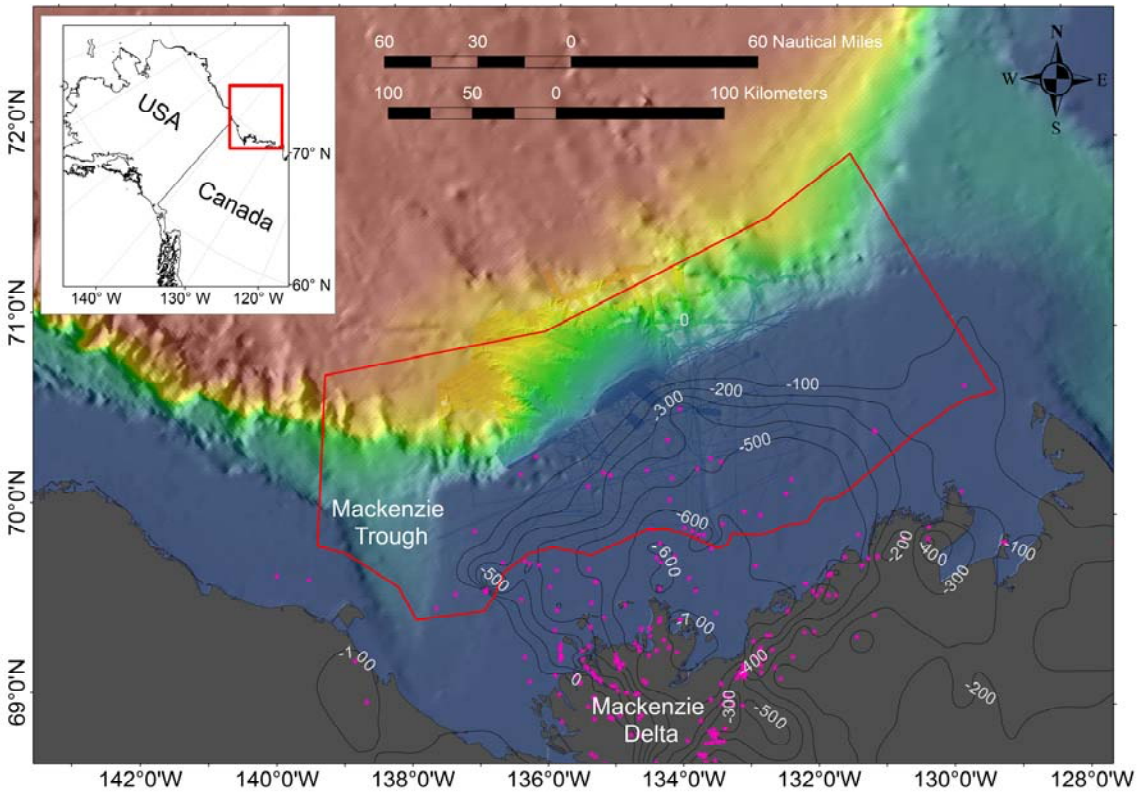

Figure 2.1 Location map of Beaufort Shelf study area showing location of industry wells (purple stars) and contour-lines of the depth (in m) to the base of permafrost. The figure also shows a portion of the outer shelf where detailed multi-beam data allow consideration of the detailed morphology of the shelf/slope transition area. The study permit area is outlined by the red line.

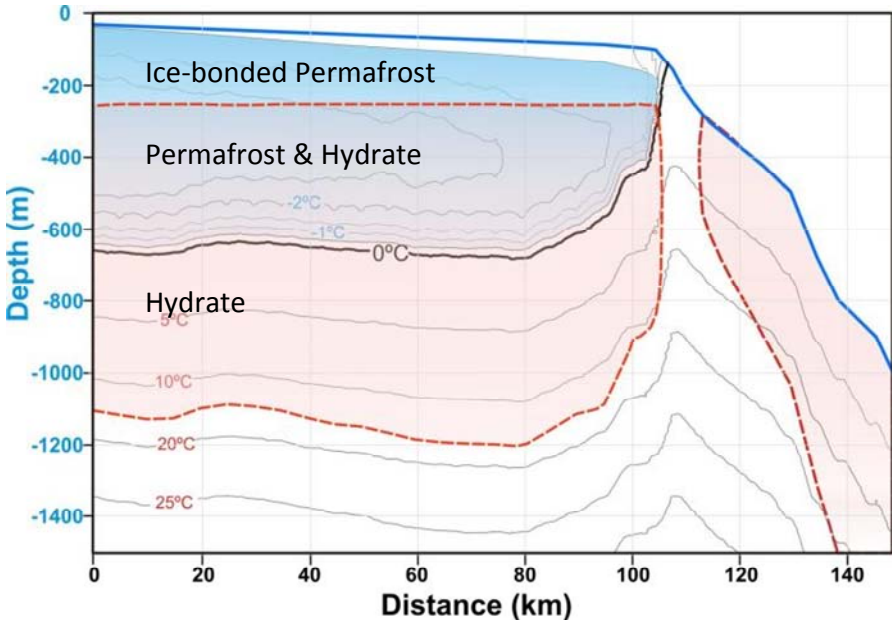

Figure 2.2 Cross-section showing the distribution of ice-bonded permafrost, permafrost-associated gas hydrate stability field, and the deeper water marine gas hydrate stability field across the Beaufort shelf based on geothermal modeling (Taylor et al., 2013).

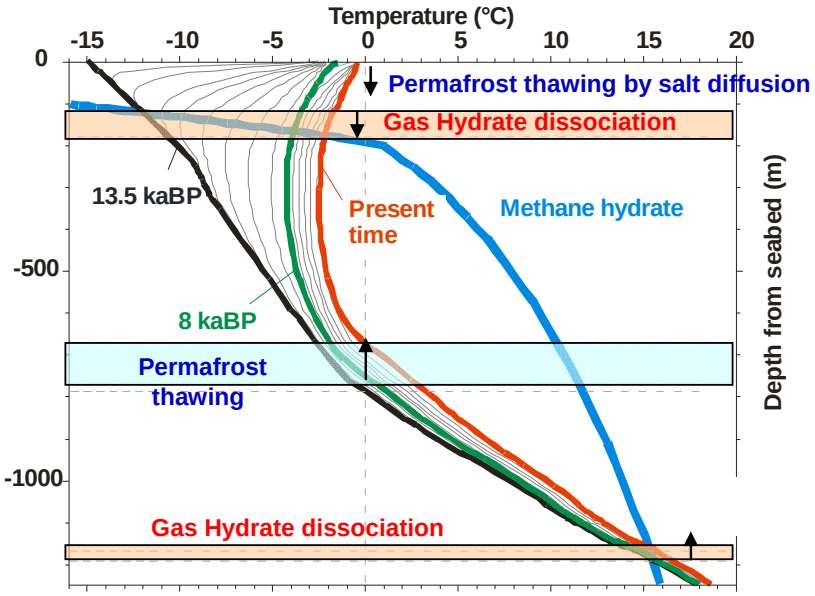

Figure 2.3 Example of evolution of ground temperature field resulting from the abrupt change from terrestrial to marine conditions (methane hydrate stability conditions are shown in blue). While the changes in the ground temperature regime occur relatively slowly, the implications of thawing of permafrost and degradation of gas hydrates are quite substantial in terms of changes in sediment strength and the possible generation of overpressure from release of bound water and natural gas.

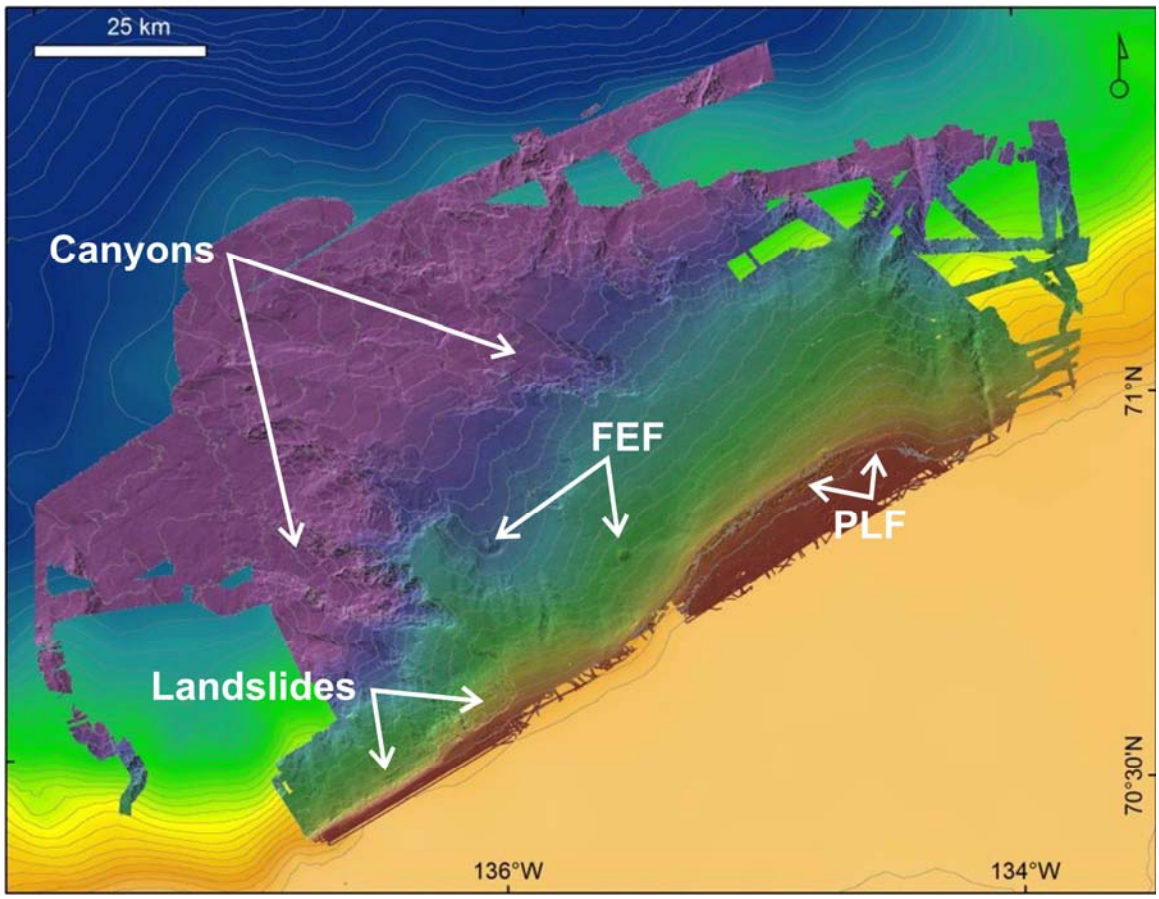

Figure 2.4 Map with general locations of features of interest in the study region: canyon and head-wall scarps with slope failures, fluid-expulsion features (FEF), pingo-like features (PLF), and landslides.

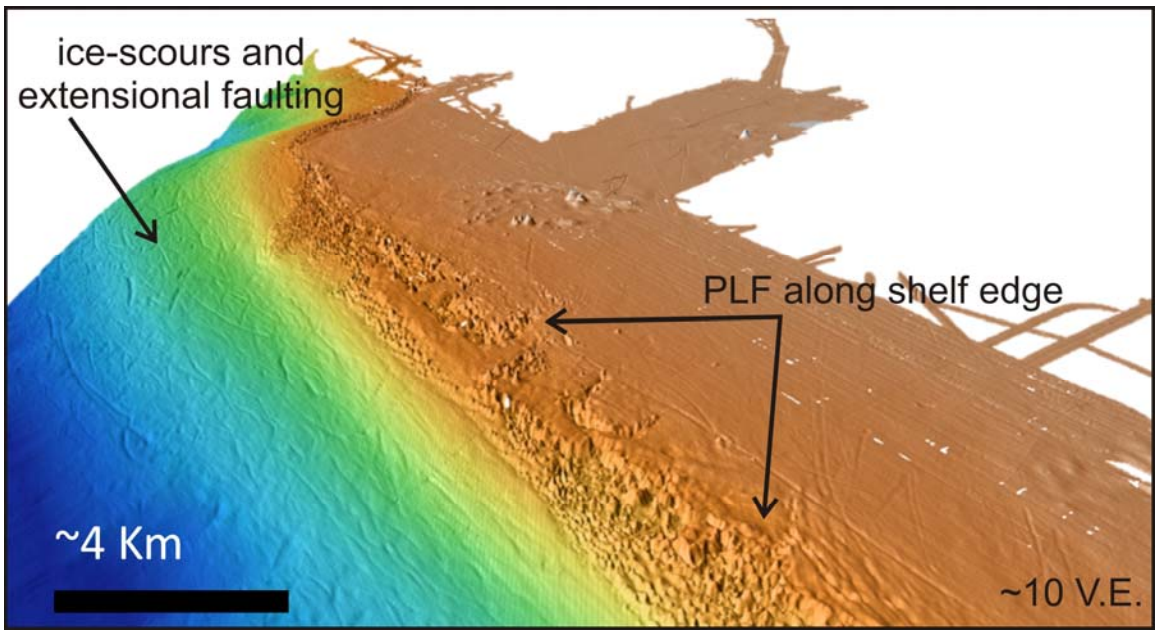

Figure 2.5 Example of pingo-like features exposed at the shelf edge.

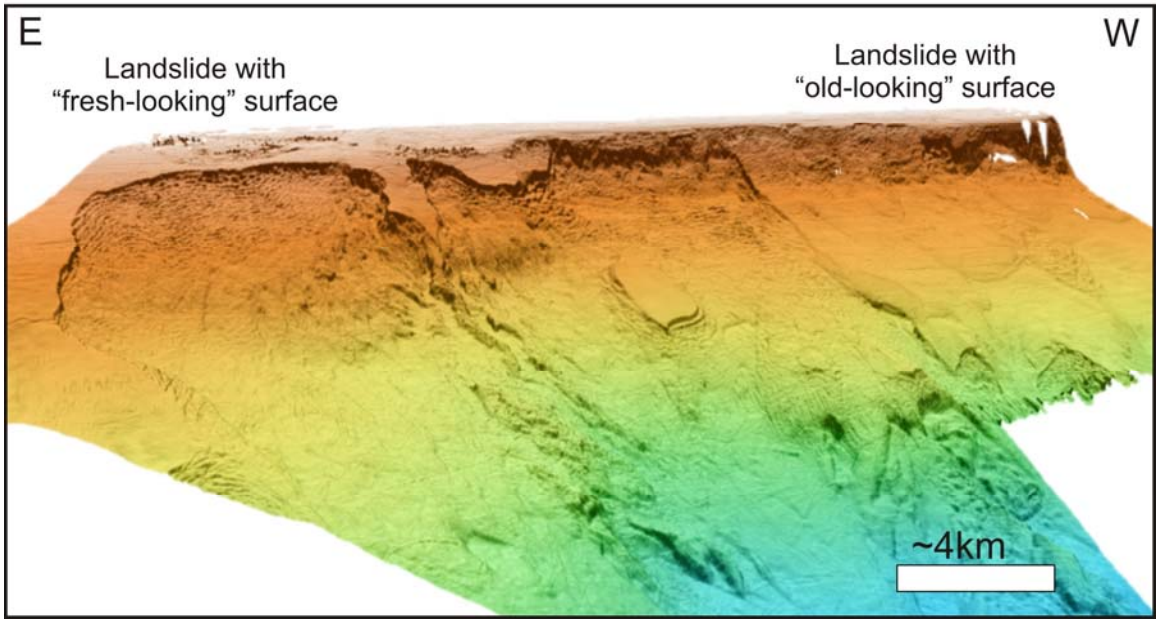

Figure 2.6 Example of large-scale landslides on the shelf edge. The landslide on the eastern portion of the image appears to be recent, while those on the western portion have a smoother appearance, suggesting they are older.

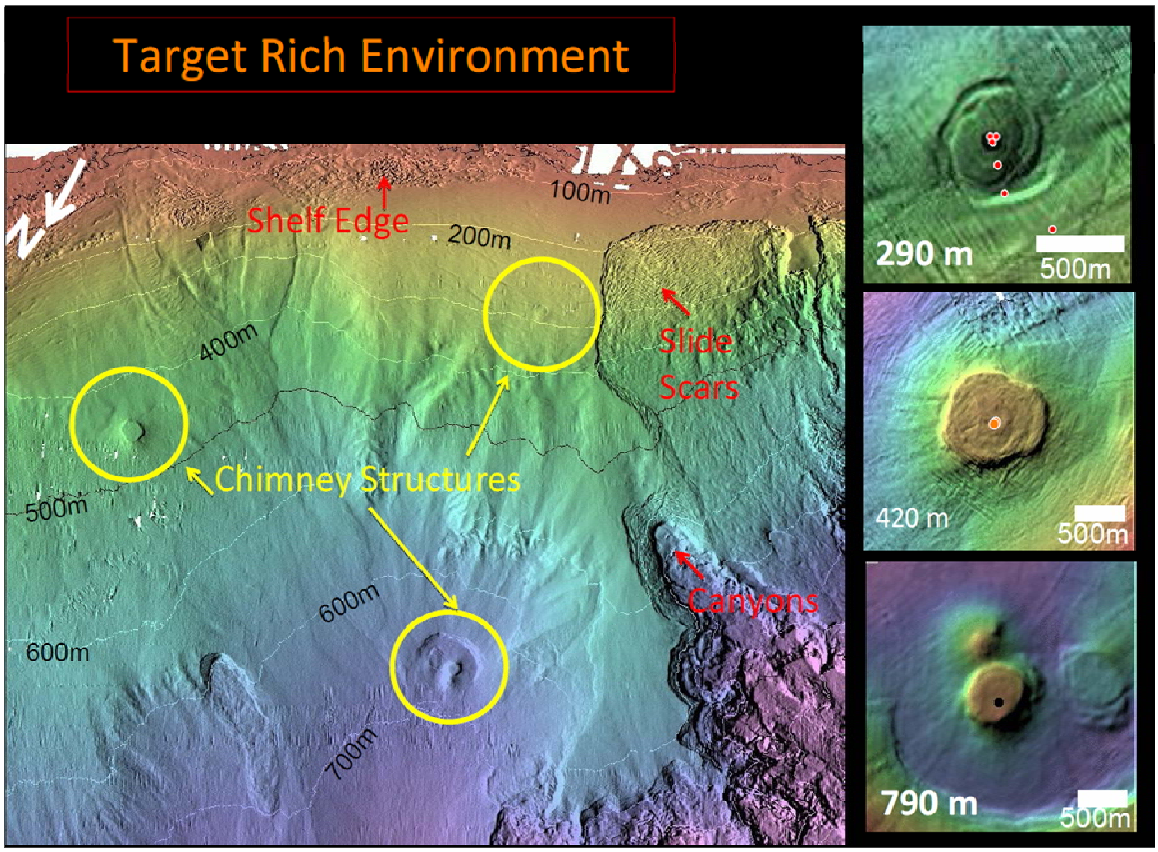

Figure 2.7 Main map on left: perspective view on the bathymetry of the Beaufort slope and shelf edge region with three deep-water expulsion features highlighted by yellow circles. Image on right-hand side show (from top to bottom): Fluid expulsion feature at 290 m water depth (also called "Coke Cap"), Fluid expulsion feature at 420 m water depth with prominent elevated, but almost flat plateau, and fluid expulsion feature at 790 m water depth with three visible mound-structures.

Chapter 3 Multi-channel seismic survey

J. K. Hong, M. Riedel, Y. K. Jin, D. S. Shin, H. Choi, H. J. Kim, H. S. Kim, M. Ulmi, S. Kim

3.1 Introduction

The multi-channel seismic survey was conducted on the outer continental shelf of the Beaufort Sea from September 14 to September 21, 2013 during ARA04C cruise in order to investigate sub-bottom structures, stratigraphy and velocity information. The seismic data consist of fourteen survey lines, 435 L-km, and 4,564 shot-gathers. Several times during the survey, the compressors were unable to maintain the working pressure over the 140 bar due to air leakage. The shot interval was set to 93.75 meter and ship speed was kept below 4.5 knots to maintain the working pressure. The processed seismic data shows detail stratigraphy and deep tectonic structures and there are refracted waves on the shot gathers from shallow water data.

3.2 Methods

3.2.1 The multi-channel seismic system on Araon

The multi-channel seismic system on Araon consists of an airgun array, a streamer, two compressors, and survey control systems (Figure 3.1). The airgun array has eight airguns, G-Gun II made by Sercel, and a float that maintains the source depth at 6 meters in the water (Figure 3.2, Figure 3.3). The airguns release compressed air at the same time and generate an acoustic wave that is used as the source wave of the multi-channel seismic survey. The airguns have four different volumes: Gun 1 and 2 were 250 in^3, Gun 3 and 4 were 200 in^3, Gun 5 and 6 were 90 in^3, and Gun 7 and 8 were 60 in^3. The total volume of the source is 1,200 in^3 (equivalent to 19.7 liter). The streamer has ten solid sections that record reflected acoustic wave and other signals like direct wave, refracted wave and background noise using hydrophones in the streamer in the water. The group interval and channel number of the streamer are 12.5 meter and 120 channels, respectively. Total length of the streamer is 1.8 km, including the tail buoy, fluid section

and lead-in cable. Eight cable levelers (birds) are attached on the streamer every 300 meters that maintain the streamer depth in the water (Figure 3.4). Compressors make compressed and inject the air into the airguns. The compressor system of Araon consists of a primary and a back-up compressor. The compressors are alternated every 12 hours. The working pressure is set between 120 to 150 bar (1,740 – 2030 psi). The survey control system in the Main Dry Lab consists of a navigation control system, an airgun controller, a bird controller, a recording system, a quality control system and a navigation editing system (Figure 3.5). The navigation system, NaviPac from EIVA, makes seismic lines and controls the event type, shooting interval, event start/stop with the gun controller and recording system. The airgun controller, Bigshot from RTS (Real Time Systems), receives the event signal from NaviPac and triggers airguns to make acoustic waves. The Bigshot shows the shooting timing, quality and wave shape. The bird controller defines streamer depth and displays the location and heading of birds. The recording system, Baby Seal from Sercel, records the seismic data and sends it to a large storage system. The quality control system, e-SQC pro from Sercel, displays the real-time data such as shot gather and near trace gather. The navigation editing system, NaviEdit from EIVA, transforms the NaviPac survey file to a standard navigation file such as UKOOA P1/90 or other formats.

3.2.2 Acquisition parameter

Table 3.1 shows the acquisition parameters of the multi-channel seismic survey in ARA04C cruise. The shooting interval was set at 93.75 m for most survey lines. The group interval was 12.5 meter and 120 channels made 8 folds of coverage. The source depth was 6 meter and the streamer depth set as same value. The work pressure was set to approximately 150 bars. The recording length and sampling rate were 10.0 seconds and 1 millisecond, respectively. The recording file format was SEG-D. Figure 3.6 shows the offset of the seismic survey.

3.3 Results

3.3.1 Data acquisition

The multi-channel seismic data were acquired on the outer shelf of the Beaufort

Sea from 14 September to 20 September 2013. The data consist of 14 survey lines, 435 L-km and 4,564 shot gathers (Table 3.2, Figure 3.7). From the first line to eighth line, the airguns had problems maintaining pressure. When the compressors were unable to maintain the working pressure over 140 bars, all airguns were turned off. After line #5, the total volume dropped to less than 300 in^3 which is too low to image deep structures because the weak high frequency energy quickly attenuates at the shallow depth. The airgun array was retrieved, reassembled and cleaned after line #7. From the line #8, the seismic data showed high-resolution data with 860 in^3 volumes. The first part of the survey finished after line #12. The second part of the survey started at line #21, but very low pressures (< 100 bars) were insufficient to conduct the multi-channel seismic and OBS surveys. Once again the airgun array was retrieved and repairs were performed. Line #22 started with sustainable pressure over 150 bars and recycle time was under the 30 seconds. The shooting interval was decreased from 93.75 meter to 75 meter. Unfortunately, after only one hour, the pressure decreased again and the seismic survey was terminated at 1:55 on 21 September. The tail buoy and the 8^{th} bird were lost after a collision with floating ice at 20:33 on 20 September. A search was undertaken in an attempt to find the tail buoy, but it was unsuccessful.

3.3.2 Data processing and analysis

The acquired seismic data were processed with VISTA 10.0, a seismic data processing software to make brute-stack section. The seismic data processing sequence consists of a number of steps: SEG-D file read, band-pass filtering, recording delay correction, geometry setting, velocity analysis, normal moveout (NMO) correction and common mid-point (CMP) stack. Since the survey area had shallow water depth about 60 m, the direct wave and refracted waves overlapped with primary reflection signals. In order to remove the direct wave and refracted wave, a top mute was added in the processing sequence. The top mute cut the lineal signals after 10 traces. The trace kill was applied to remove bad shot gathers.

The brute stack section of ARA04C-SS-08, line #8, shows stratigraphy under the seafloor and deep structure below 1.0 second (Figure 3.8). Refracted waves were also recorded in the shot gathers acquired at shallower depths across the continental shelf

portion of the survey lines (Figure 3.9).

3.4 Summary

The multi-channel seismic data were acquired on the outer continental shelf of Beaufort Sea with 14 lines, 435 L-km and 4,564 shot gathers from 14 September to 21 September 2013. During the survey, issues in maintaining airgun pressure and harsh weather conditions resulted in generally poor data quality and resulted in some damaged to the streamer. However, good quality data were acquired on some lines, showing deep structures and clear refracted wave.

Table 3.1 Seismic acquisition parameters.

Shot Interval	93.75 m
Channel Number	120 ch
Group Interval	12.5 m
Source Depth	6 m
Streamer Depth	6 m
Fold of Coverage	8 folds
Work Pressure	150 bar
Recording Length	10.0 sec
Sample Rate	1 ms
Tape Format	SEG-D

Table 3.2 Seismic survey line log.

Line Name	SOL (Start of Line)						EOL (End of Line)						FGSP	LGSP	Shot Gather
	SP	Date/Time	Latitude (- / South)		Longitude (- / West)		SP	Date/Time	Latitude (- / South)		Longitude (- / West)				
ARA04C-SS-01	1043	2013:09:14:11:03:49.617	70.9598328	70 57.5900	-134.9756819	-134 58.5409	1750	2013:09:14:19:41:41.523	70.4725520	70 28.3531	-134.0124095	-134 00.7446	1043	1722	708
ARA04C-SS-02	2001	2013:09:14:19:50:54.163	70.4635566	70 27.8134	-134.0169594	-134 01.0176	2256	2013:09:14:23:02:03.540	70.4082265	70 24.4936	-134.6196280	-134 37.1777	2026	2241	256
ARA04C-SS-03	3001	2013:09:14:23:03:35.512	70.4082865	70 24.4972	-134.6248699	-134 37.4922	3458	2013:09:15:04:41:14.123	70.7007339	70 42.0440	-135.3309766	-135 19.8586	3004	3458	458
ARA04C-SS-04	4001	2013:09:15:04:52:03.645	70.7056254	70 42.3375	-135.3613550	-135 21.6813	4142	2013:09:15:06:42:28.349	70.6519624	70 39.1177	-135.6802081	-135 40.8125	4026	4123	142
ARA04C-SS-05	5001	2013:09:15:06:48:45.781	70.6452424	70 38.7145	-135.6914683	-135 41.4881	5432	2013:09:15:11:52:56.717	70.3584343	70 21.5061	-135.0697817	-135 04.1869	5015	5420	432
ARA04C-SS-06	6001	2013:09:15:12:20:05.025	70.3356883	70 20.1413	-135.0880822	-135 05.2849	6166	2013:09:15:14:26:05.091	70.3235118	70 19.4107	-135.4884534	-135 29.3072	6011	6160	166
ARA04C-SS-07	7001	2013:09:15:14:37:08.039	70.3320614	70 19.9237	-135.4795911	-135 28.7755	7040	2013:09:15:15:05:24.281	70.3455273	70 20.7316	-135.3932994	-135 23.5980	7012	7040	40
ARA04C-SS-08	8001	2013:09:16:00:59:34.162	70.4360323	70 26.1619	-135.9422627	-135 56.5358	8559	2013:09:16:07:36:29.919	70.5969178	70 35.8151	-134.6585254	-134 39.5115	8028	8550	559
ARA04C-SS-09	9001	2013:09:16:07:41:31.721	70.5969807	70 35.8188	-134.6403589	-134 38.4215	9165	2013:09:16:09:35:08.269	70.4993618	70 29.9617	-134.3619125	-134 21.7147	9024	9145	165
ARA04C-SS-10	10001	2013:09:16:09:38:05.162	70.4959476	70 29.7569	-134.3620239	-134 21.7214	10614	2013:09:16:17:02:04.917	70.3005040	70 18.0302	-135.7440375	-135 44.6422	10020	10613	614
ARA04C-SS-11	11001	2013:09:16:17:05:31.585	70.3008774	70 18.0526	-135.7535191	-135 45.2111	11266	2013:09:16:20:07:17.405	70.4491344	70 26.9481	-136.2304483	-136 13.8269	11023	11257	266
ARA04C-SS-12	12001	2013:09:16:20:09:28.154	70.4510966	70 27.0658	-136.2352078	-136 14.1125	12199	2013:09:16:22:24:52.925	70.5907314	70 35.4439	-136.4856117	-136 29.1367	12008	12188	199
ARA04C-SS-21	21021	2013:09:19:05:10:19.947	70.4789661	70 28.7380	-133.5184403	-133 31.1064	21158	2013:09:19:07:40:58.452	70.6148162	70 36.8890	-133.8291506	-133 49.7490	21024	21158	138
ARA04C-SS-22	22001	2013:09:20:19:28:30.446	71.0738283	71 04.4297	-134.9174777	-134 55.0487	22421	2013:09:21:01:24:53.966	70.7463133	70 44.7788	-134.1314508	-134 07.8870	22028	22421	421

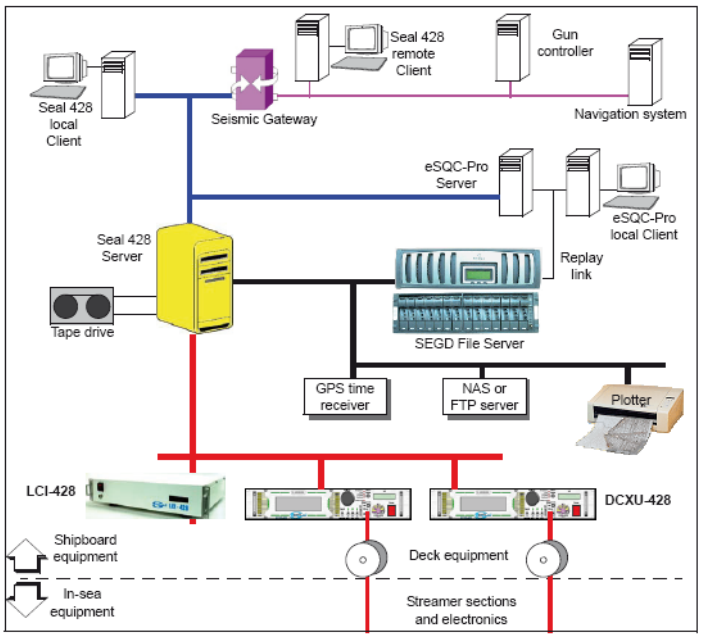

Figure 3.1 Schematic diagram of the multi-channel seismic system on Araon.

Figure 3.2 Airguns attached on the airgun array.

Figure 3.3 The airgun array launching into the Beaufort Sea.

Figure 3.4 The streamer is launched. The cable-leveller (bird) is attached to the streamer and tested.

Figure 3.5 The seismic survey control system including navigation, airgun controller, bird controller, recording system and quality control system in Main Dry Lab.

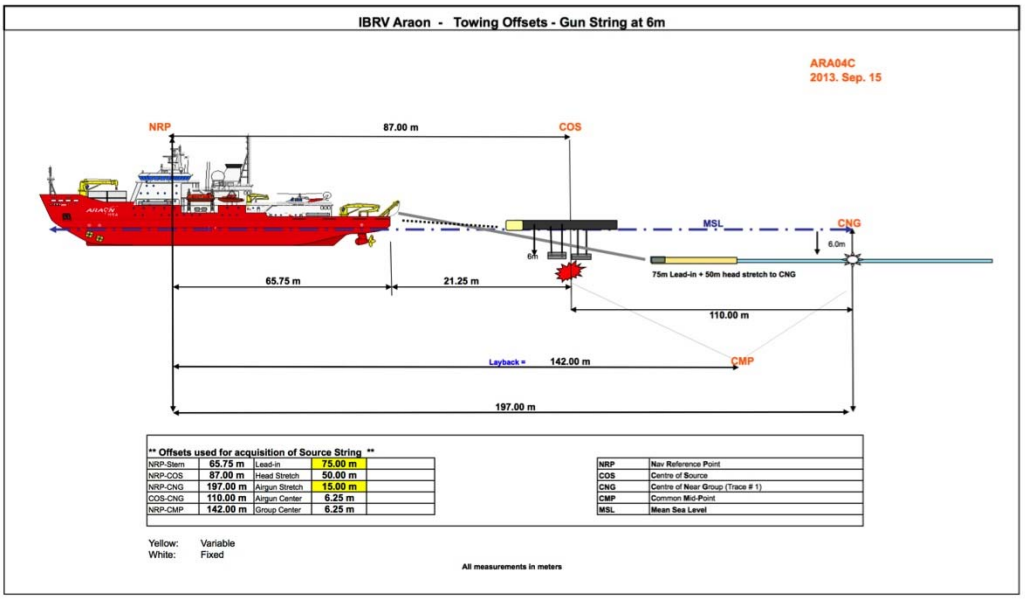

Figure 3.6 The offset information for the seismic survey.

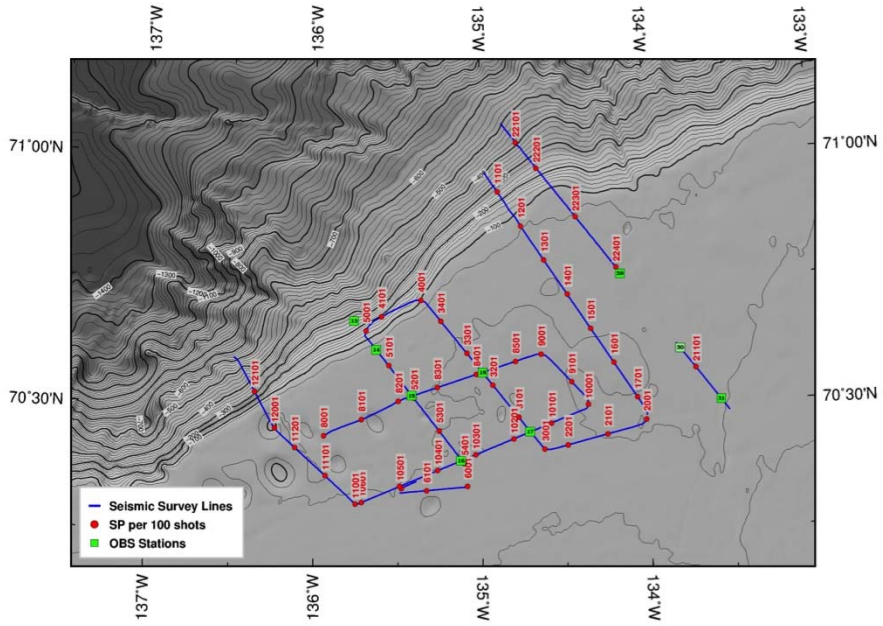

Figure 3.7 Track-chart of the seismic survey of ARA04C showing the seismic lines and the location of the OBS mooring.

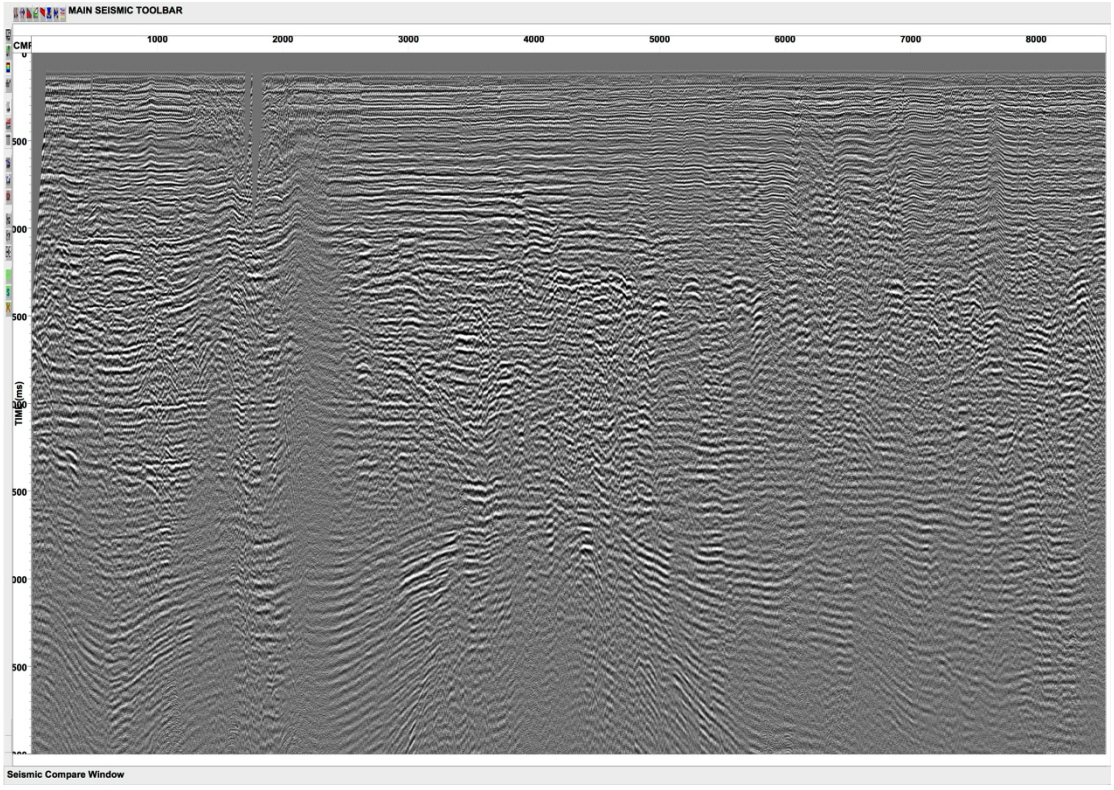

Figure 3.8 Brute stack section of ARA04C-SS-08.

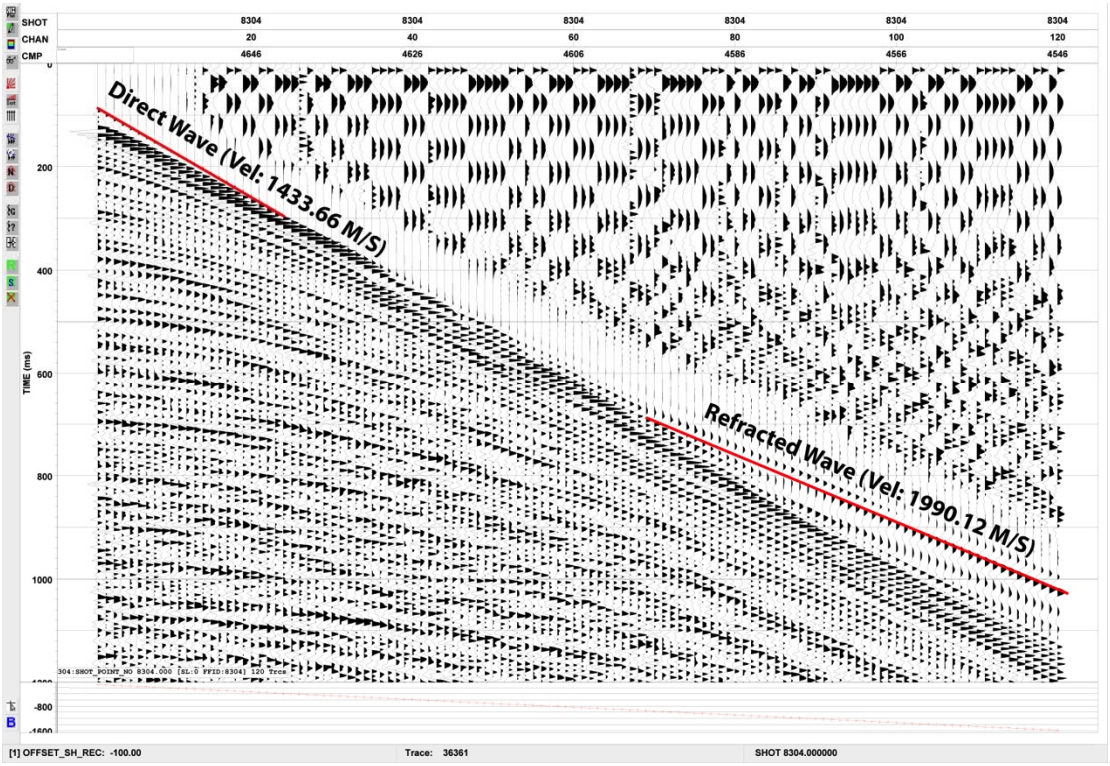

Figure 3.9 Common shot gather of shot #8304 in ARA04C-SS-08 shows refracted wave arrival with an apparent velocity of ~1990 m/s.

Chapter 4 Ocean Bottom Seismometer Survey

M. Riedel, G. Standen

4.1 Introduction

The combination of the multichannel seismic survey with ocean bottom seismometers (OBS) offers a unique opportunity to study permafrost settings. To enhance our understanding of the presence (or absence) of permafrost in the subsurface is a key objective of this expedition, and is a cornerstone of the IODP pre-proposal 806. Predictions of the offshore permafrost distribution were made in the past using several techniques including borehole temperature data and refraction seismic studies (Pullan et al., 1987). The offshore-edge of the permafrost in ~100 m water depth is the most critical boundary for understanding the sediment and hydrogeologic regimes associated with the degrading permafrost. Following the strategy of collecting data along main shelf-edge perpendicular transects, described in the introduction chapter of this report, we deployed several OBS along three transects bracketing the area of apparent continuous permafrost with ice-bonded sediments to the southeast and the ice-free, no permafrost zone at the northwest end of the transects (Figure 3.1). Two areas of across-shelf transects were chosen: Area 1 focusing on the "yellow" priority transect and Area 2 focusing on the "red" priority transect (transect priority and colour-coding are explain in the Background Chapter). Six OBS were deployed and airgun data were acquired along a set of lines crossing the OBS along the "yellow" priority transect from September 13 to17, 2013. After repeated airgun failures, repairs were carried out on September 18. A second deployment of consisting of three OBS took place. Limited data were collected from September 19 to September 21, 2103, along the "red" priority transect due to airgun array failures.

Sea ice conditions were challenging throughout the entire expedition. Therefore a deployment scheme was required that allowed airgun data collection for the OBS seismic reflection and refraction experiment and assured OBS retrieval in ice-free waters. Due to extensive ice along the "red" priority transect, we began data acquisition along the

"yellow" transect and only attempted work along the "red" priority transect later in the program, when ice had moved farther to the north. Although ice conditions were more favorable when operating along the "red" priority transect, the program was interrupted by a storm with winds over 40 knots and seas of up to 5 meter wave height. While weathering the storm, the streamer collided with sea ice, resulting in the loss of the tail-buoy and one streamer-leveling bird.

4.2 Method and instrument description

The NRCan owned ocean bottom seismometers (OBS) are instruments, which are designed to collect seismicity data while on the ocean floor. Each unit has a packaged array of three geophones (one vertical, two horizontal) and a single hydrophone which measures either passive or directed seismic events (Figure 3.2). The OBS units consist of one large and two smaller Benthos spheres mounted to a frame. This frame has half moon cut-outs on ether side where the OBS cylinder is fastened using bottom support brackets cut to the same design. The whole unit is then placed on an anchor plate and fastened using the release rod. The geophones are secured to the frame using galvanic release pins. This allows the geophones to release when the unit reaches the ocean floor so that they do not become tangled when the unit is descending (Figure 3.2). A trailing rope is used to recover the unit. The OBS were deployed using the Araon's A-frame and a simple slip-hook, releasing the OBS is lowered to water level (Figure 3.3).

The electronics are contained in a full ocean depth pressure housing. The housing also contains the batteries which provide the voltage for running the digital acquisition stage and analog boards.. The data are written and stored on a 16 Gigabyte flash card, which is removed upon retrieval for data processing.

A key element to recording useful data during this experiment is to ensure that the time series on the OBS is the same as that of the ship. The individual airgun shots are triggered onboard the ship using the ship's GPS antenna and time settings. Meanwhile, the computer on the OBS, will have some clock drift relative to the vessel's time, which needs to be corrected upon OBS-recovery. Another important element is that the exact time of each airgun shot needs to be recorded to sub-millisecond accuracy to allow for clock-drift corrections and exact shot-point location calculations. To ensure these key

elements are achieved, two separate GPS antennae were mounted on the 2nd deck (helicopter-deck level) on the starboard side (Figure 3.4) connected by BNC cable to two individual time-servers in the dry lab. The OBS time server was connected to the recovered OBS and clock-drift was calculated (Table 3.1). This drift will be corrected during the post-processing of the OBS data onshore. The second time server matched incoming trigger data with the exact time and navigation data from the GPS antenna. This will be used to define relative shot locations. The post-processing of OBS data will then define absolute distances (offsets) from OBS to airgun shots using an OBS-relocation inversion algorithm.

The OBS are programmed to start logging at a given time after deployment and also have a back up time for auto-release, if the forced acoustic release attempts fail. Once the airgun program is completed a coded acoustic released command is sent to the individual OBS. A low voltage high current circuit is used to short out to seawater/ground Minell wire, which then releases the rod holding the anchor and OBS together. After an eight minute burn the unit then rises at approximately 1 meter per second to the surface. Once the unit is at the surface a flashing strobe and a radio direction finder (RDF) tone is emitted, which helps locate the float assembly.

4.3 Results

The OBS experiment was split into two separate deployment periods. The first set of six OBS was deployed in the night of September 13 to 14, 2013 (Table 3.1) at the start of the airgun and multichannel seismic program. This deployment focused on two lines across the shelf and shelf edge zone of the Transect 1 Area (Figure 3.1). All six OBS were recovered successfully and data quality check confirmed that all OBS recorded data on all four channels of the vertical and horizontal geophone components and hydrophone (Figure 3.5). Refraction and reflection arrivals will be used post-expedition for a detailed velocity analysis using ray-tracing-based inversion algorithms as well as full-wave-form inversion. Due to ice over the intended route (Figure 3.6), two lines crossing the OBS-A (station ARA04C_13OBS_001) had to be shortened at the northern limit, resulting in no direct coverage of OBS-A.

The second deployment was carried out focusing on the Transect 2 Area over the

"red" priority transect. This deployment took place once the sea ice coverage in this area decreased and allowed complete line coverage over features of interest. The OBS were deployed in the night of September 18, 2013 (Table 3.1). Two attempts in collecting airgun seismic data along this OBS transect were made: a first attempt started at 17:00 on September 18 along the south-eastern end of the transect with two airgun ramp-up procedures, but no sustainable airgun volume could be reached, and the operation was halted. The ship maintained a route along the intended seismic line towards the north-west as the gear could not be recovered during night. After a short airgun repair operation, a second attempt was made to collect seismic data in the afternoon of September 20, 2013. After only 3 hours of operation, airgun leakage problems returned and the line was finally abandoned by 19:00 on September 20 at about OBS-D (Station ARA04C_29OBS_001).

Data recorded during this second deployment were limited. Only two of the three OBS deployed were retrieved (OBS-D and OBS-P) OBS-L was not retrieved despite a lengthy attempt at the retrieval sequence. It is speculated that the OBS did release upon the first attempt, but the vessel was too far away from the OBS surfacing point to see it in the twilight and the strobe may not have activated. With the upcoming winter and sea-ice formation, it is highly unlikely the device will be washed ashore intact where it could be found.

4.4 Summary

The combined multichannel seismic and OBS data will allow detailed velocity analyses to investigate the permafrost signature and help mapping zones of high-velocity sediments indicative of the presence of ice along the four main lines crossing the OBS stations in the Transect 1 Area). Initial analysis of individual shot gathers show clear refraction arrivals with velocities around 2000 m/s (see Chapter 3 for more details) in areas of expected permafrost occurrence, and shot gathers lacked such arrivals in zones where the permafrost was predicted to be absent. It is therefore expected that the OBS data, once post-processed will also show clear refracted arrivals for velocity analyses.

Table 4.1 OBS stations deployed during expedition ARA04C**.**

OBS-ID	Station	Latitude	Longitude	Water depth (m)
OBS-A	ARA04C_13OBS001	70°39.8856	135°45.8101	254
OBS-E	ARA04C_14OBS001	70°36.4466	135°37.7178	74
OBS-F	ARA04C_15OBS001	70°30.9717	135°25.0372	64
OBS-H	ARA04C_16OBS001	70°23.1932	135°07.4192	57
OBS-J	ARA04C_17OBS001	70°26.5783	134°42.5861	55
OBS-K	ARA04C_18OBS001	70°33.7002	134°59.4760	57
OBS-D	ARA04C_29OBS001	70°45.3078	134°09.3476	68
OBS-L	ARA04C_30OBS001	70°45.2910	134°09.2436	67
OBS-P	ARA04C_31OBS001	70°36.2777	133°48.2597	68

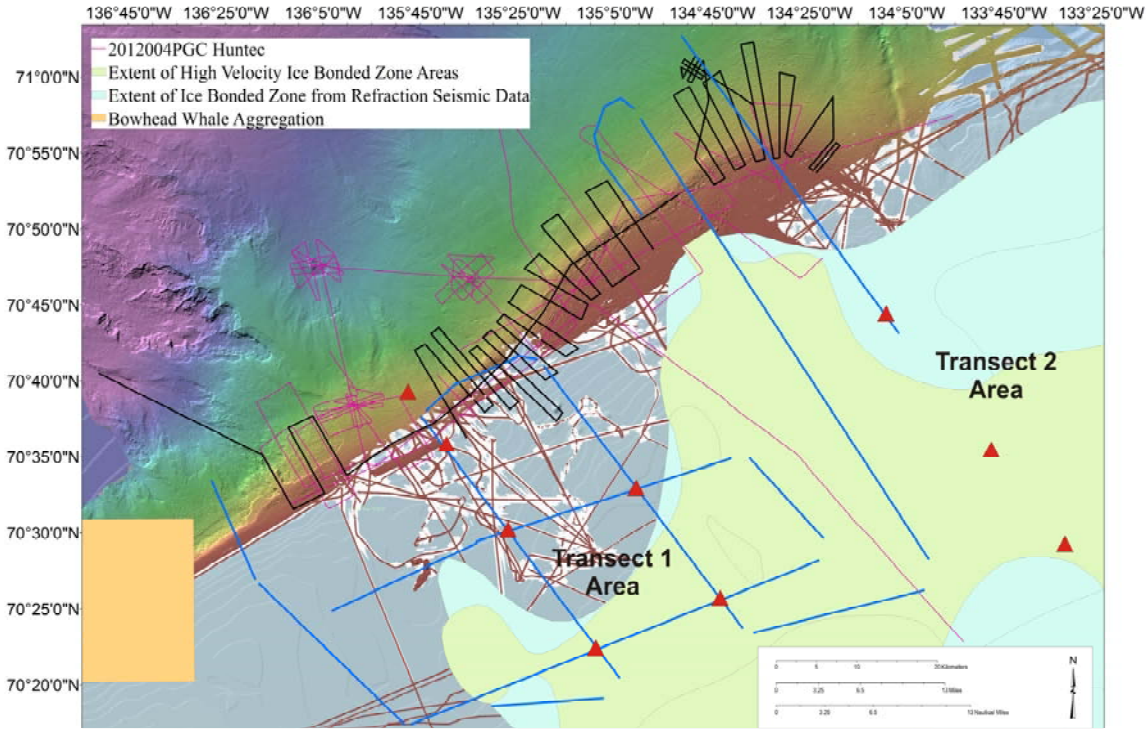

Figure 4.1 Layout of the OBS (red triangles) to study the degrading permafrost edge along two main transect areas. Transect Area 1 follows the concept of the "yellow" priority transect and Transect Area 2 follows the "red" priority transect. Lines drawn in blue are collected with the airgun array and multichannel streamer, lines in black were collected with the sub-bottom profiler only.

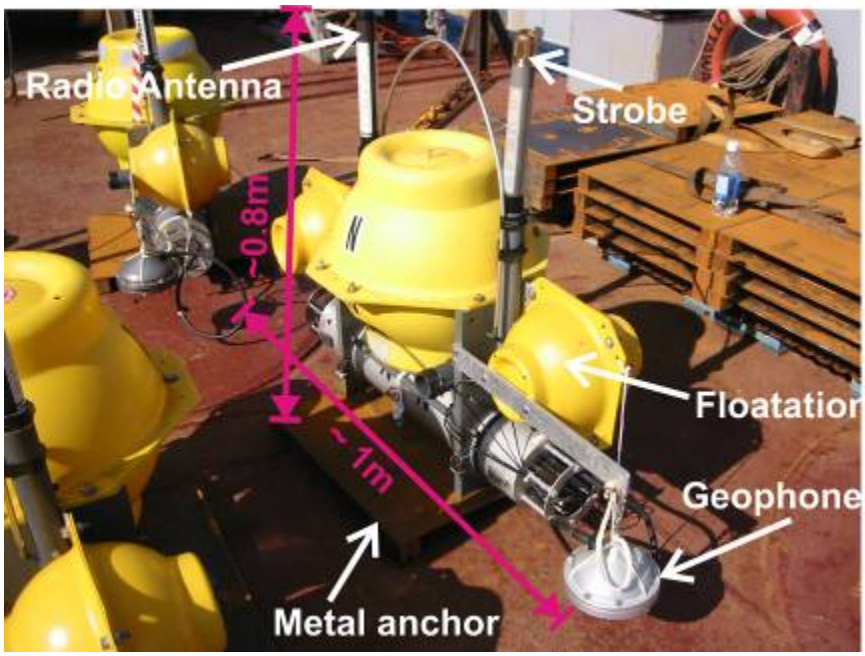

Figure 4.2 Image of a fully assembled OBS on deck.

Figure 4.3 Graham Standen operating the release-hook while deploying OBS from the stern of the Araon.

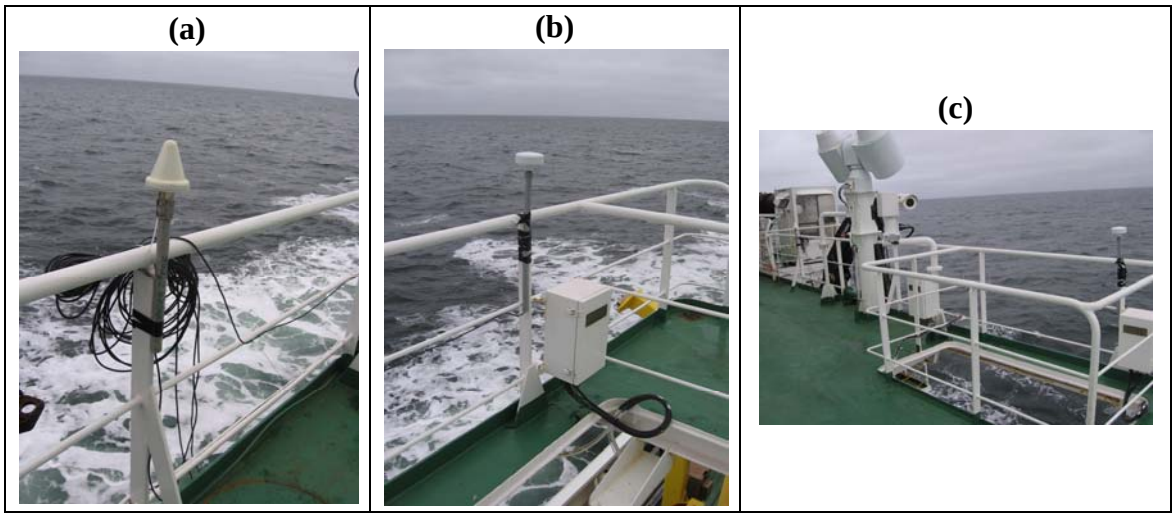

Figure 4.4 Antennae mounted on the helicopter-deck (Deck 2 level), 33 m towards the stern of the main ship's antenna reference point: (a) Antenna for GPS clock-drift calculations, (b) Antenna for shot-time logging equipment, (c) setup of both antennae on the starboard side of the helicopter deck (Deck 2 level).

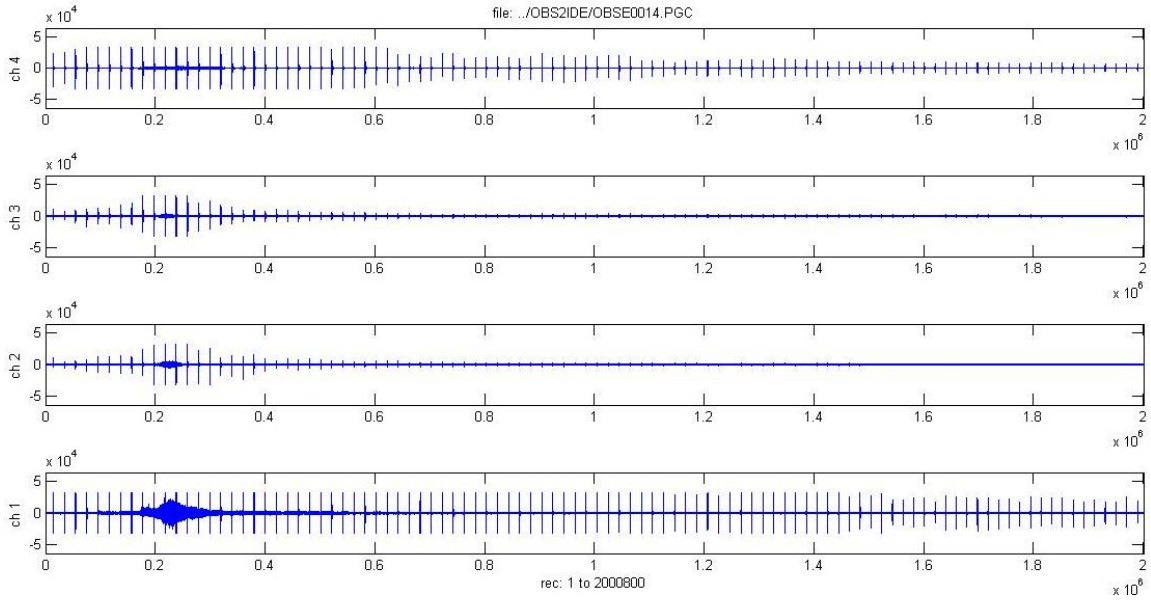

Figure 4.5 Example of seismic records on OBS-E (Station ARA04C_14OBS001) showing regular airgun arrivals on all channels: Ch1=vertical geophone component, Ch2 and Ch3=horizontal geophone components, Ch4=hydrophone. The time when the Araon is directly over the OBS location can be seen by the increase high frequency noise on the hydrophone data.

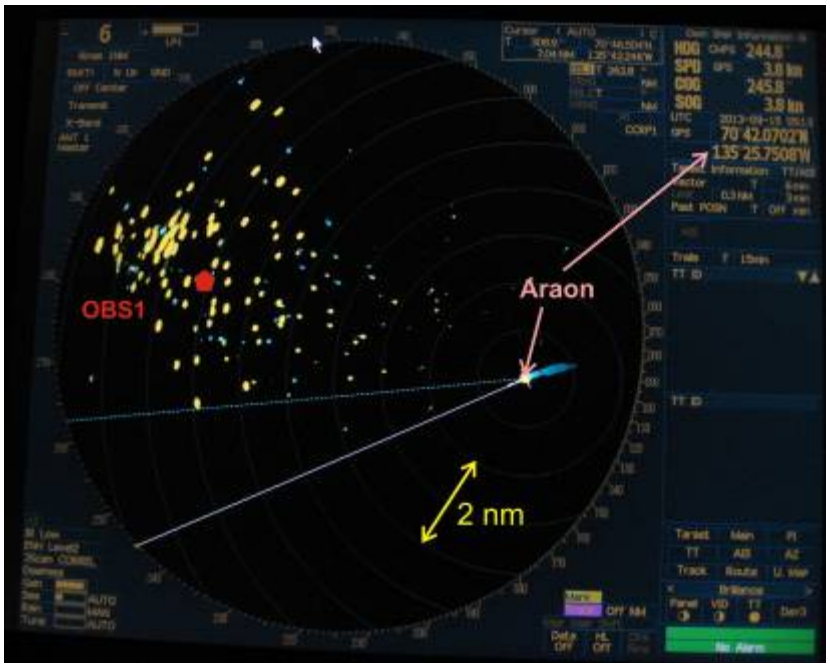

Figure 4.6 Screenshot of the ship's radar showing location of floating ice (yellow spots) and the location of OBS-1 (station ARA04C_13OBS_001) was inserted manually on this image. Location of the Araon is also shown. The occurrence of the ice deflected the line orientation for seismic data acquisition. No direct crossing of this OBS station was completed during this expedition.

Chapter 5 Sub-bottom profiler survey

M. Riedel, J.K. Hong, K. Conway, D.S. Shin, S. Kim, H.J. Kim, H.K. Choi, Y.-G. Kim, N. Seo, M. Ulmi, H.S. Kim, E.J. Byun, Y.J. Lee

5.1 Introduction

Subsurface images obtained from sub-bottom profiler (SBP) show precise sediment structure below surface. Conventional SBP equipment transmits 3.5 KHz acoustic signals and receives reflections. The resolution of SBP is the highest among other reflection methods such as Sparker, Boomer, and air-gun seismic instruments. Theoretically, SBP can detect layers of thickness up to 10 cm, depending on the sediment P-wave velocity structure. In most cases, vertical resolution is ~0.5 m.

In the survey area of the Canadian Beaufort Sea, many subsurface structures are closely related to the geologic evolution of permafrost and gas expulsion as introduced in Chapter 2. Pingo-like structures, for example, are distinct features in permafrost environments and mud volcanoes are related to gas expulsion from the subsurface. Sub-bottom images will provide additional insight on these features. Sub-bottom images are also utilized to define the optimum site for sediment coring and heat flow measurements.

5.2 System Description

The SBP120 Sub-bottom profiler installed on the ARAON is an optional extension to the EM122 Multibeam echo sounder. Figure 5.2 shows the SBP system diagram. The receiving transducer hydrophone array used by the EM122 multibeam system is a broadband system; by adding a separate low frequency transmitting transducer and electronic cabinets and operator stations, the EM122 can be extended to include the sub-bottom profiling capability, as provided by the SBP120. System beamwidth is 12 degrees with 24 transducers, equivalent to a footprint of 20m in 100 m water depth (or 20% of water depth). The frequency range of the SBP120 is 2.5 to 7 kHz. The SBP120 beam is electronically stabilized for roll and pitch. It can also be steered to take into account bottom slope. The ping rate is synchronized to that of the multibeam

echo sounder transmitter if both are running simultaneously. The data produced by SBP120 are logged in the Topas .raw format and can be converted to SEG-Y format that allows post-processing by standard seismic processing software packages. During ARA04C cruise, we used SBP120 settings as summarized in Table. 5.1.

5.3 Results

5.3.1 Pingo-like structures at "Gary Knolls"

The area of the "Gary Knolls" has not been mapped extensively prior to this Expedition and data obtained provide new insights into the formation and evolution of the Knolls. The Knolls are identical in character to pingo-like features (PLFs) mapped in many locations across the study zone. The zone mapped with multibeam and backscatter (see Chapter 6 for more details) reveals three types of Knolls, or PLFs: (a) individual conical mounds protruding several 10s of meters above the surrounding seafloor with a semi-circular and almost symmetrical moat, (b) individual mounds without a moat, and (c) mounds mostly buried and extending only few meters above the seafloor, covered with laminated sediments (see Chapter 6), but underlain by acoustic wipe-out zones likely PLF-structures that yet not extended to the surface.

5.3.2 Pingo-like structures at shelf edge zone

The shelf edge is a critical boundary for processes related to degrading permafrost. The deep-water laminated sediments are being truncated and pierced at water depth around 100 m to 120 m by conical-shaped pingo-like features (Figure 5.5). These structures, acoustically transparent but with high seafloor backscatter (see Chapter 6) are widespread and cover a zone of approximately 1 km width all around the shelf edge around the 100 m isobath.

5.3.3 Mud volcano in 420 m water depth

As introduced in Chapter 2, several deep water fluid-expulsion features exist in the study zone. Several of these features were inaccessible during the Expedition due to ice cover. However, the feature at 420 m water depth was visited twice for coring, CTD, and heat-flow measurements. The mud volcano is characterized by an almost circular and

flat plateau that shows little seafloor elevation changes. At the western flank, a stack of mud flows are identified as high-amplitude events, covering the otherwise regular laminated sediments. The plateau is acoustically transparent from the presence of free gas, which results in the high backscatter images (see Chapter 6). Free gas is also seen being emitted form the plateau in echosounder data (Figure 5.7) as well as the multibeam water column data (Figure 5.8).

5.3.4 Newly developing mud volcano

During the SBP survey, we crossed over a feature that resembles a newly forming mud volcano (Figure 5.9). The feature has several near-seafloor edifices, as imaged in the SBP and multibeam data (see also Chapter 6 for detailed map). The mud volcanoes (or deep water expulsion features) seen long the study area (introduced in Chapter 2) show more pronounced seafloor elevation, large-scale plateaus, thick stacks of mud flows and degassing at the surface. However, this feature is just forming, as seen by the slight seafloor deformation from mud-intrusions at depth, minor deformation of the overlying strata, with lamination still intact, and only one shallow, near-seafloor deposit of a recent mud flow.

5.3.5 Sub-surface permafrost

The presence of sub-seafloor permafrost and ice-bonded sediments is a critical element of Expedition ARA04C. Using the SBP data, the presence of ice-bonding sediments can be detected by mapping acoustically transparent zones, of little penetration depth of the SBP data (Figure 5.10). The presence of ice in the sediment changes its acoustic properties (higher impedance contrast on top and high energy absorption) and thus the SBP data cannot penetrate deep into the sediment. In zones, where channels or paleo-lakes were present the bottom was not permanently frozen and these zones appear as patches along the SBP profiles, where acoustic penetration of the data is suddenly increased. The SBP data will be post-processed for the occurrence of shallow permafrost and compared to the multichannel seismic data where the presence (or absence) of high-velocity material produces refractions (see Chapter 3 for more details).

5.3.6 Slump-feature

The shelf edge in the western portion of the study zone shows distinct seafloor failures and slump-deposits (see Chapter 2 for a detailed multibeam image). While most of the area was covered by sea ice during the Expedition ARA04C, a few attempts were made to collect data across these features. In total four crossings were made at line-locations filling in the data set acquired in 2012 with the Huntec system, providing valuable additional insights in slump-dynamics and initiation.

5.3.7 IODP pre-proposal #753 coring sites

The deep-water section of the Mackenzie Trough is an interesting study zone for paleontology and reconstruction of the ice-shelf. Although the area is dominated by canyon-topography (compare to Chapter 6 for a multibeam image), the hope was, to core on top of prominent ridges and collect an intact and deep record of Holocene sedimentation. Two core sites were previously defined as part of IODP pre-poposal #753 based on low-resolution bathymetry data and few seismic lines. Therefore, the core-site locations were modified after multibeam mapping and SBP data collection to target the optimal location of laminated and un-deformed sediments.

5.4 Summary

During Expedition ARA04C, more than 3000 line-kilometers of sub-bottom profiler (SBP) data were collected, co-located with multibeam and backscatter data. These data are an essential part of the study of sub-seafloor permafrost distribution and further provide insights into sediment dynamics at critical boundaries, especially the shelf edge. Here, the occurrence of pingo-like features (PLFs) result in a characteristic, rugged landscape with thousands of PLFs piercing through the otherwise laminated sediments. More than 30 crossings of this critical shelf-edge boundary were made during this expedition, with locations specifically chosen to complement data acquired in 2012 with the Huntec system and previous vintage 3.5 kHz data that were provided by ArcticNet as part of the regional multibeam map of the study area. Critical new insights were gained at deep-water fluid expulsion zone, not previously imaged in the detail achieved during Expedition ARA04C. Critical new data was also acquired over the area of the "Gary Knolls", where PLF structures occur at the shelf edge in water depth of only 50 to 60m. All SBP data from this expedition will be post-processed and analyzed for the presence of sub-seafloor permafrost, occurrence of the PLF structures and indications for fluid and gas migration.

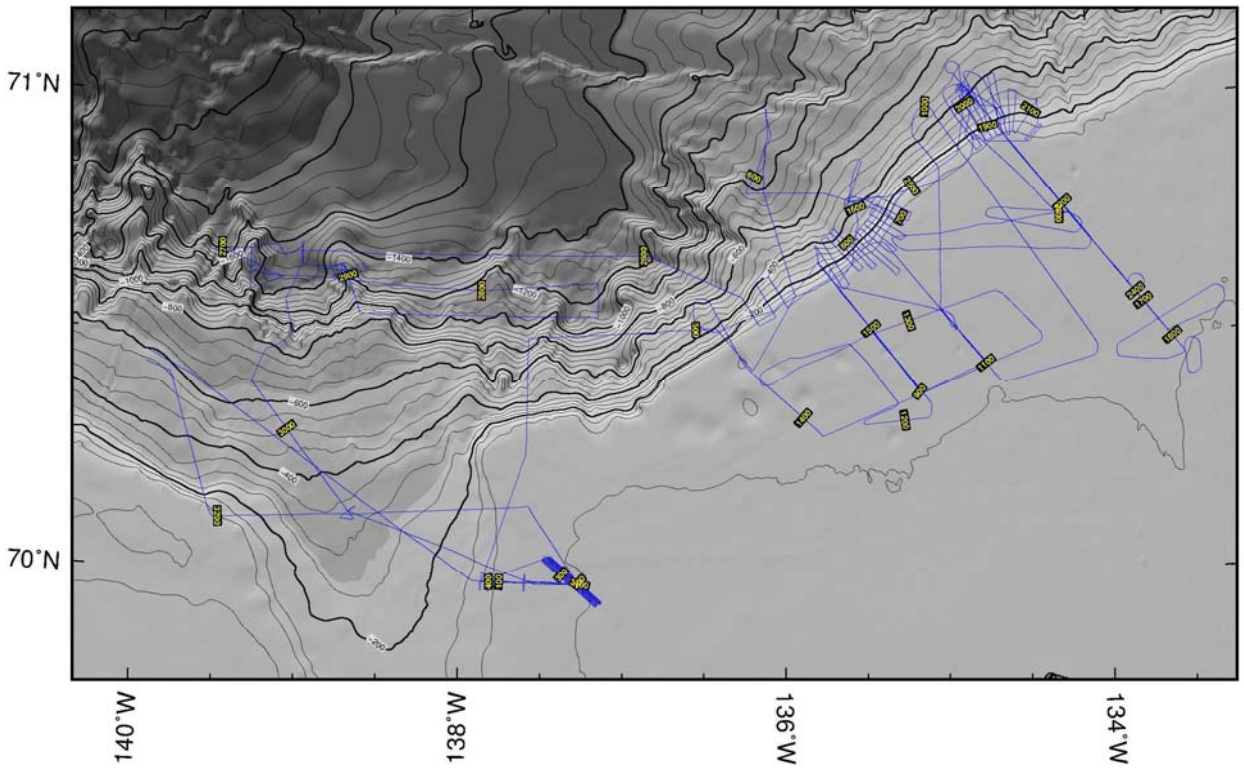

Figure 5.1 Map showing all tracks of the Expedition ARA04C. Total length of the lines is more than 1800 nautical miles (> 3300 km). SBP data were recorded when the vessel moved along survey lines, but was stopped when the vessel stayed for coring, CTD, and heat flow measurements.

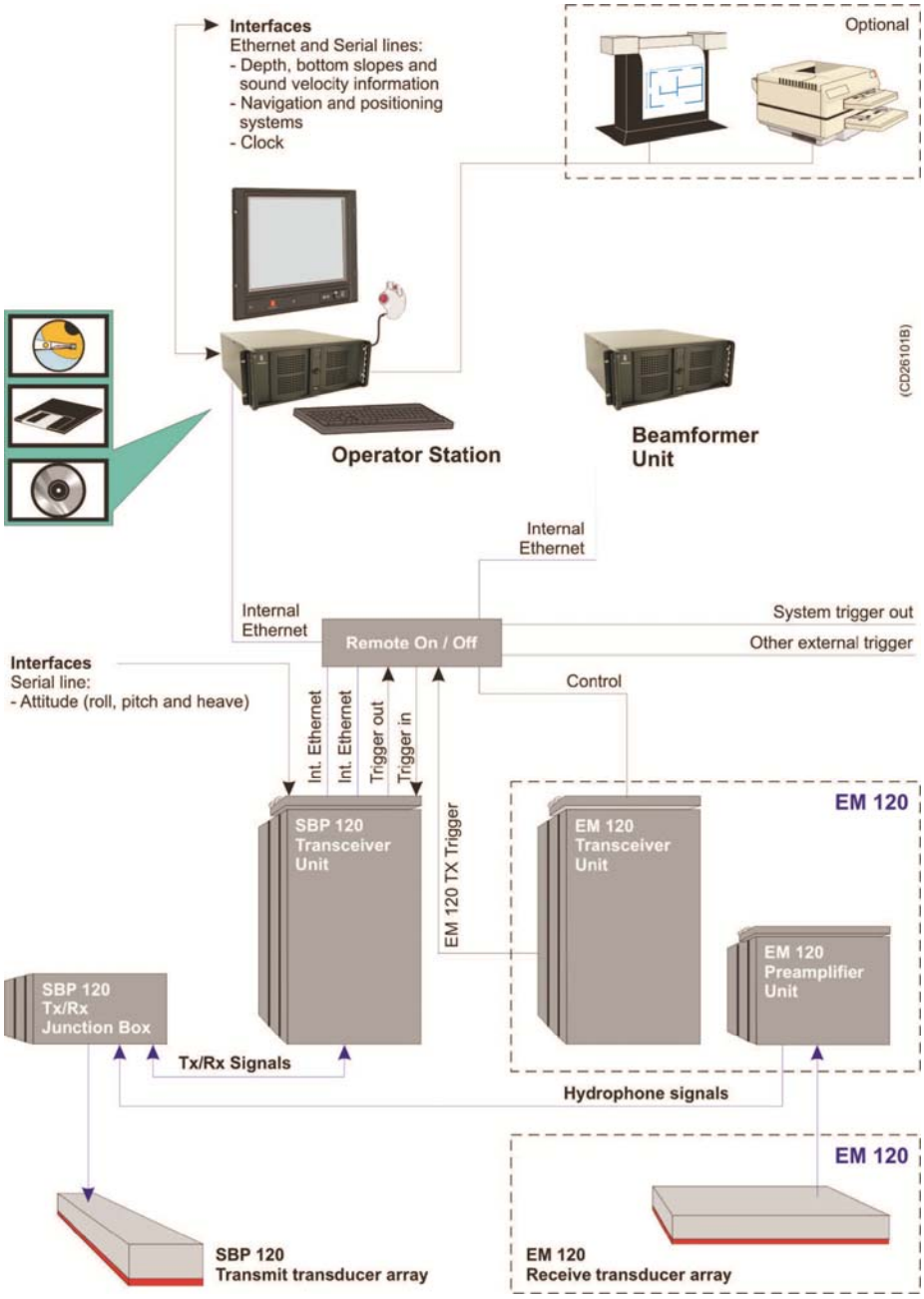

Figure 5.2 SBP 120 system units and interfaces.

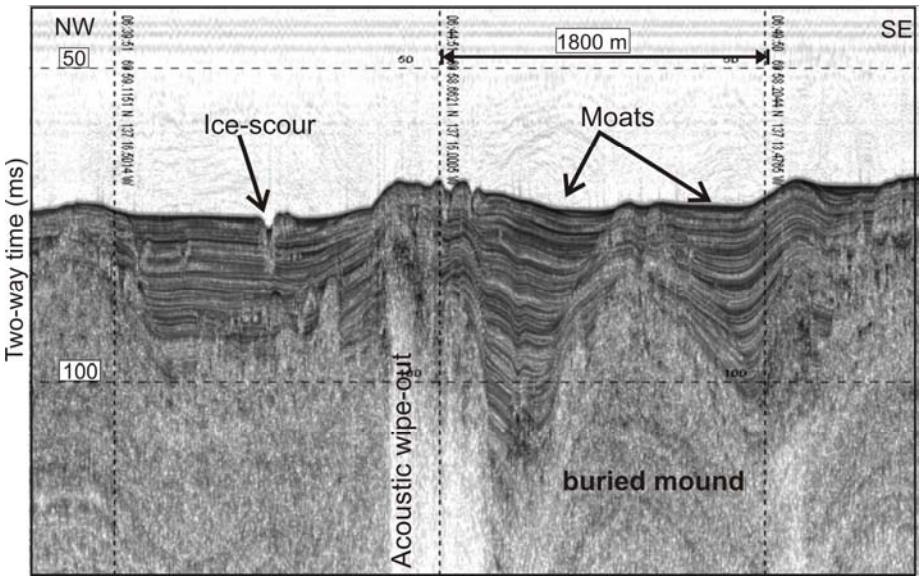

Figure 5.3 Section of 3.5 kHz data across the "Gary Knolls" area showing moats filled with laminated sediments and acoustically transparent "knolls", partially buried or barely outcropping at the seafloor. Vertical scale is in ms two-way time (50 ms markers, equivalent to ~40 m sub-seafloor depth).

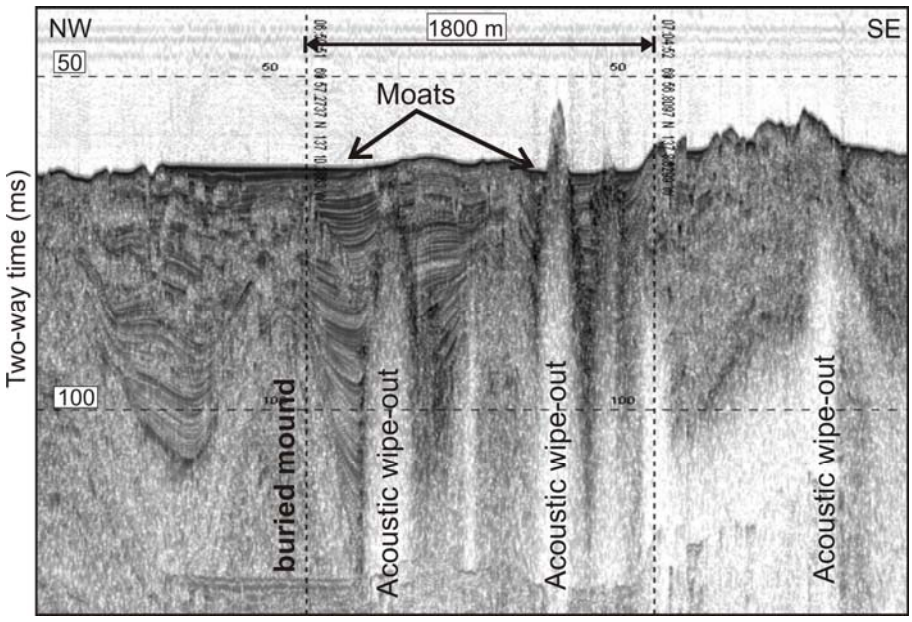

Figure 5.4 Section of 3.5 kHz data across the "Gary Knolls" area showing moats filled with laminated sediments and acoustically transparent "knolls", penetrating through the seafloor. Vertical scale is in ms two-way time (50 ms markers, equivalent to ~40 m sub-seafloor depth).

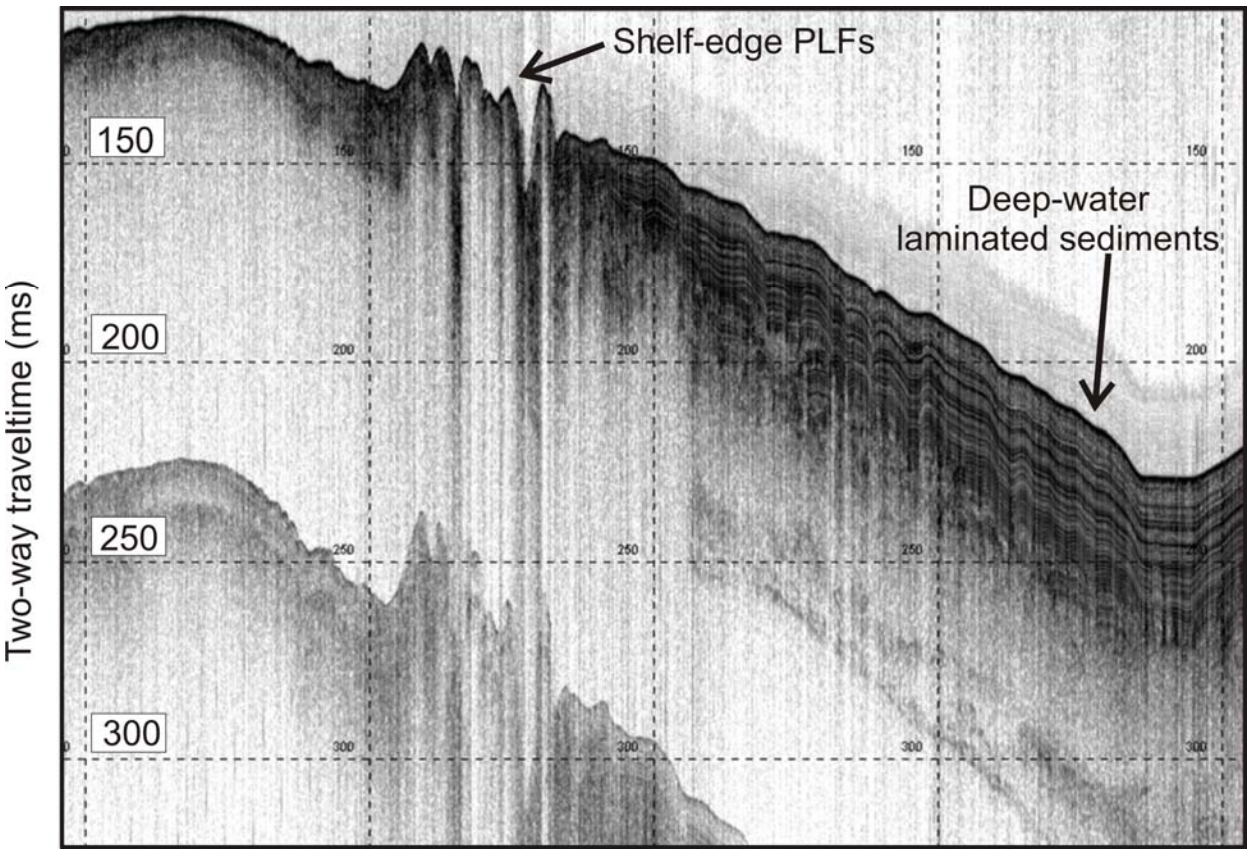

Figure 5.5 Example of SBP data across the shelf edge showing the sudden truncation and piercement of deep water laminated sediments by the pingo-like features (PLFs). Vertical scale is in ms two-way time (50 ms markers, equivalent to ~40 m sub-seafloor depth).

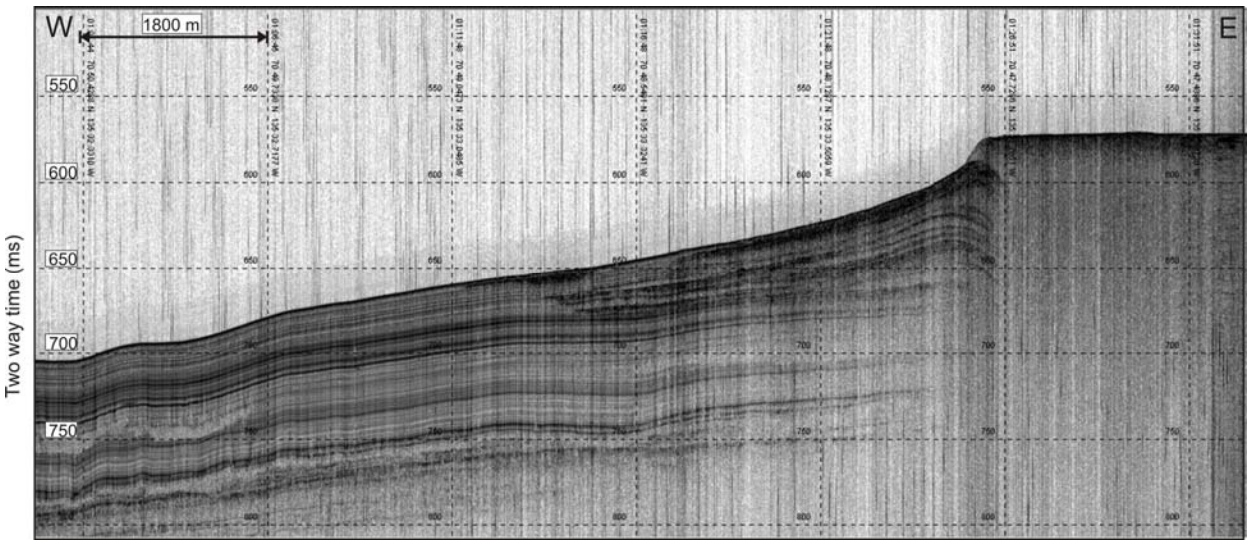

Figure 5.6 Image of sub bottom profiler data from Araon across 420 m mud volcano feature showing a flat-top plateau. Note the stack of mudflows on the western edge of the mud volcano as well as the complete acoustic wipe-out underneath the plateau of the feature caused by the presence of free gas (as seen being emitted from the seafloor, Figure 5.7 and 5.8). Vertical scale is in ms two-way time (50 ms markers, equivalent to ~40 m sub-seafloor depth).

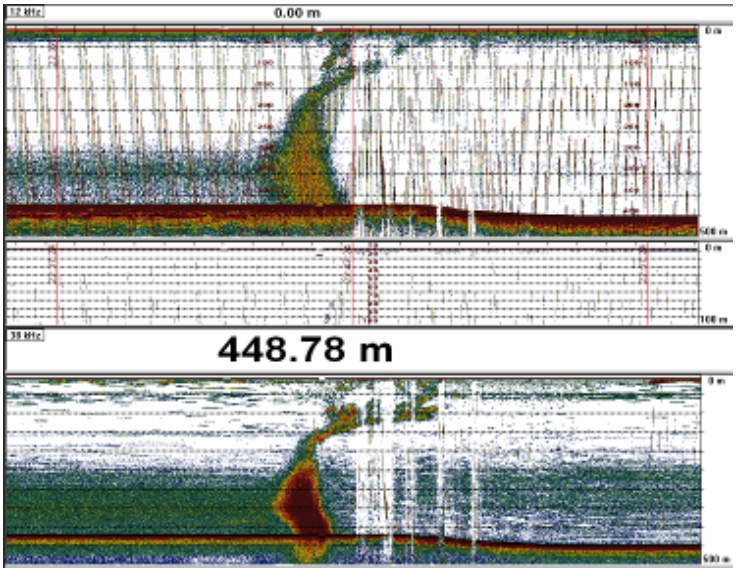

Figure 5.7 Image of the 12 (upper) and 38 kHz (lower) echo sounder across the gas flare of the 420 m mud volcano.

(a)

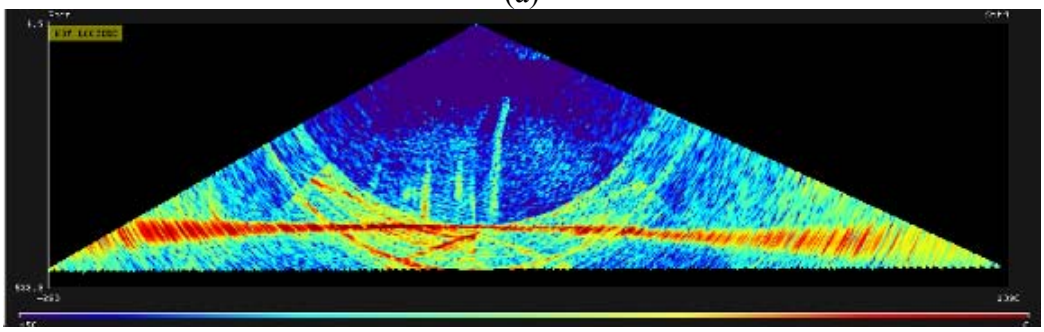

(b)

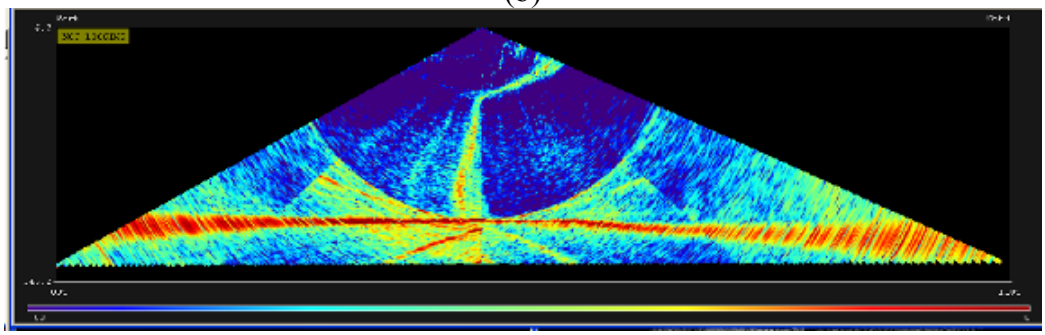

(c)

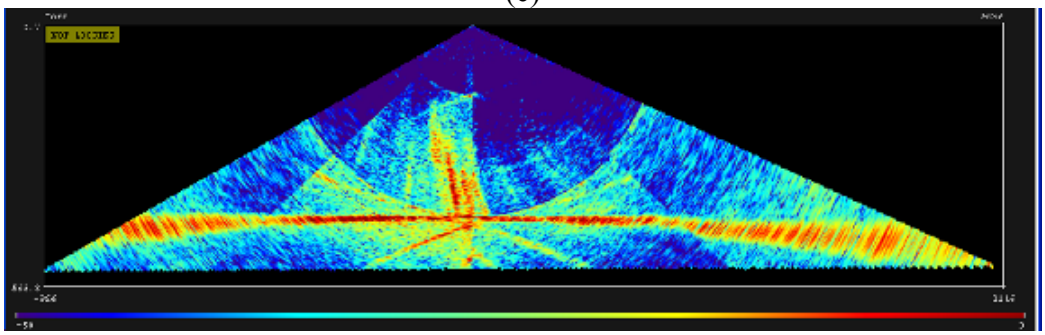

(d)

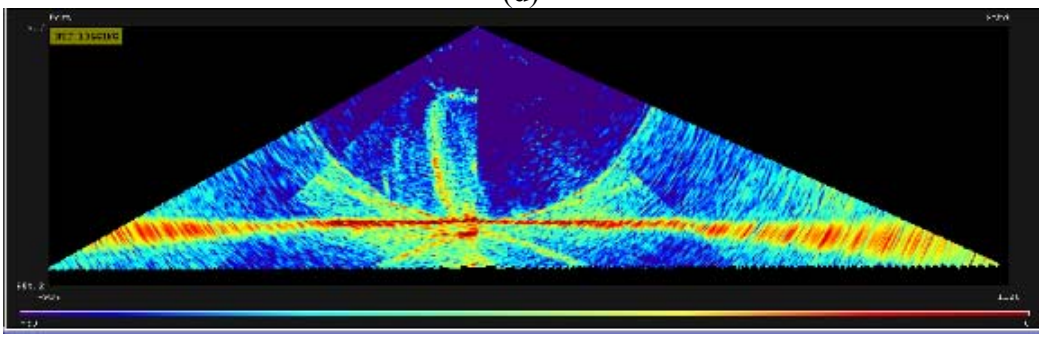

Figure 5.8 (a) - (d): Four images of the gas flare at the 420 m mud volcano from the multibeam water column scan.

(a)

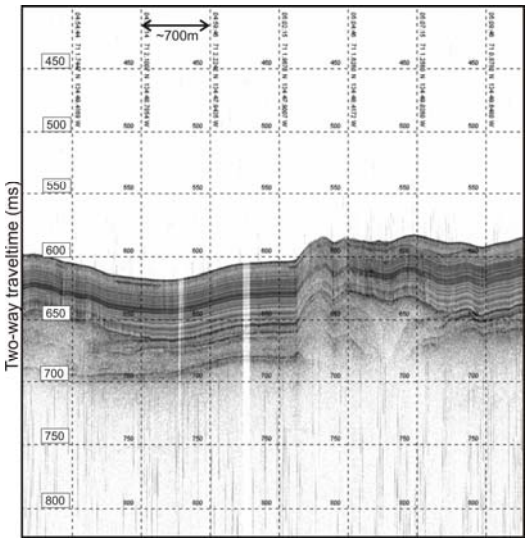

(b)

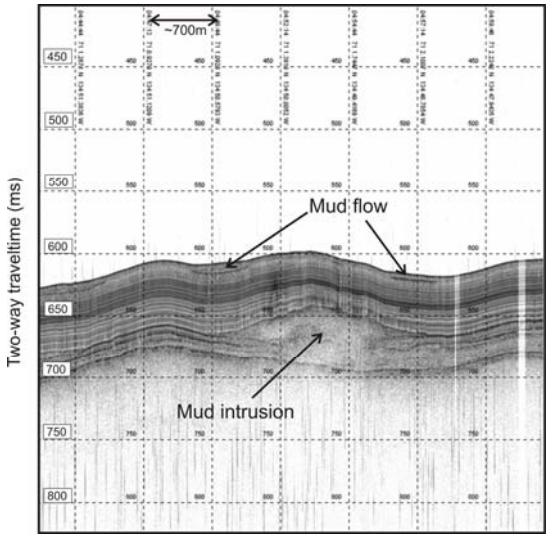

Figure 5.9 (a) section of SBP data across the new mud volcano showing early deformation of the upper-lying stratigraphy, (b) section of SBP data across the new mud volcano showing mud-intrusion at depth and one shallow, near-seafloor mud-flow. Vertical scale is in ms two-way time (50 ms markers, equivalent to ~40 m sub-seafloor depth).

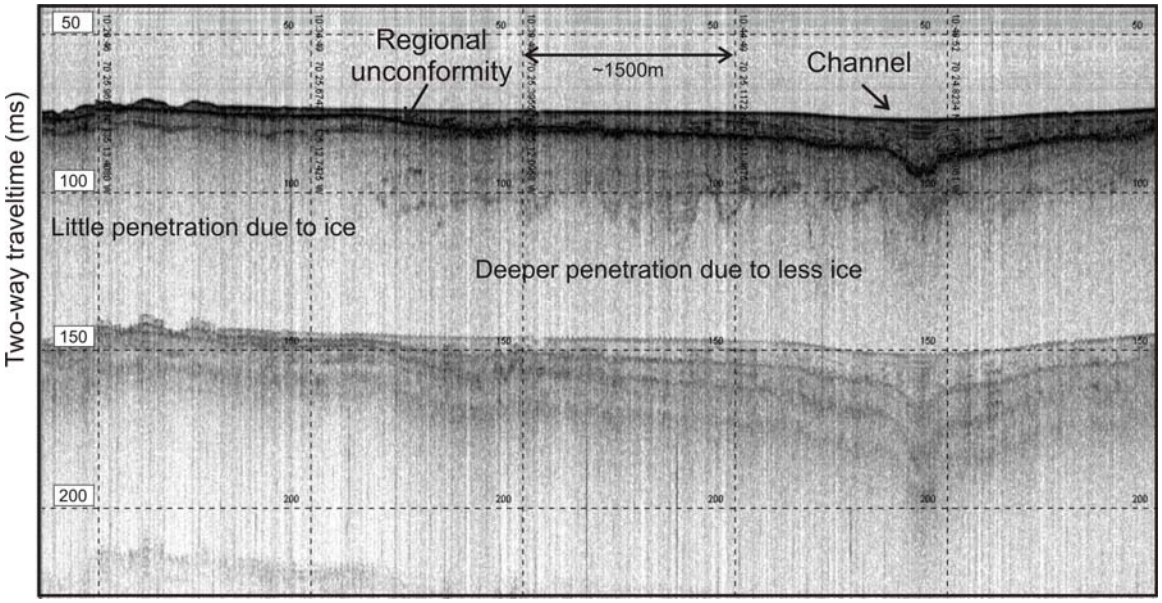

Figure 5.10 Example of SBP data across a portion of the shallow shelf showing zones of permafrost occurrence with little acoustic penetration and zones of a channel, where the bottom was not permanently frozen, and allowing deeper penetration of the SBP data. Vertical scale is in ms two-way time (50 ms markers, equivalent to ~40 m sub-seafloor depth).

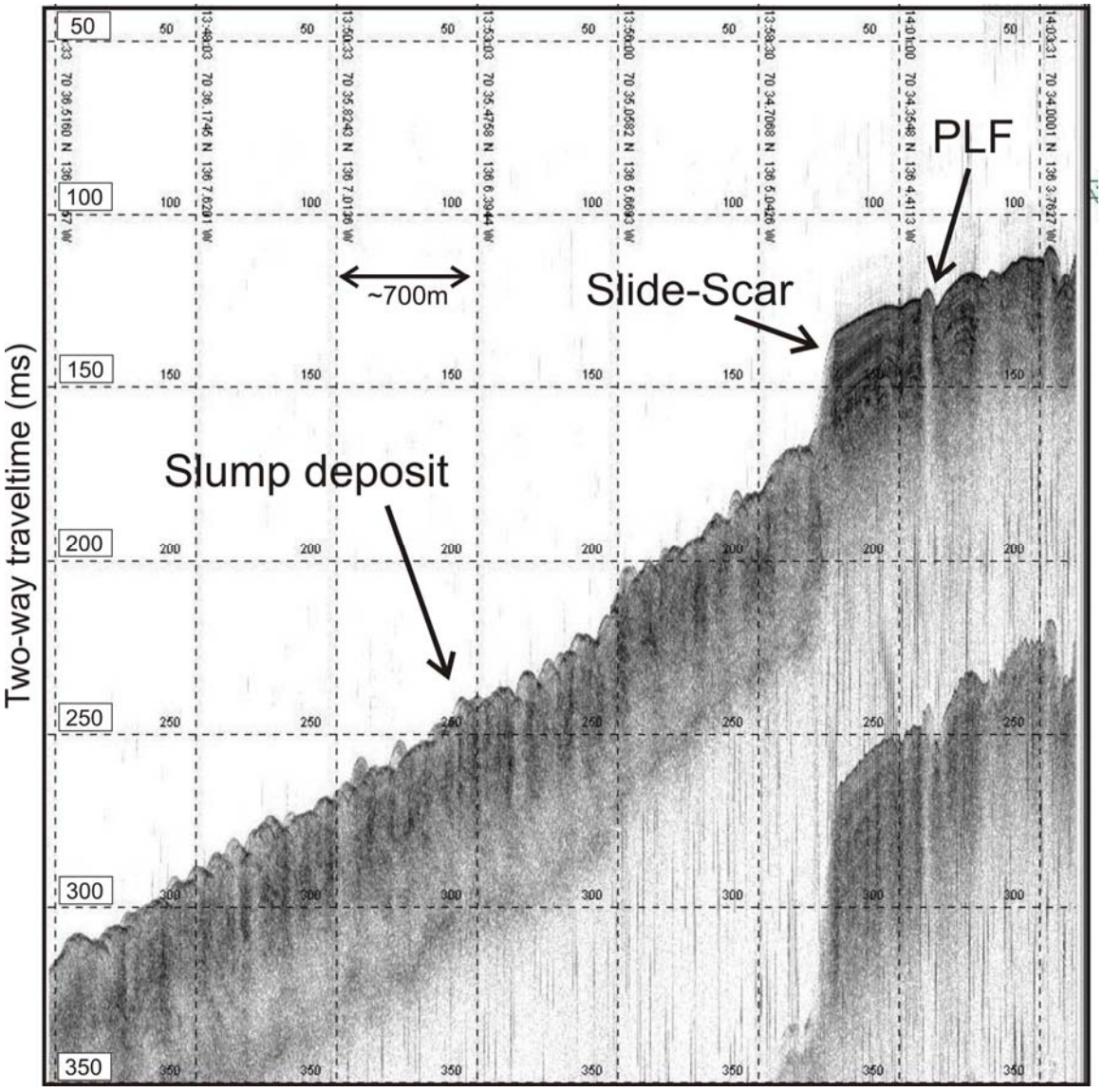

Figure 5.11 Example of SBP data across slump-feature, clearly showing the sharp head-wall scarp abruptly truncating the laminated sediments on the shelf. Vertical scale is in ms two-way time (50 ms markers, equivalent to ~40 m sub-seafloor depth).

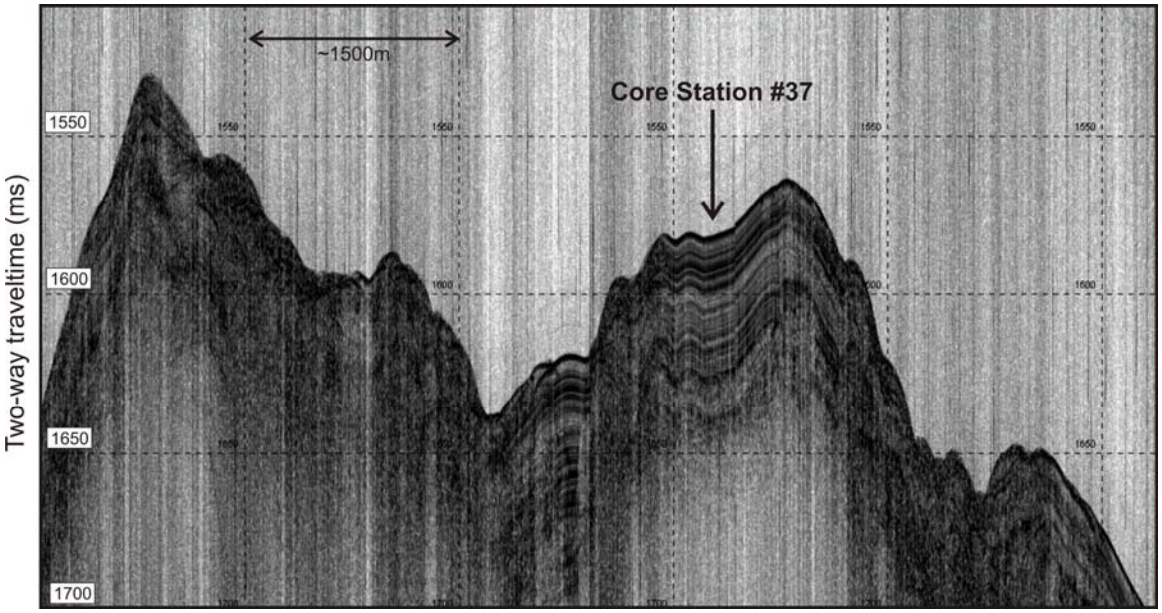

Figure 5.12 Section of SBP data across core station #37, in support of IODP pre-proposal #753. The core site was chosen to target the package of well laminated sediments on top of the western ridge seen in the area (compare to Chapter 6 for a multibeam image of this site). Vertical scale is in ms two-way time (50 ms markers, equivalent to ~40 m sub-seafloor depth).

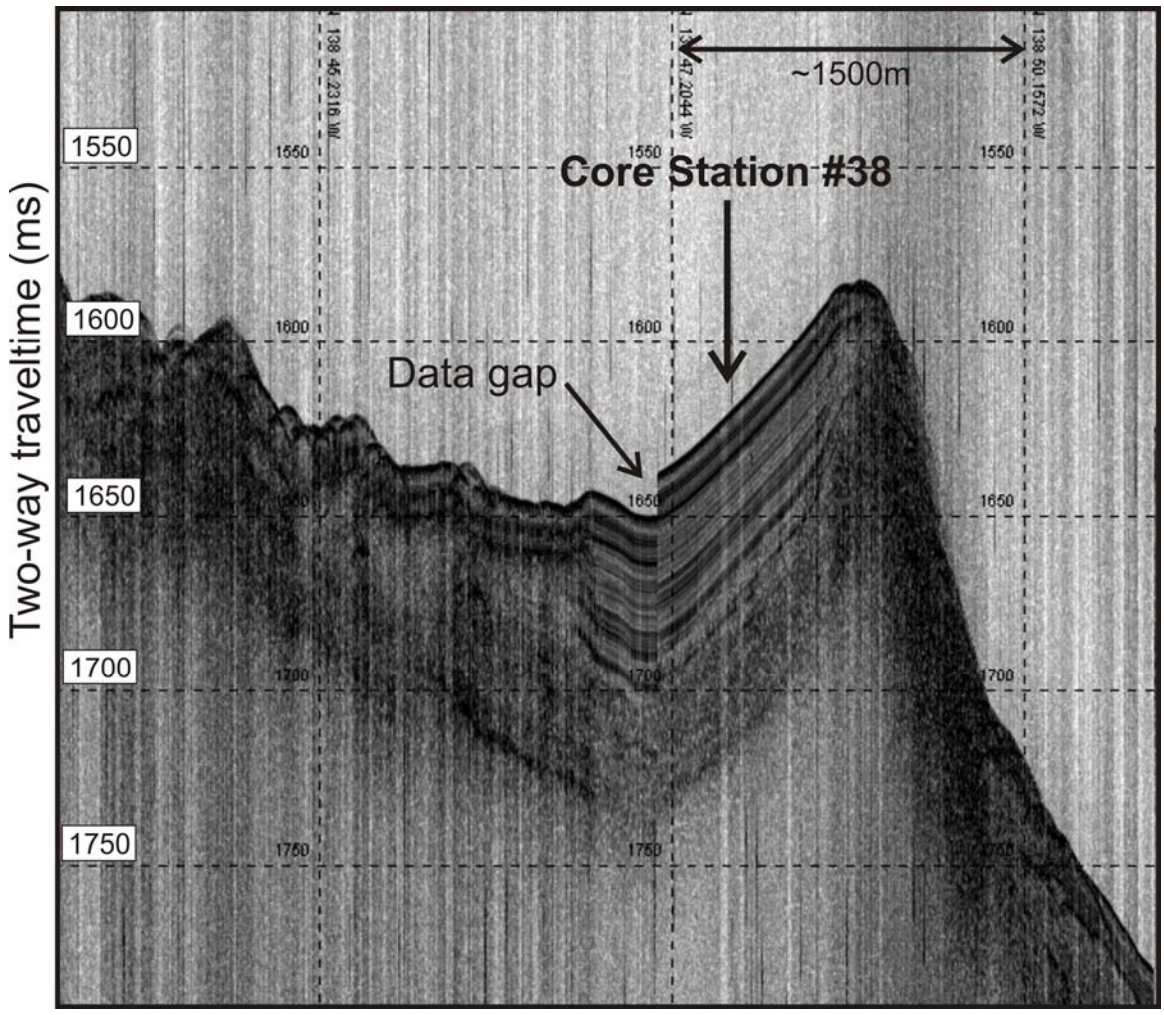

Figure 5.13 Section of SBP data across core station #38, in support of IODP pre-proposal #753. The core site was chosen to target the package of well laminated sediments on top of the western ridge seen in the area (compare to Chapter 6 for a multibeam image of this site). Vertical scale is in ms two-way time (50 ms markers, equivalent to ~40 m sub-seafloor depth).

Table. 5-1: Setting information of SBP 120 during cruise ARA04C.

Used Settings	**Value**	**Unit**
Runtime Parameter		
Transmit mode	normal	
Synchronization	Fixed ping rate	ms
Acquisition delay	Manual & automatic	ms
Acquisition window	400	ms
Pulse form	Linear chirp up	
Sweep low frequency	2500	Hz
Sweep high frequency	6500	Hz
Pulse shape	80	%
Pulse length	30	ms
Source power	0	dB
Beam widths Tx	Normal	
Beam widths Rx	Normal	
Number of Rx beams	1	
Beam spacing	3	1 deg
Calculate delay from depth	X	
Delay hysteresis	30	%
Bottom screen position	50	%
Automatic slope corrections	On	
Gain	36	dB
Bottom tracker		
Window start	40	ms
Window length	20	ms
Threshold	80	%
Time Variable Gain		
TVG control	manual	

Chapter 6 Multibeam survey

J.K. Hong, M. Riedel, H.J. Kim, D.S. Shin, S. Kim, K. Conway, H.K. Choi, Y.-G. Kim, N. Seo, M. Ulmi, H.S. Kim, E.J. Byun

6.1 Introduction

A continuous multibeam survey using the EM122 system was conducted to acquire swath bathymetry and backscatter data during the entire period of the expedition. Vertical sound speed profiles were obtained from CTD casting stations and these velocities were applied to the acquisition system for corrected depth calculations. Acquired bathymetry data were processed onboard using CARIS, a specialized bathymetry-processing software.

The major purpose of the multibeam survey is to aid in the regional bathymetric mapping of the study zone, reveal unknown features not previously mapped, and to confirm specific seafloor morphological features of target areas recognized through earlier studies. Figure 6.1 highlights some areas of where numerous features of interest occur. Processed seafloor bathymetric images were also utilized to determine sites of geological sampling and heat flow measurement. Some of the processed data will also contribute to the international bathymetry data sets (i.e. International Bathymetric Chart of the Arctic Ocean (IBCAO), and General Bathymetric Chart of the Ocean (GEBCO)).

Recording errors occurred during the survey, mainly due to a malfunction of the supporting navigation system (Seapath system). When a navigation error occurred, the water depth can not be calculated correctly. In most cases the navigation error recovered automatically after several minutes, but occasionally a reboot of the navigation system was required, resulting in data gaps of approximately one hour.

6.2 System description

The multibeam system consists of a hull-mounted transmit and receive transducer, a transceiver unit, and an operator station (Figure 6.2). EM122 has a wide beam angle (-70 ~ 70 degrees) and a capability of measuring into the deep ocean. The technical specifications of EM122 are listed at Table. 6.1.

6.3 Preliminary Results

6.3.1 Data acquisition

More than 3000 line-kilometers of survey data were acquired with multibeam and backscatter data. While the seafloor bathymetry data were processed initially onboard for immediate interpretation and cruise-planning, backscatter and multibeam bathymetry data will be re-processed on shore post-cruise. The following sections highlight a few initial results in key areas of interest.

6.3.2 Pingo-like features at the "Gary Knolls"

Most of the "Gary Knolls" area was previously uncharted. Existing multibeam data are sparse, due to the shallow water depth of 50 - 60 m, resulting in a narrow width of the survey swatch mapped by each line. During this cruise, 10 new multi-beam lines, covering an area of approximately 15 km (SE-NW direction) by 2 km (SW-NE direction), were acquired (Figure 6.3). The data reveal a series of pingo-like features (PLFs) with different morphologies. Three types of PLFs can be defined: (a) individual conical mounds protruding several 10s of meters above the surrounding seafloor with a semi-circular and almost symmetrical moat, (b) individual mounds without a moat, and (c) mounds mostly buried and extending only few meters above the seafloor, covered with laminated sediments (see Chapter 5), but underlain by acoustic wipe-out zones. The area covered by the multibeam data also shows numerous ice-scours oriented in various directions. The striations will be analyzed by GSC scientists and incorporated in the ice-scour database for the Mackenzie Trough region (Figure 6.4).

Two coring sites were selected within the area mapped by the new multibeam data, specifically targeting an unconformity at the onset of the "Gary Knolls" (Station 40) and within a broad moat, possibly containing a detailed record of the Holocene

sedimentation (Station 41). These cores will help understand the history of the PLF development.

6.3.3 Mud volcano, 420 m water depth

Prior to the expedition ARA04C, several deep-water fluid expulsion features were identified, mapped and cored (see Chapter 2, Figure 2.7). After the investigation of the northern extent of the ice-margin was complete on September 12, survey lines were chosen to approach the shelf edge zone in preparation for the airgun deployment. While on approach to the deployment site, we surveyed the 420 m mud volcano (Figure 6.5). Its high backscatter return is indicative of the presence of shallow gas in the sediments (Figure 6.6). This feature was revisited twice for heat-flow analyses and gravity coring later in the expedition.

The backscatter image specifically reveals ring-like details of the mound structure representing mud-flow episodes as well as lineations extending from the edge of the mound to deeper water, likely being mud-flows that broke through walls at the edge of the volcano.

Orientation of the image is along the track-path shown in Figure 6.5 (i.e. almost east-west, and water depth generally decreases from bottom to top along the image). The circular nature of mound is clearly visible, but details of the backscatter show ring-structures at the edges of the mound, as well as mud-flows to the bottom of the image (western edge). Note, the abrupt change of backscatter at the upper end of the feature (eastern edge), possibly delineating the extent of mudflows in shallower water. High backscatter values are in white. Horizontal tick marks are in 3 minute intervals (here equivalent to approximately 900 m). Horizontal tick marks are approximately 300 m, given a beam-angle of 60° and 420 m water depth (half-width of swatch is ~700 m).

6.3.4 Shelf edge and slope region

The shelf edge and slope region is a critical boundary for studying the degrading permafrost on the shelf and the onset of the marine gas hydrate regime in deeper water of the slope. As shown in Chapter 2, thermal modeling predicts P-T conditions that would support the occurrence of marine gas hydrate to start at approximately 240 m water depth.

Two sub-regions were imaged in surveys during periods of airgun maintenance on September 12-13, 2013 (Area B, Figure 6.6), and September 19 - 20, 2013 (Area C, Figure 6.7). The multibeam data show the typical nature of the shelf-edge zone with the high abundance of PLFs (Figure 6.8), introduced in Chapter 5 (Figure 5.5). However, the backscatter images reveal interesting structures of these PLFs and their surrounding sediments (Figure 6.9). High backscatter values are seen over the almost circular PLFs themselves, but in many cases, the high backscatter values cover elongated ridges.

The multibeam survey on September 19 - 20, 2013 also covered a small, newly developing mud volcano (see also Chapter 5). The seafloor elevation of the volcano is subtle (Figure 6.10) and is only few tens of meters. Several smaller mounds have developed so far and a small moat around the feature is developing. No degassing was seen at this site and images of the sediments in the sub-bottom profiler show mud intrusions, shallow mud flows and early sediment doming.

6.3.5 IODP 753 site

Area D mapped during this expedition (Figure 6.11) is the location of IODP pre-proposal #753 and is within the Chevron 3D block. This area is in the deep-water (> 1000 m water depth) portion of the Mackenzie Trough. No multibeam bathymetry data have previously been collected in this area. The seafloor is characterized by many canyons and steep ridges with sharp edges. Coring was performed in this area at three sites: Two cores on top of ridges in support of IODP pre-proposal #753 (Stations 37, 38) and one core in the canyon between the two ridges in support of work by Chevron.

6.4. Summary

New multibeam and backscatter data were collected during Expedition ARA04C in key areas of the study zone. These data will help advance the scientific understanding of the degrading permafrost on the shelf and at the shelf edge, the nature of pingo-like features (PLFs), deep-water fluid expulsion zones, and the eastern-shelf of the Mackenzie Trough and its deep-water extension area. Data are of general high quality revealing formerly unknown details, such as the Mackenzie Trough "Gary Knolls" zone with many PLFs and moats, the canyon-type setting of the deep-water Mackenzie Trough, as well as a newly developing mud volcano site.

Post-processing of the backscatter data will be carried out at KOPRI and the GSC after the expedition and will be integrated with the multibeam data.

Table 6.1 Technical specifications of EM 122.

Operating frequency		12 kHz
Depth range		20 – 11000 m
Swath width		6 × Depth, to approx 30 km
Pulse forms		CW and FM chirp
No. of beams		432
Swath profiles per ping		1 or 2
Motion compensation	Yaw	± 10 degrees
	Pitch	± 10 degrees
	Roll	± 15 degrees
Sounding pattern		Equi-distant on bottom/equiangular
Depth resolution of soundings		1 cm
High resolution mode		High Density processing
Sidelobe suppression		-25 dB
Modular design, beamwidth		0.5 to 4 degrees

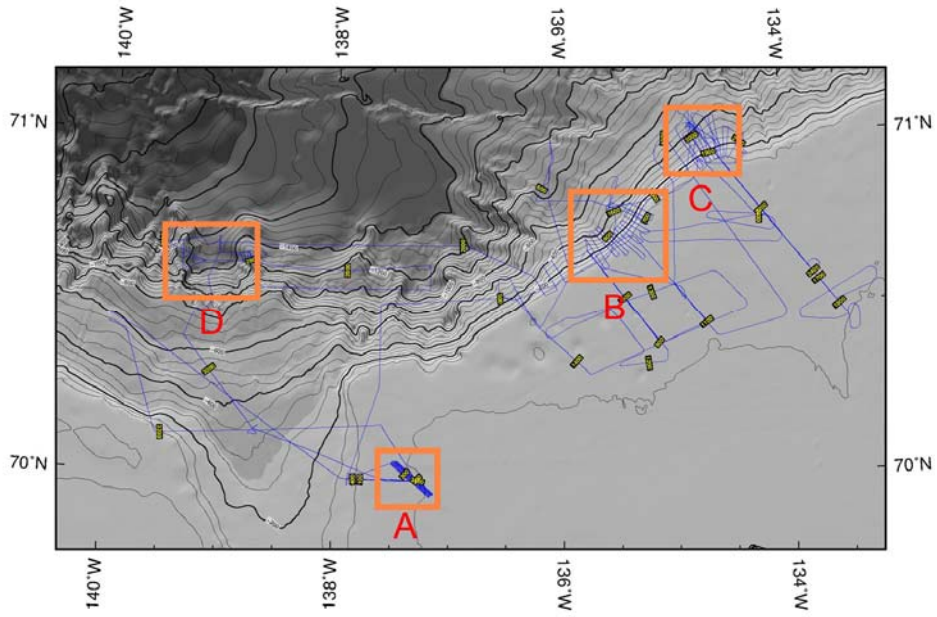

Figure 6.1 Multibeam survey area in the Canadian study zone of the Beaufort Sea. Area A is known for many Pingo-like features (PLFs), also referred to as "Gary Knolls", Areas B and C are at the shelf edge and slope, where many PLFs and fluid expulsion features are observed. Area D is covering two sites for IODP pre-proposal 753 and the Chevron 3D seismic data block.

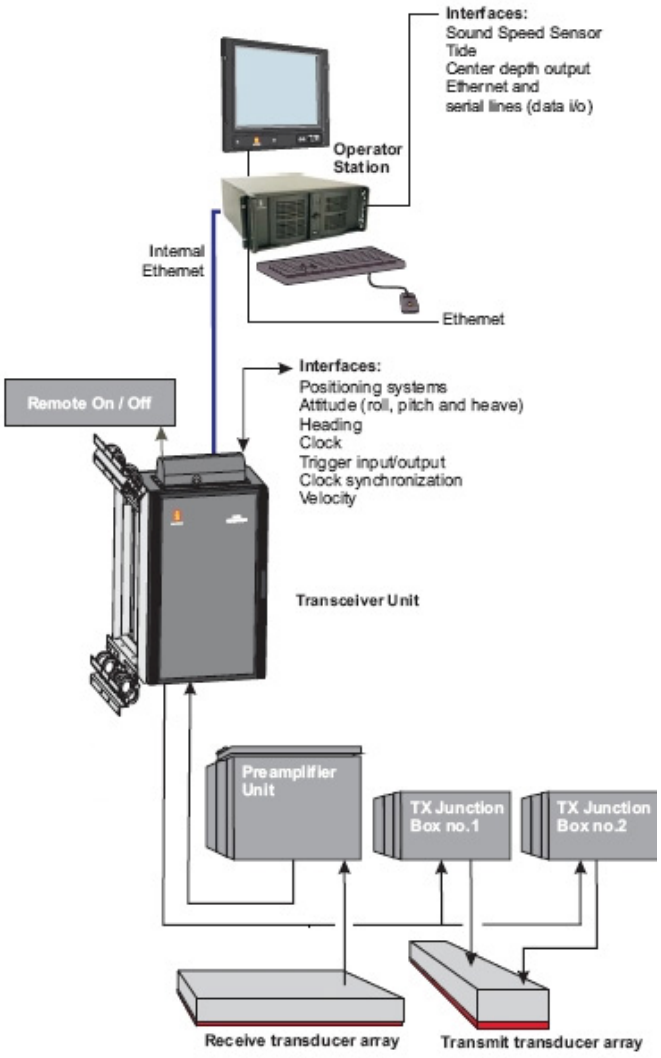

Figure 6.2 System diagram of EM122 multibeam system.

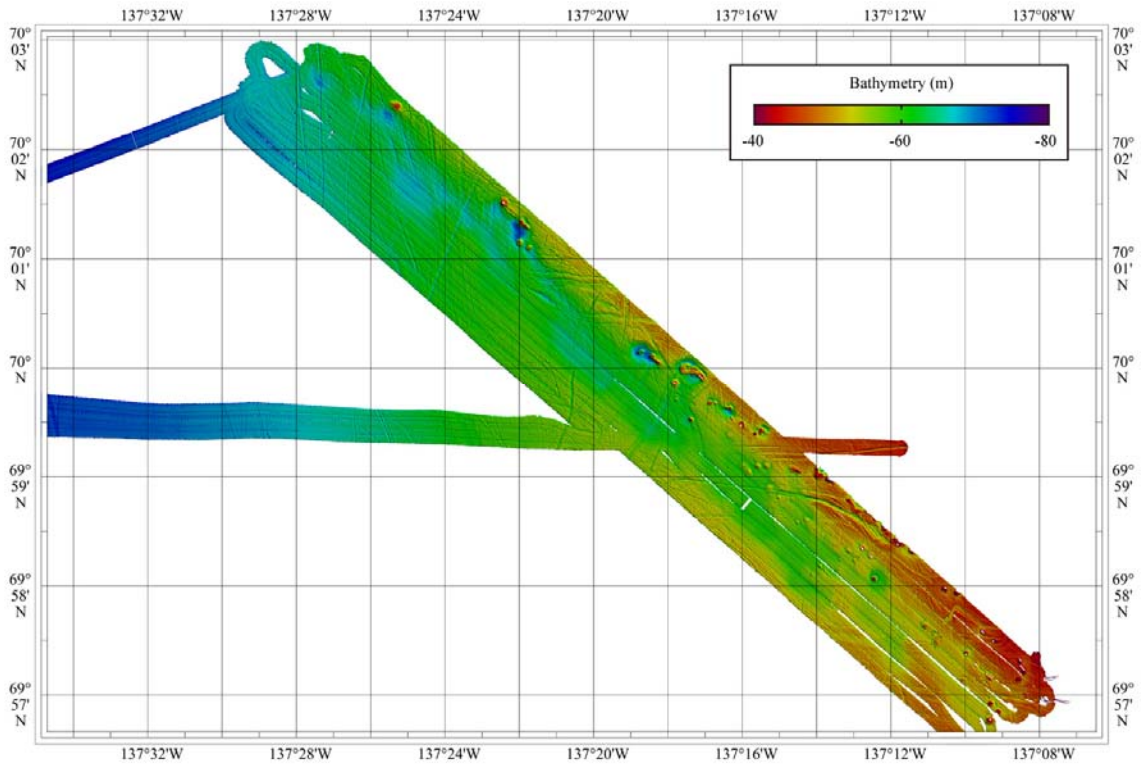

Figure 6.3 Seafloor image showing pingo-like features at the "Gary Knolls" area. The east-west oriented multibeam swatch is along the approach line to the study zone, running over the same coordinates of the 2012 Huntec line. This line is also chosen for a coring transect to study the development of the eastern Mackenzie Trough sedimentation.

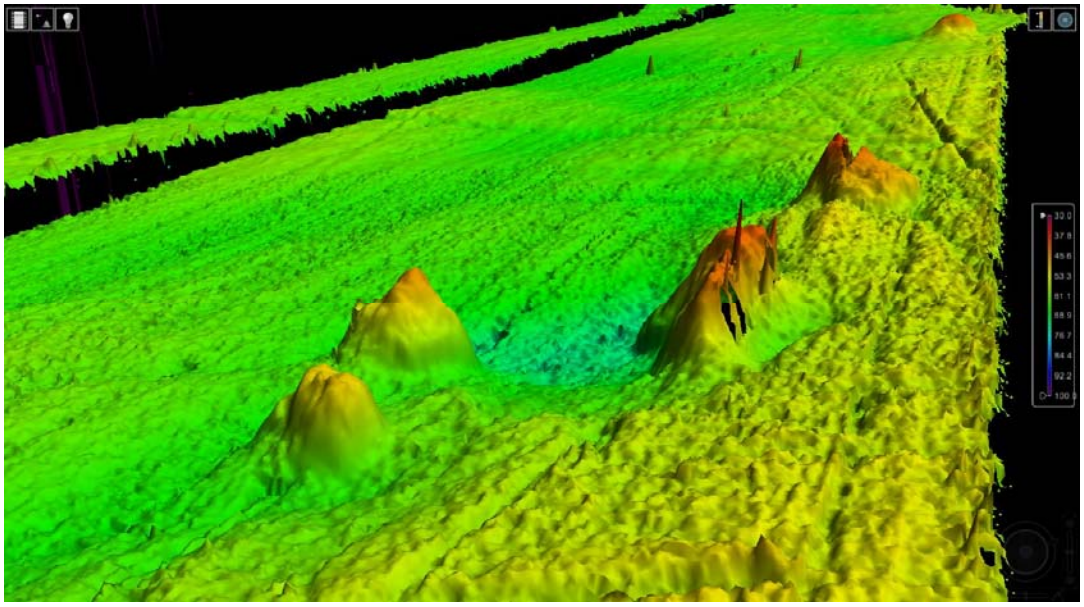

Figure 6.4 Perspective view of the Pingo-like features at "Gary Knolls" showing type-(a) and type-(b) mounds in the foreground (tall mounds with and without moat), and the ice-scoured landscape in the background.

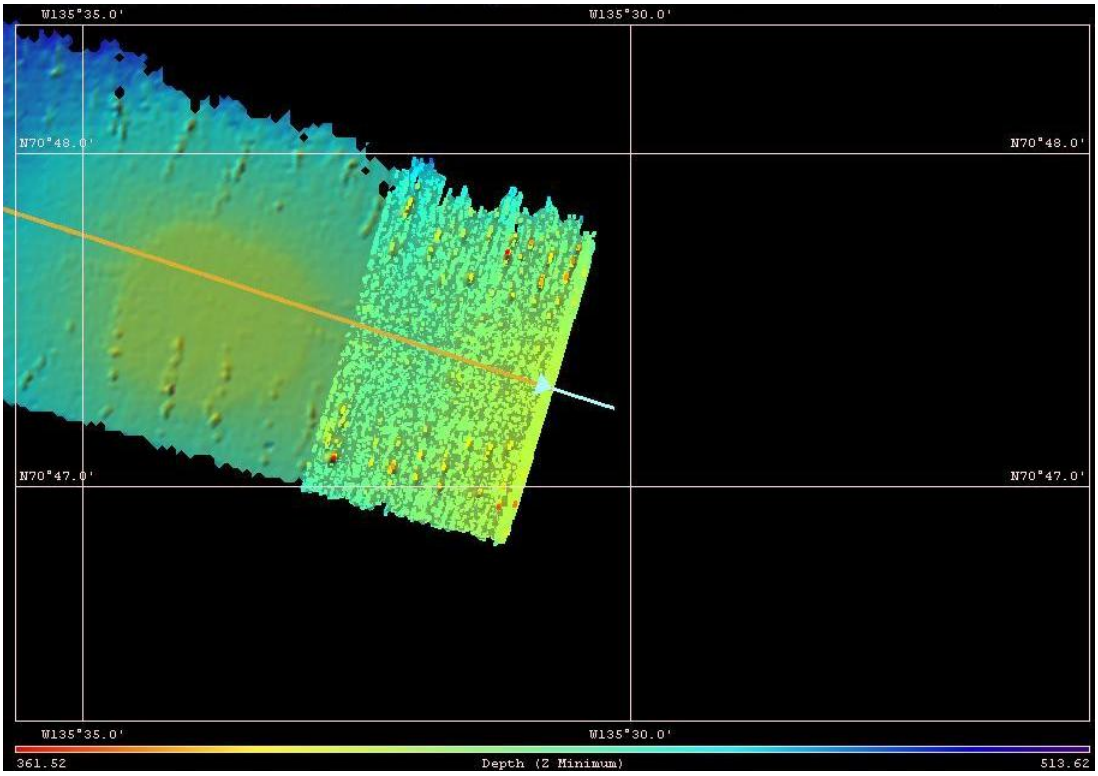

Figure 6.5 Screen image of multibeam bathymetry (un-processed) over the 420 m water-depth mud volcano with a characteristic circular shape. The path of data acquisition is shown as an orange line, with the vessel at the end of the line shown as white triangle.

Figure 6.6 Image of the backscatter over the 420 m water-depth mud volcano. High backscatter values are shown in lighter (grey) color.

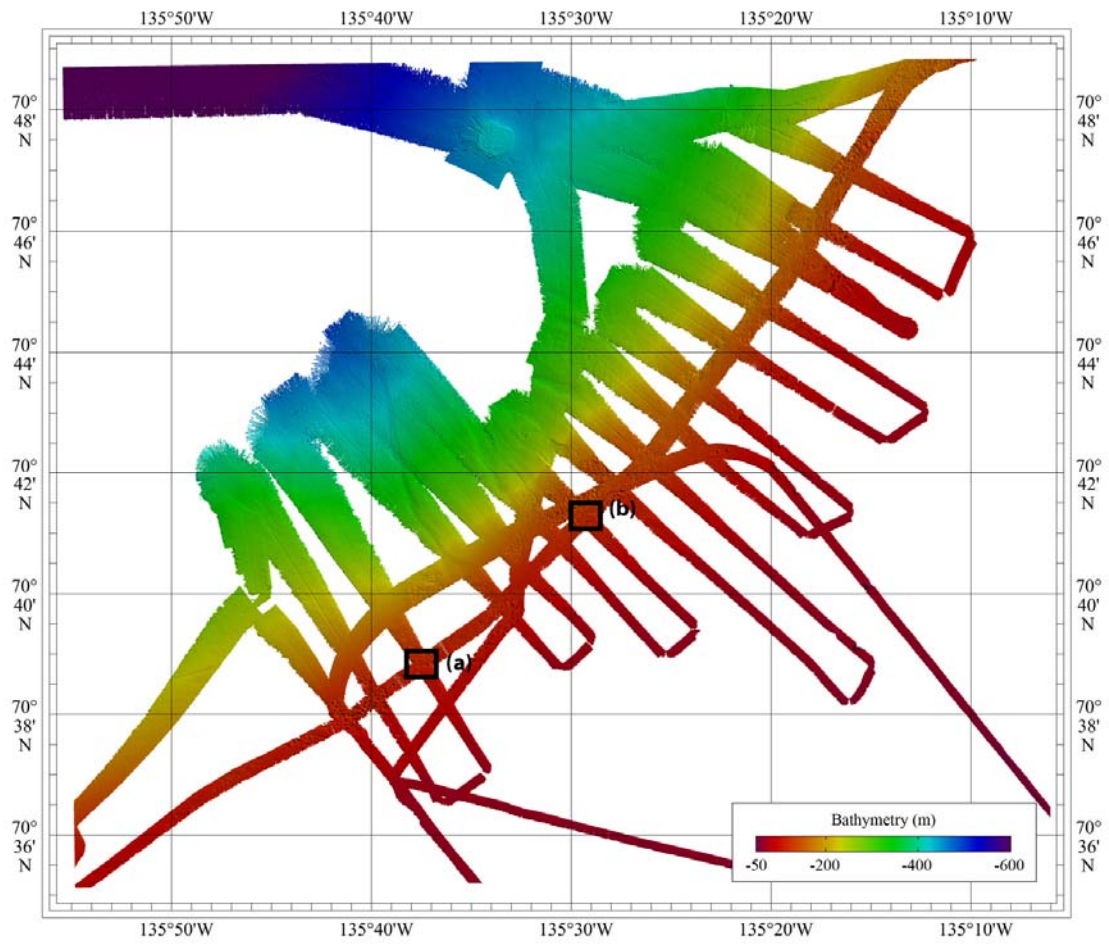

Figure 6.7 Seafloor image of multibeam bathymetry on Area B. Inset shows location of backscatter images of Figure 6.9 (a) and (b). At the northern edge of the image, the 420 m water depth mud volcano can be clearly seen with its characteristic almost circular mound structure.

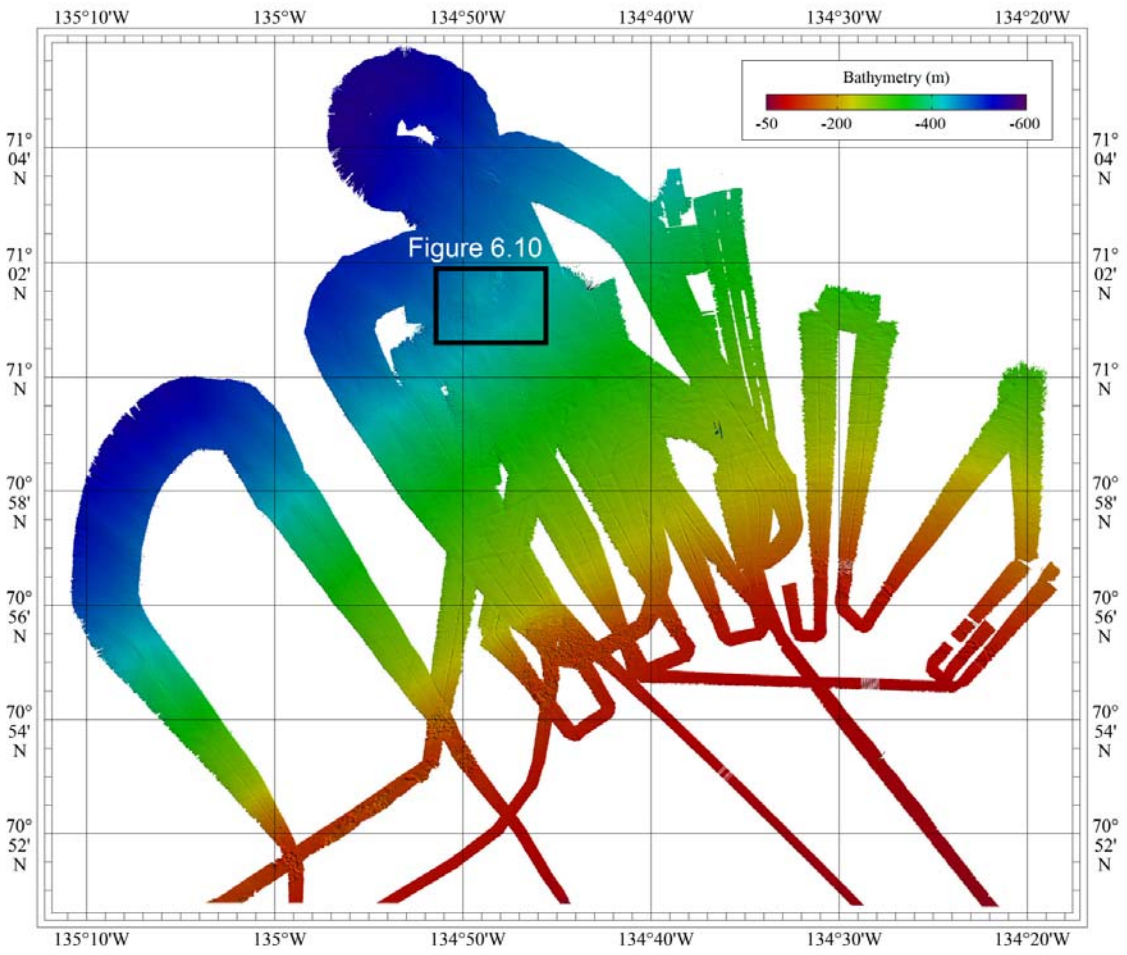

Figure 6.8 Sea floor image of multibeam bathymetry on Area C. The inset shows the location of the newly developing mud volcano (Figure 6.10).

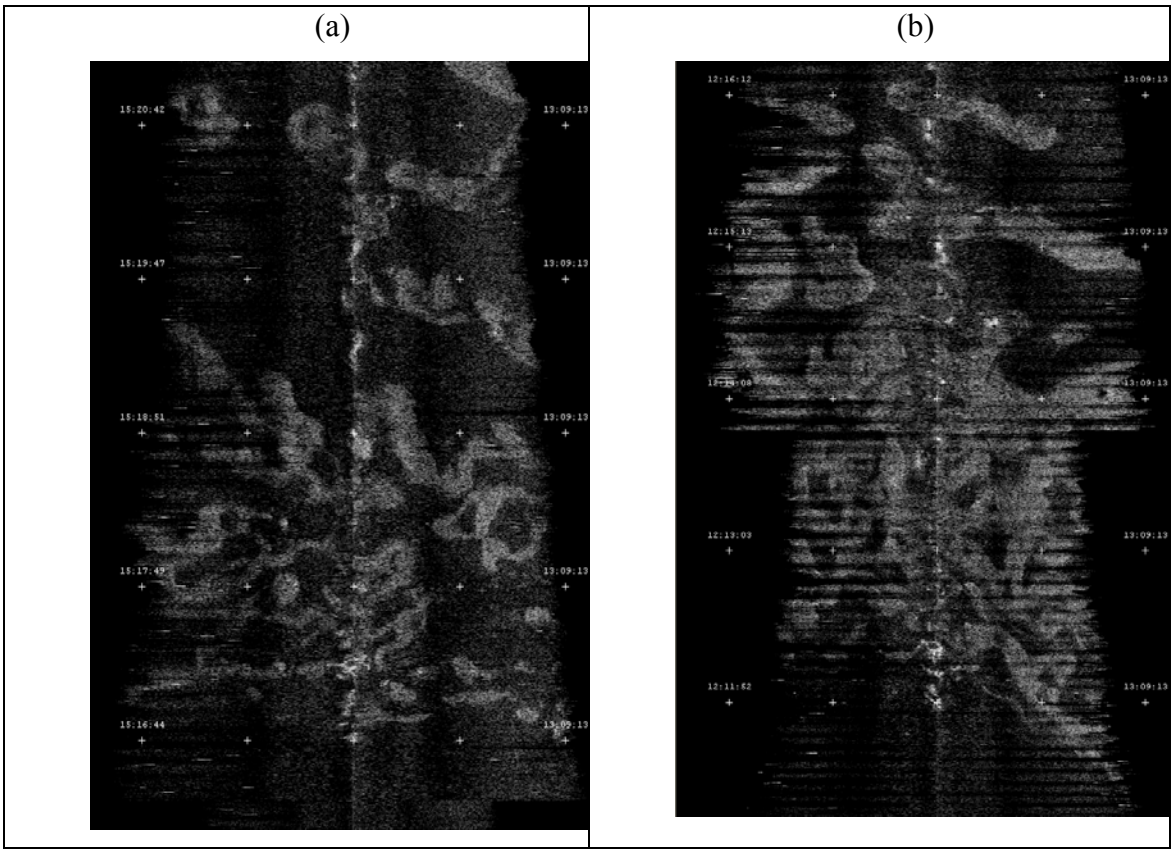

Figure 6.9 Examples of backscatter values across the shelf edge PLF landscape: (a) Image taken at 70°38.8337′N, 135°37.4541′W, (b) Image taken at 70°41.2722′N 135°29.325534′W. Location of these two images is shown in Figure 6.7.

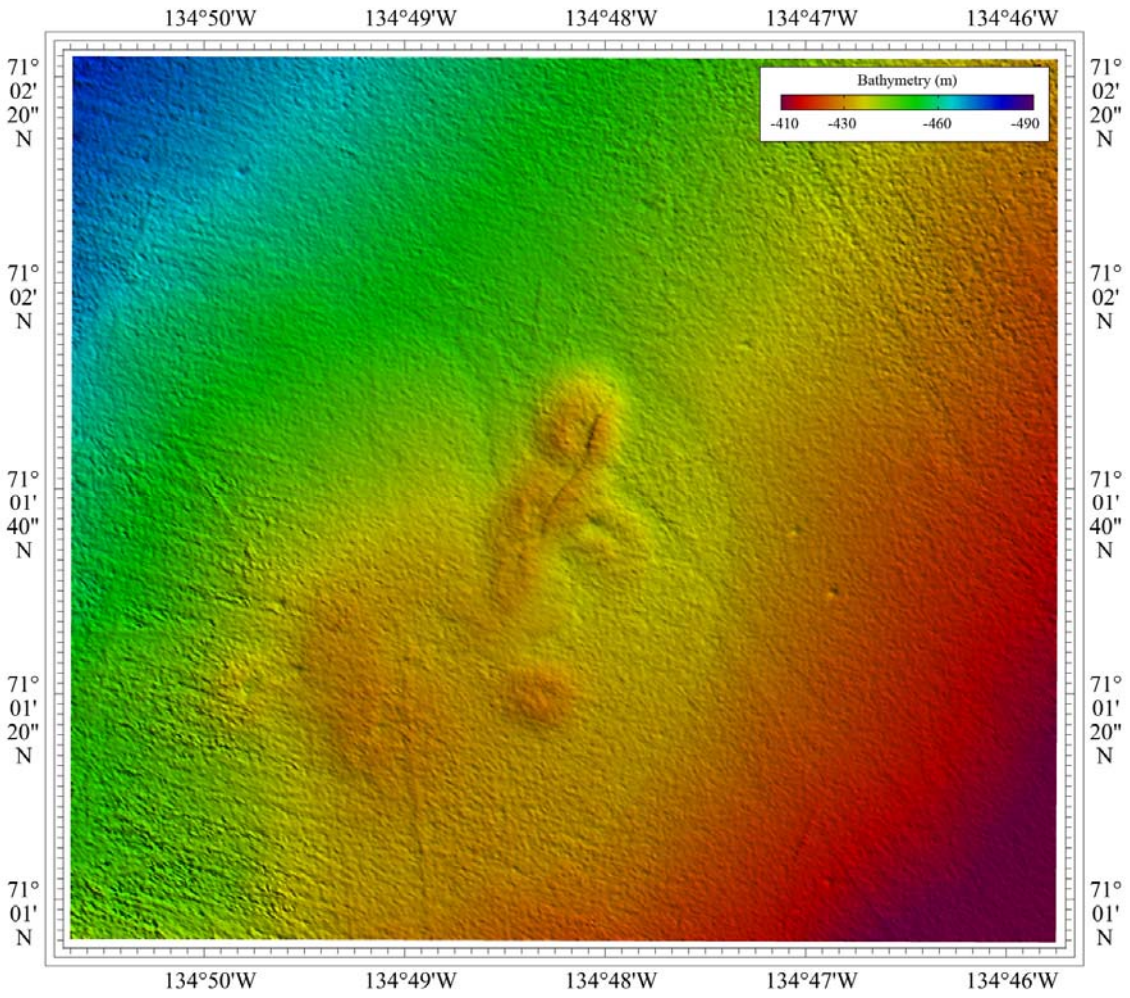

Figure 6.10 Detailed image of the newly developing mud volcano. Many small mound edifices are seen and a shallow moat has started to develop. Sub-seafloor structures from the sub-bottom profiler data are shown in Chapter 5.

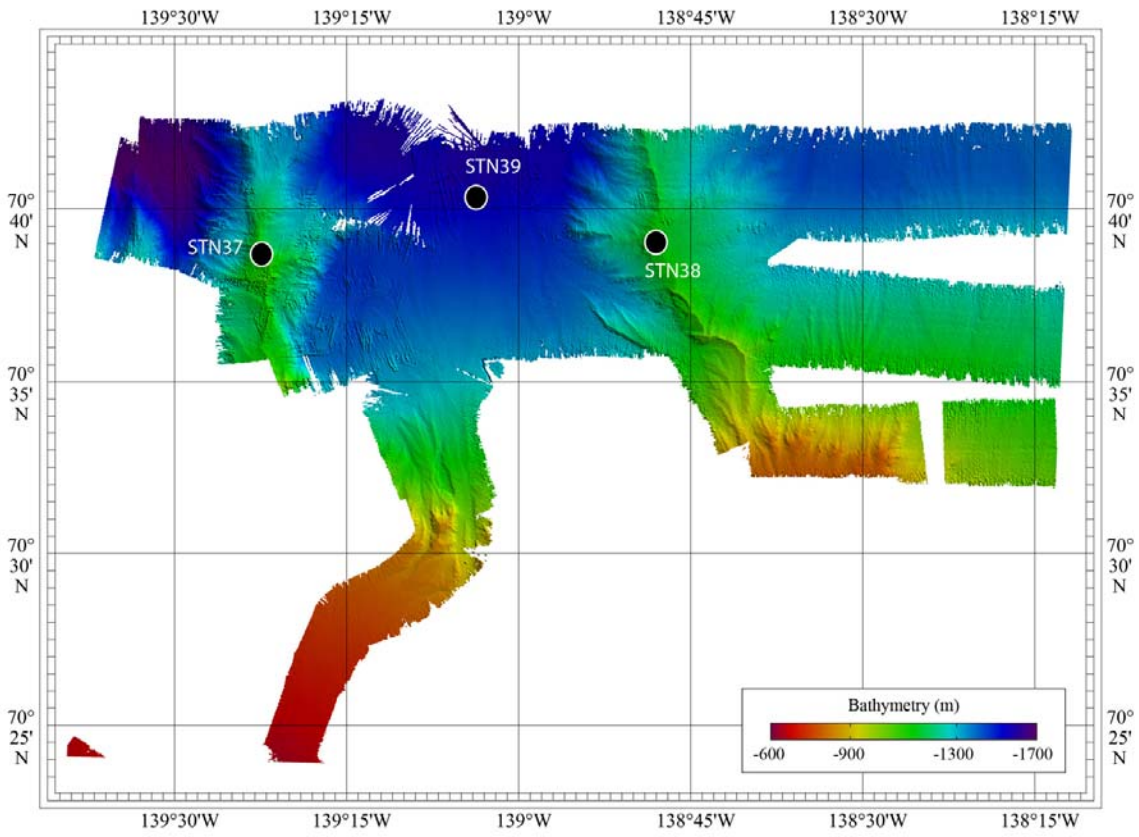

Figure 6.11 Seafloor image in Area D over Chevron 3D block, covering core Stations 37, 38, and 39. Stations 37 and 38 are in support of IODP pre-proposal #753, Station 39 is in support of work by Chevron.

Chapter 7 Heat Flow Measurements

Y.-G. Kim

7.1 Introduction

Regional heat flow distributions are used to understand the thermodynamics of the inner Earth as well as surficial process within sediments (e.g., Von Herzen and Uyeda, 1963). The local heat flow distribution may be useful to unravel surficial process such as fluid expulsion from sediments to sea water, and in the detection of ice within sediments, which is expected to be present within the area of the ARA04C heat flow survey. Furthermore, defining geothermal gradients is a common approach to estimate the extent of the gas hydrate stability zone (e.g. Yamano et al., 1982; Kim et al., 2010). During Expedition ARA04C, heat flow measurements have been carried out at eight stations in the Canadian Beaufort Sea (Table 7.1; Figure 7.1), ranging from the shallow waters of the shelf to the deep waters on the edge of the continental shelf. Five heat flow stations were located along a west-east transect at the eastern Mackenzie Trough, two stations were used to investigate heat flow at a mud volcano, and one station was located at a deep water site serving as regional reference.

In this heat flow survey, a Ewing-type heat probe was used to measure in-situ thermal conductivity as well as geothermal gradients with a single penetration of the probe into the sediments (Table 7.2; Figure 7.2a and b). The probe has been used at two research study site around Japan and Korea (e.g., Yamano et al., 2008; Kim et al., 2010), but this survey is the first use of the tool in Polar Regions. Operation in the Beaufort Sea during Expedition ARA04C was challenging due to extremely cold air/water temperature, sea ice, and "sticky" sediments. However, the experiences gained during this work showed that the heat probe is fully suitable for polar environments.

In order to prevent the probe from damage and to ensure the acquisition of reliable data, careful site selection is required. Use of the sub-bottom profiler data obtained prior to any deployment, and use of the dynamic positioning system of the vessel to maintain station-position during the measurement period (typically 1 hour) are

key elements to obtaining good quality data. The IBRV Araon fully satisfies these conditions with providing high quality sub-bottom profiler data (e.g., Figure 7.1a to c) and dynamic positioning with less than a few meters deviation from the intended location during the heat flow survey. In particular, the dynamic positioning system allows measurements at quite shallow water depth of ~60 meter.

7.2 Methodology

Marine heat flow is determined by two physical properties: geothermal gradient within a sediment section and thermal conductivity of sediments penetrated. Marine heat flow is observed mainly by using a heat probe which consists of frame (weight and barrel) and electrical parts (sensors, data logger, and thermistors) for the top-most several meters below the seafloor. In general, the data logger containing several kinds of sensor is inserted into the top-weight, and thermistors are attached to the core barrel and connected below the top-weight. Thus, deployment of the heat probe is very similar to that of gravity corer.

The Ewing-type heat probe used during Expedition ARA04C has an ability to measure the geothermal gradient and in-situ thermal conductivity simultaneously (Figure 7.2a and b). To accomplish this, heat-generating thermistors as well as passive thermistors are attached on the barrel. The probe has nine thermistor channels in total, with three heating channels and a maximum six passive thermistors. In-situ thermal conductivity is determined based on the speed of heat dissipation on temperature-time curves after a given amount of heat is provided, which is known as the transient method (Von Herzen and Maxwell, 1959; Carslaw and Jaeger, 1959). Shock and tilt sensors are used to determine appropriate tool-conditions to generate heat after penetration of the probe into the sediments (Table 7.2). In addition, a pinger and transponder are used to accurately determine the position of the probe in the water column (Figure 7.2a).

The standard procedure to calculate marine heat flow using the Ewing-type probe is as follows: deployment of the probe after setup (Figure 7.2c and d), standby for 10 minutes at several tens of meters above the seafloor, penetration of the probe into the seafloor, standby for 20 minutes after penetration of the probe into sediments, pull-out and standby for 5 minutes in the water above seafloor, and re-insertion and standby for 15

minutes in the sediments, final removal of the tool and data retrieval from the data logger via RS-232 to a PC.

Two measurements are carried out at each station (Depth in Figure 7.3 upper panel) to increase reliability of the measurements. The raw data observed at the thermistors are transformed into temperature values based on the individual thermistor-calibration functions. The data are quality controlled by screening for erroneous temperature (i.e. resistance) data using simultaneous change of both tension and tilt, and general data trends (Figure 7.3 upper panel). The geothermal gradient and in-situ thermal conductivity are then calculated from the temperature-time curves.

7.3 Results

7.3.1 Stations visited during the expedition

Heat flow measurements were carried out at eight stations during Expedition ARA04C (Table 7.1). The heat flow stations were chosen to understand local heat flow variations where a change stemming from the subsurface geologic feature is expected over short lateral distances. Five stations, (St. 40, 11, 10, 09 and 08 from deep to shallower water depths) were occupied along the transect across the eastern Mackenzie Trough. Laminated sediment layers in deeper water become more disrupted or acoustically obscured (transparent) toward shallower water depths by progressive occurrences of ice and/or free gas. Stations 12 and 28 are located in- and outside the mud volcano at 420-m water depth, where fluid and gas emissions from sediments into the seawater occur (Figure 7.1b and c). On the plateau of the mud volcano, a strong gas flare is acoustically observed by the EA600 echo sounder and high methane concentrations in water samples collected closed to the top of the mud volcano were measured. Station 39, located in the central Mackenzie trough region in ~1500 m water depth, is chosen as a reference site for the survey area in general.

Preliminary results from Stations 12, 28, and 39 are presented in this report. A comparison of the three sites clearly supports that fluid expulsion occurs at the mud volcano.

7.3.2 Resistance-time curves

Using a simple linear relationship to resistance, raw data observed from thermistors are first transformed into resistance prior to yielding temperature. On the plot of resistance with time, erroneous curves (dashed lines in Figure 7.3 lower panel) are screened based on the methodology described above. Particularly, curves having irregularities over the period of penetration of the probe into sediments are excluded from the analysis. The tool penetration into the sediment can easily be detected from a depth-time curve. At the three stations chosen in this report a minimum of four data points are available, which is sufficient for a linear regression analysis to yield geothermal gradients (see also Table 7.1). Since the thermistors yield higher resistance with colder temperatures, the resistance axis is reversed to resemble a conventional temperature-scheme. The relative change of resistance prior to and after the penetration is a direct proxy for the temperatures. Post-processing of the data and conversion from resistance to temperature will be done onshore, after the calibration functions for each thermistor have been obtained

The change of thermistor resistance prior to and after the penetration at Station 12 (inside mud volcano), where it is expected that fluid expulsion occurs, is much larger than those at Station 28 and 39 where no expulsion is expected to occur. This is interpreted as evidence for heat convection in the mud volcano, where heat is transported from depth with the mud-extrusions at a speed faster than heat is conducted away, thus leading to higher subsurface temperature but lower geothermal gradients (i.e. more uniform temperature-versus-depth profiles) as suggested by Kim et al. (2013).

It also appears that fluid emitted from the top of the mud volcano has a higher temperature than anywhere else measured in the surrounding water at an equivalent depth. However, it is still uncertain whether this phenomenon is also detected on the CTD data (Figure 7.4). This is partly caused by the fact that the CTD tool was stopped at too high depth above the seafloor (typically 8-10 m above the seafloor), and partly because the flux is too weak to significantly change the surrounding water temperature. During future research programs, lowering the CTD tool nearer to the seafloor to study the fluid flux impact ion seawater may be useful or using an AUV or ROV to acquire temperature data near the seafloor.

7.4 Summary

During Expedition ARA04C, heat flow surveys using the Ewing-type heat probe were carried out successfully at eight stations. Analysis on preliminary results from Station 12 (at the mud volcano in 520 m water depth), Station 28 (outside the mud volcano), and at Station 39 (deepest water depth of ~1500 m) supports the hypothesis that fluid emission from sediments to seawater at the top of the mud volcano occurs. However, at this stage, magnitude of the fluid flux is not certain.

References

Carslaw, H. S., Jaeger, J. C., 1959. Conduction of heat in solid, 2nd edition, Claredon Press, 510p.

Kim, Y.-G., Lee, S.-M., Matsubayashi, O., 2010. New heat flow measurements in the Ulleung Basin, East Sea (Sea of Japan): relationship to local BSR depth, and implications for regional heat flow distribution, Geo-Marine Letters, 30, 595-603.

Kim, Y.-G., Lee, S.-M., Jin, Y.K., Baranov, B., Obzhirov, A., Salomatin, A., Shoji, H., 2013. The stability of gas hydrate field in the northeastern continental slope of Sakhalin Island, Sea of Okhotsk, as inferred from analysis of heat flow data and its implications for slope failures, Marine and Petroleum Geology, 45, 198-207.

Von Herzen, R. P., Uyeda, S., 1963. Heat flow through the Eastern Pacific Ocean floor, Journal of Geophysical Research, 68, 4219-4250.

Von Herzen, R. P., Maxwell, A. E., 1959. The measurement of Thermal Conductivity of Deep-Sea Sediments by a Needle-Probe Method, Journal of Geophysical Research, 10, 1557-1563.

Tishchenko, P., Hensen, C., Wallmann, K., Wong, C.S., 2005. Calculation of the stability and solubility of methane hydrate in seawater, Chemical Geology, 219, 37-52.

Yamano, M., Uyeda, S., Aoki, Y., Shipley, T.H., 1982. Estimates of heat flow derived from gas hydrates, Geology, 10, 339-343.

Yamano, M., Kinoshita, M., Goto, S., 2008. High heat flow anomalies on an old oceanic plate observed seaward of the Japan Trench, International Journal of Earth Sciences, 97, 345-352.

Table 7.1. Summary of heat flow measurements

St. #	Lat (°)	Lon (°)	WD (m)	Penetrated thermistors	Usable data	Station description	Remark
08	69.988265	-137.306623	59	8	Not determined	Along the transect in the eastern slope of Mackenzie Trough	Not presented
09	69.990495	-137.602482	73	8	Not determined	Along the transect in the eastern slope of Mackenzie Trough	Not presented
10	69.990326	-137.737682	88	8	3	Along the transect in the eastern slope of Mackenzie Trough	Not presented
11	69.991225	-137.819489	129	8	Not determined	Along the transect in the eastern slope of Mackenzie Trough	Not presented
12	70.790960	-135.564355	419	8	7	On top of mud volcano	Resistance
28	70.792722	-135.518772	430	8	5	Outside of mud volcano	Resistance
39	70.655748	-139.038375	1540	8	4	Deepest site	Resistance
40	70.133333	-138.700000	330	8	Not determined	Keel of Mackenzie Trough	Not presented

Table 7.2. Specification of heat probe

Part	Specification	
Data logger	Dimension	50 kg Ø144*775 mm
	Housing	Up to 6000 m
	Measuring channel	#1~#10 #10 for fixed resistor as reference
	Measuring interval	30 sec
	Measurable resistance	1500-6500Ω
	Depth sensor	Up to 6000 m with accuracy of 1 m
	Tilt sensor	Up to ±45 degree on X, Y axes with accuracy of 0.1 degree
	Shock sensor	
	Memory	32MB (corresponding to 0.5 million records)
	Heat pulse	On/Off When mode 'On', for 12 seconds with 5 V in 6/8/10 minutes after shock
	Pinger frequency	12/13/14/15 kHz
	Pinger pulse length	2/5 ms
	Pinger oscillation mode	3 (Heater On/Heater Off/Tilted)
	Connectivity	RS-232C
	Battery	NiCd 7.2V *1 for measurement NiCd 25.2V *1 for the pinger
Thermistor	Length	Up to 6.5 m
	Type	2 (Heat-generating/Normal thermistor)
	Measurable temperature	~1500 Ω for 80 degree 6000 Ω for 0 degree Accuracy: 0.01 degree
Frame	Head	400 kg Ø540*1330 mm
	Barrel	~35 kg/1.5 m Adjustable using 2 units (1.5 m/3.0 m)

(a)

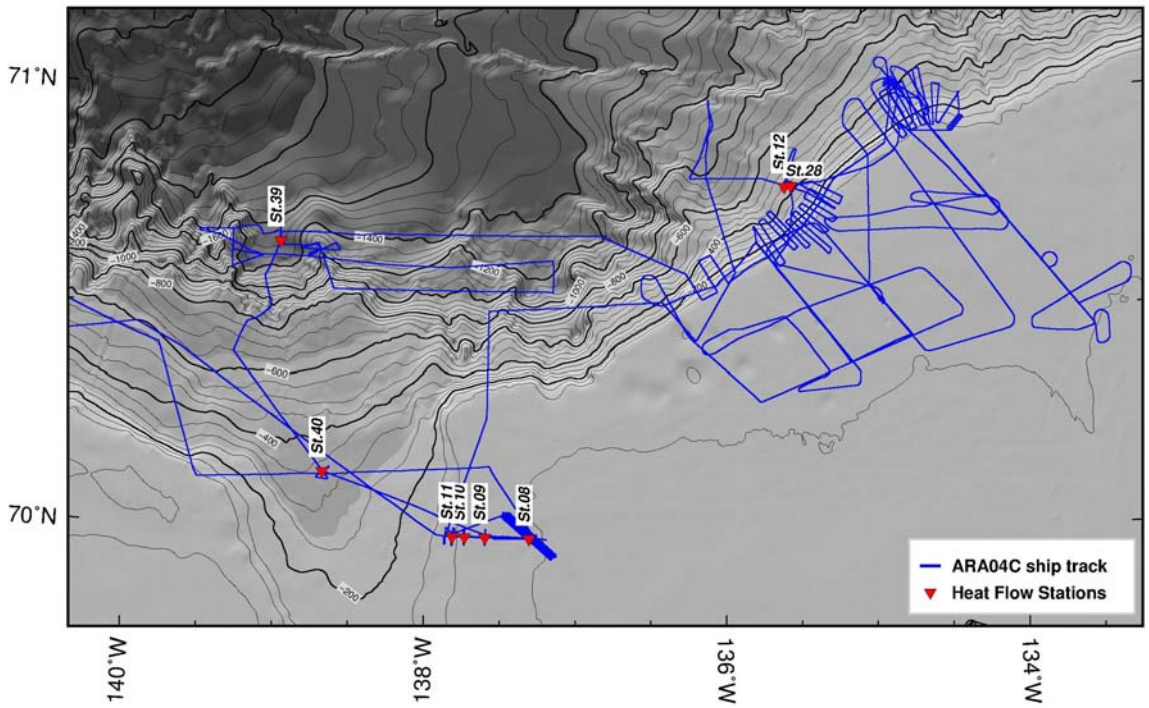
71°N
70°N
140°W
138°W
136°W
134°W
St.39
St.40
St.11
St.10
St.09
St.08
St.12
St.28
ARA04C ship track
Heat Flow Stations

(b)

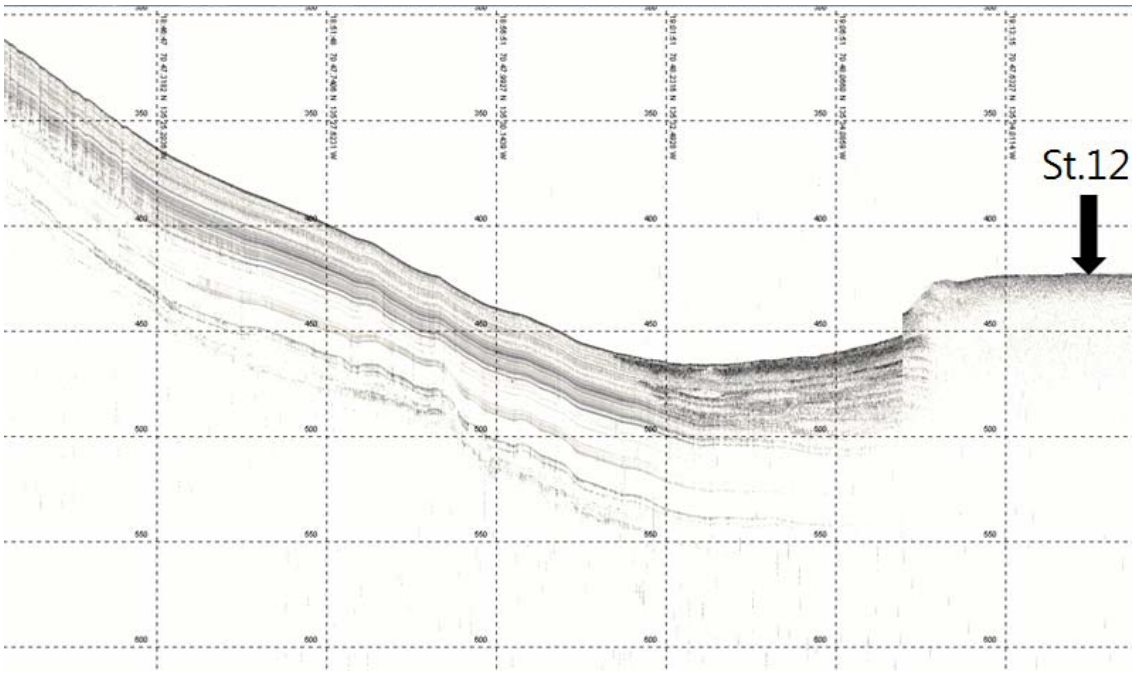
St.12

(c)

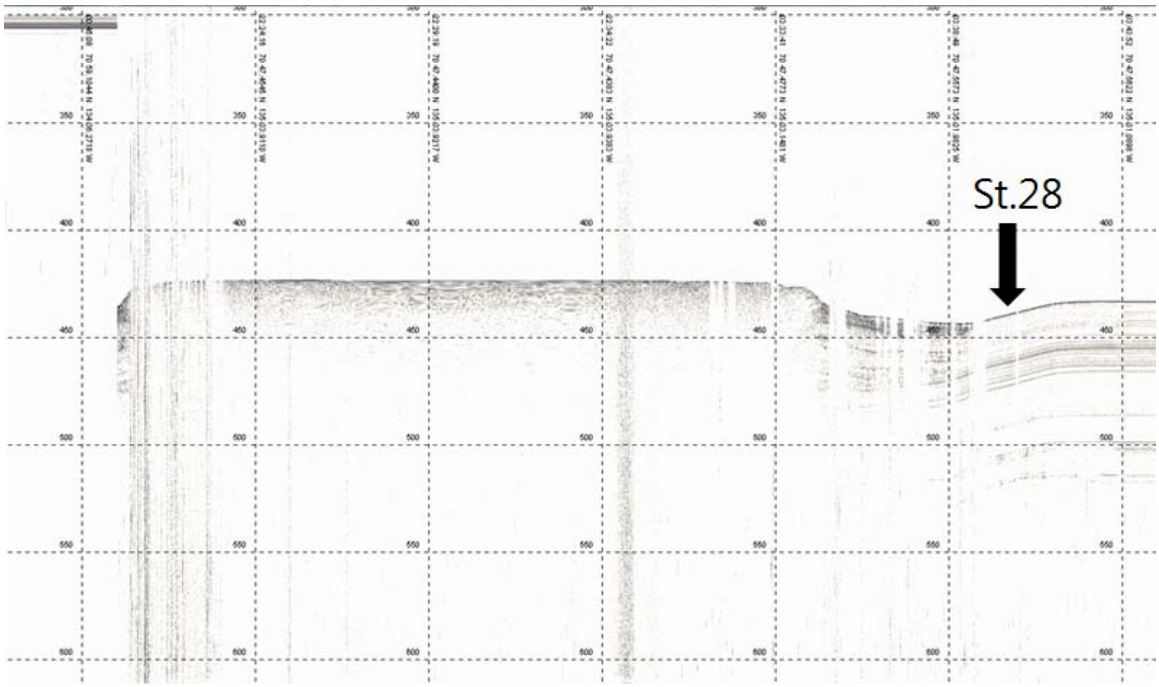

(d)

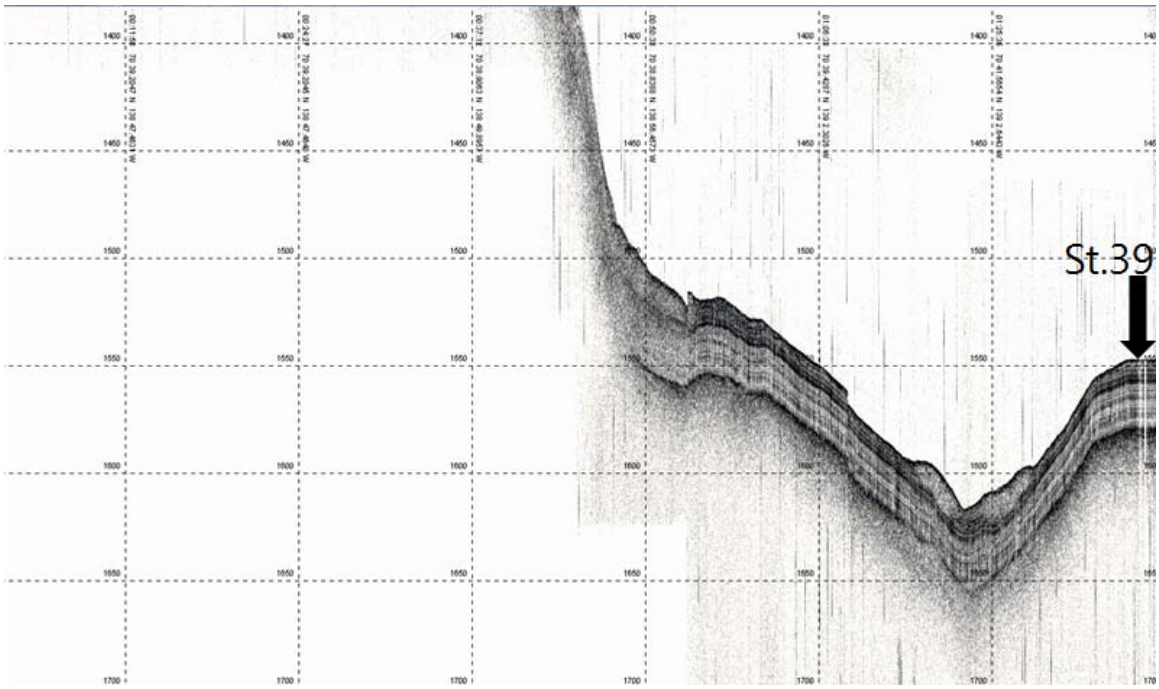

Figure 7.1 (a) Heat flow measurements (red triangles) and shiptrack (blue line) during Expedition ARA04C. Data from station 12, 28 and 39 are presented in this report. Sub-bottom profiler data for (b) Station 12, (c) Station 28, (d) Station 39.

(a)

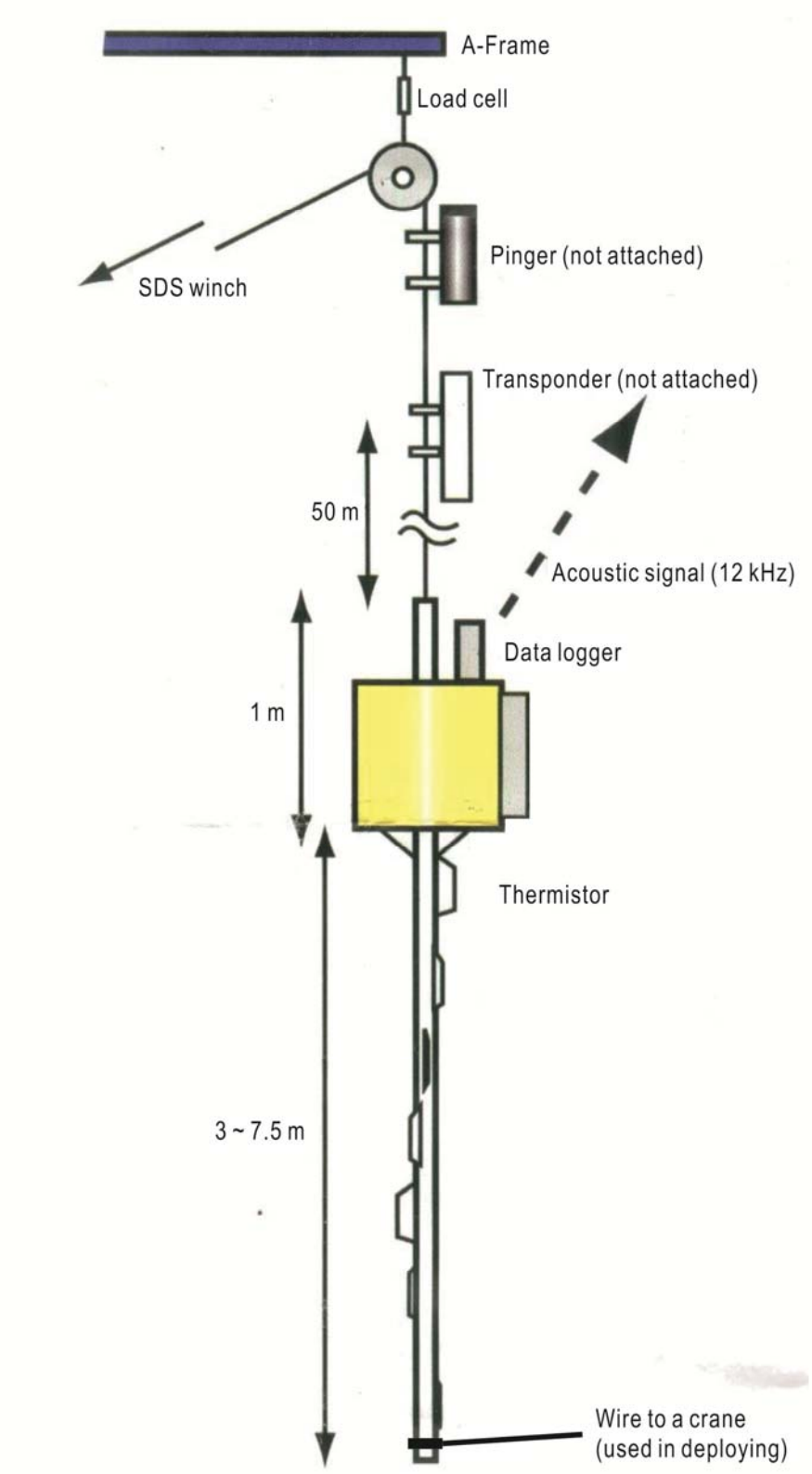
A-Frame
Load cell
SDS winch
Pinger (not attached)
Transponder (not attached)
50 m
Acoustic signal (12 kHz)
Data logger
1 m
Thermistor
3 ~ 7.5 m
Wire to a crane
(used in deploying)

(b)

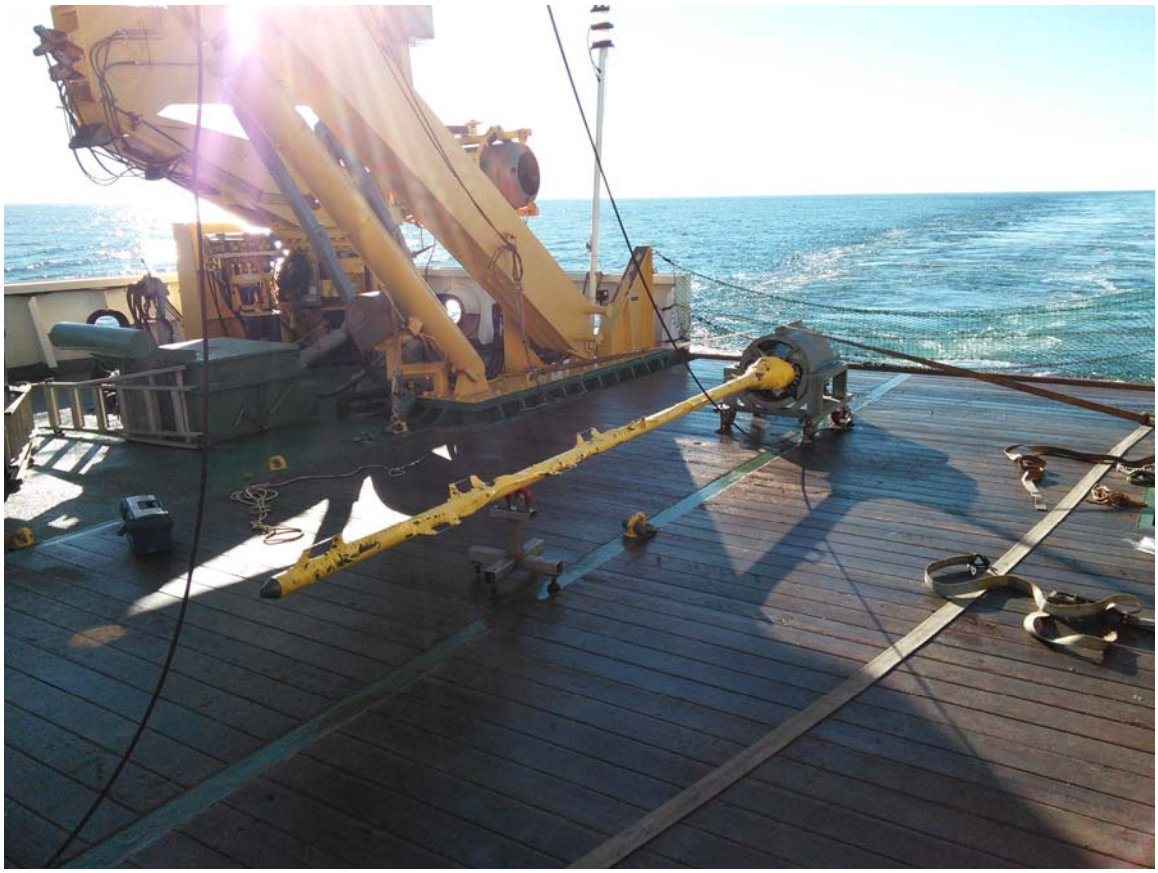

(c)

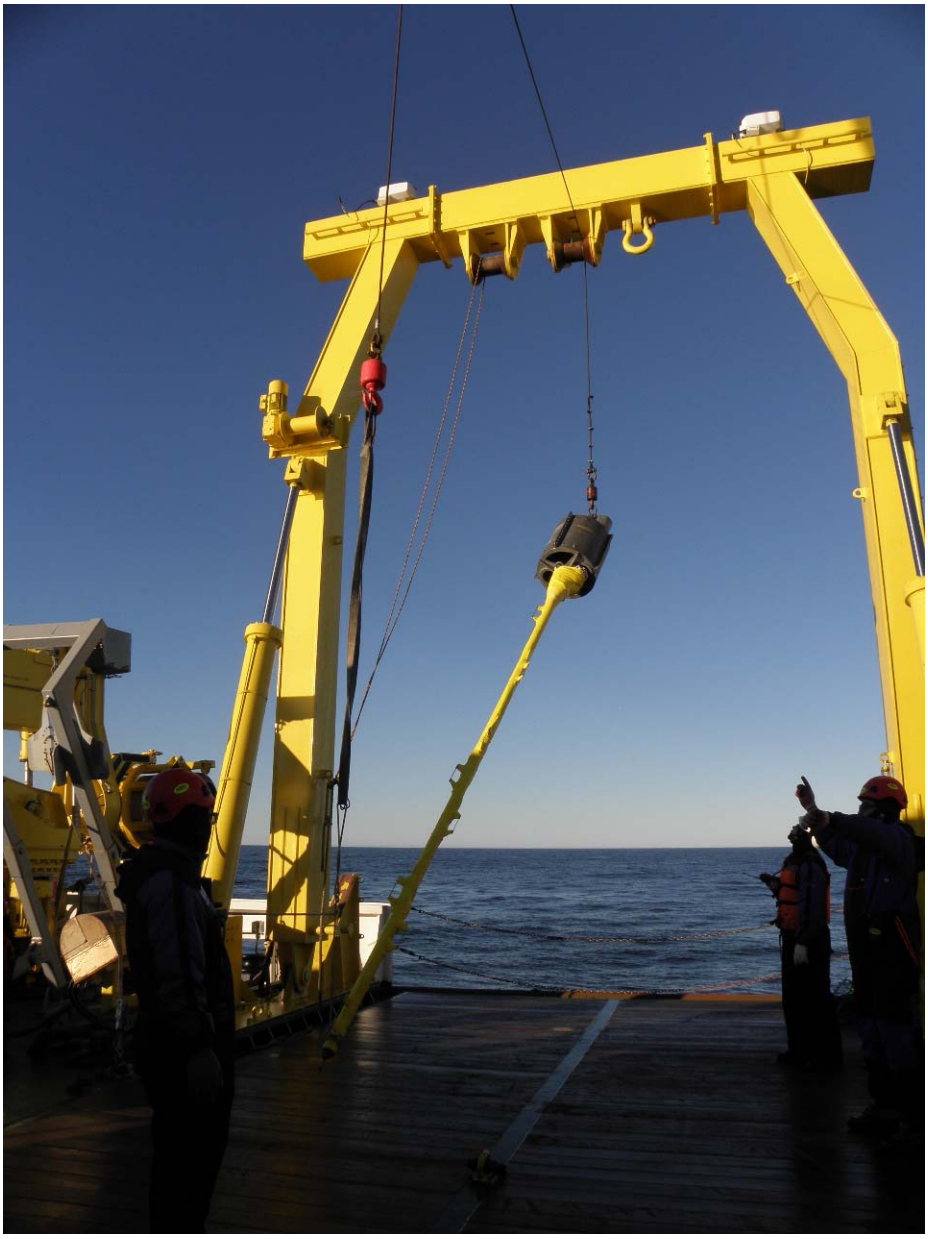

(d)

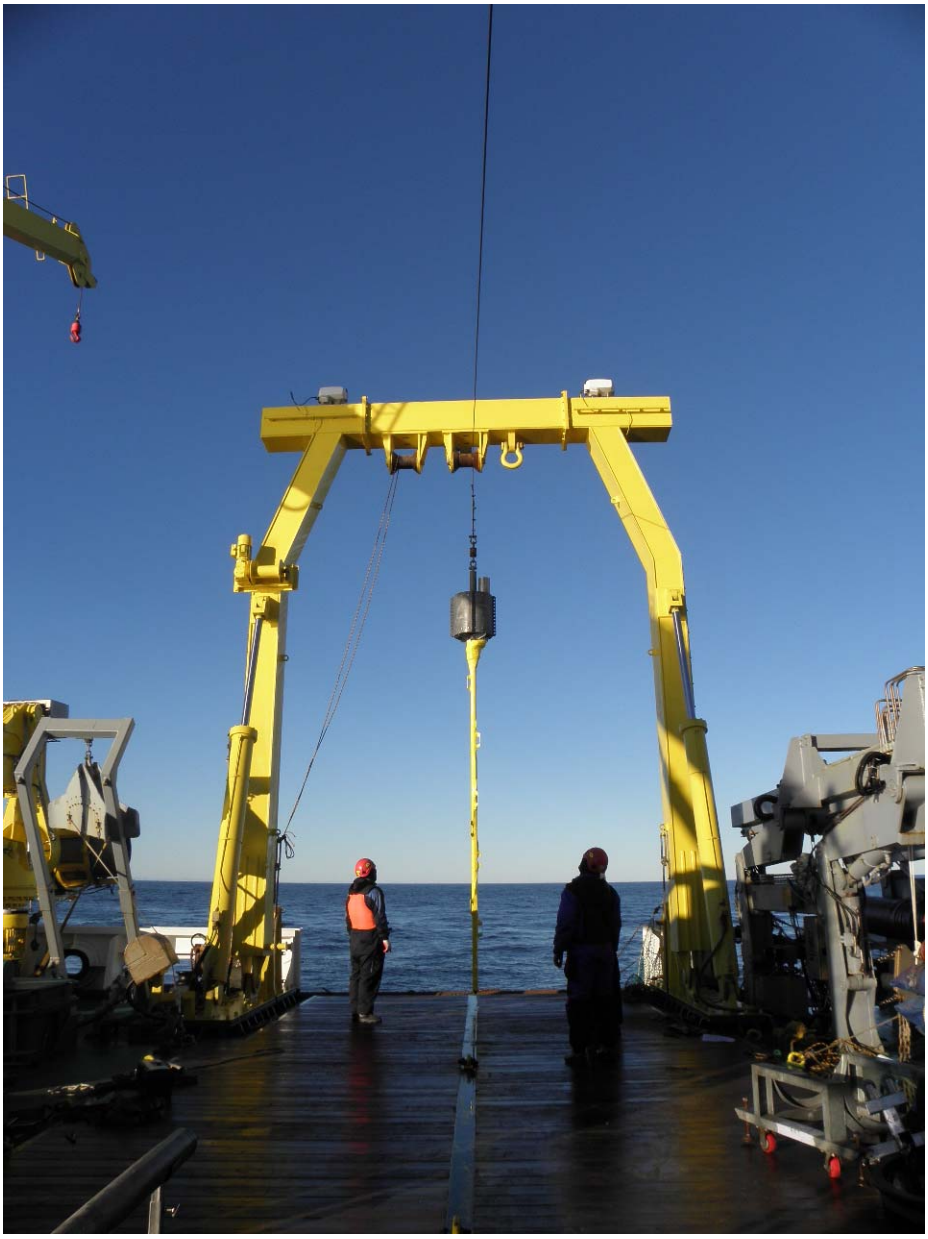

Figure 7.2 Configuration and deployment of the heat probe. Due to the size of the A-Frame the maximum length of the barrel (yellow part) is 4.5 m. A total of 8 thermistors are attached to the barrel. (a) Schematic diagram of the heat probe operation. (b) Photo of the heat probe on-deck. (c) and (d) Photos during deployment**.**

(a)

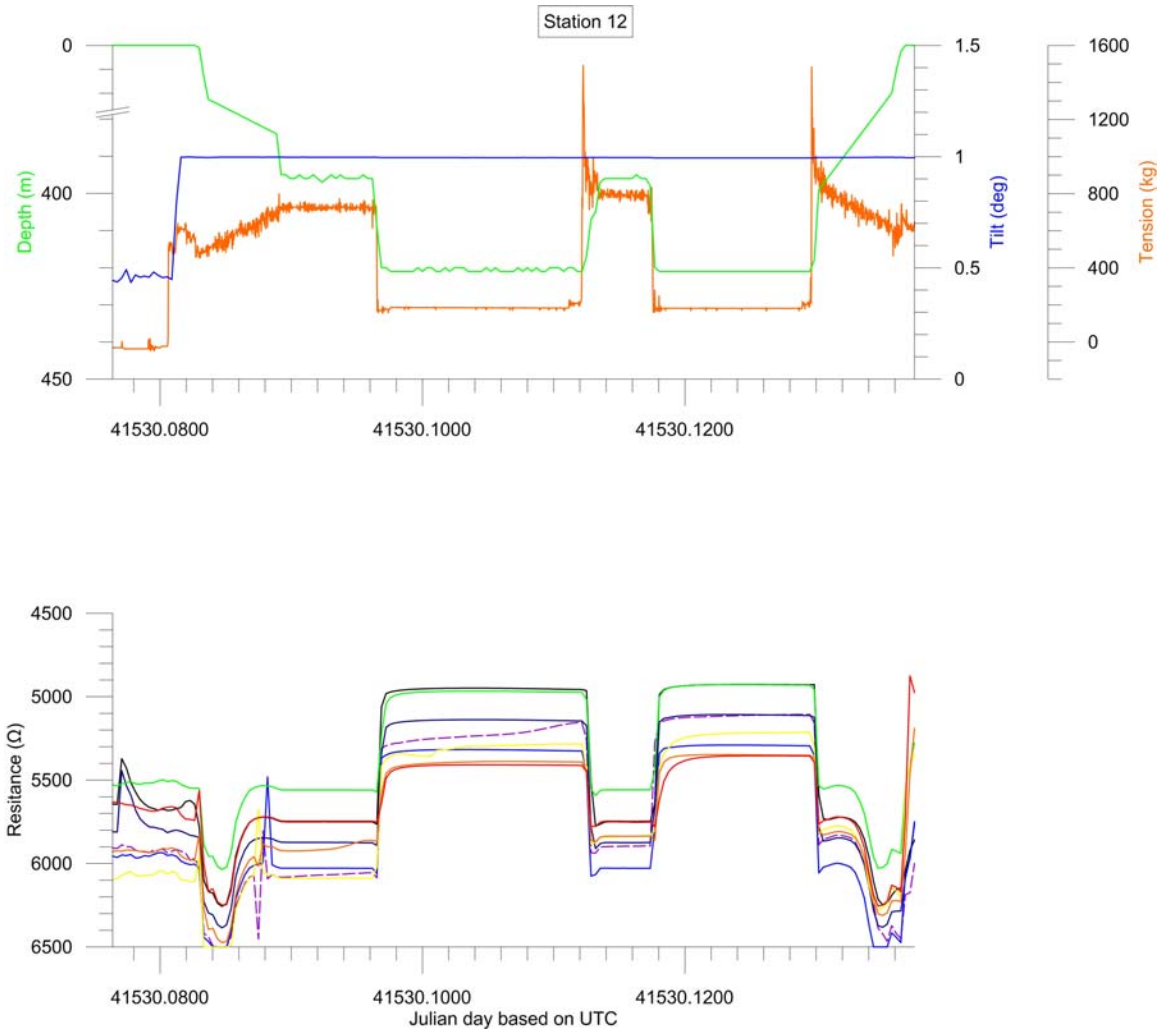
Station 12
Depth (m)
0
400
450
Tilt (deg)
1.5
1
0.5
0
Tension (kg)
1600
1200
800
400
0
41530.0800
41530.1000
41530.1200
Resitance (Ω)
4500
5000
5500
6000
6500
41530.0800
41530.1000
41530.1200
Julian day based on UTC

(b)

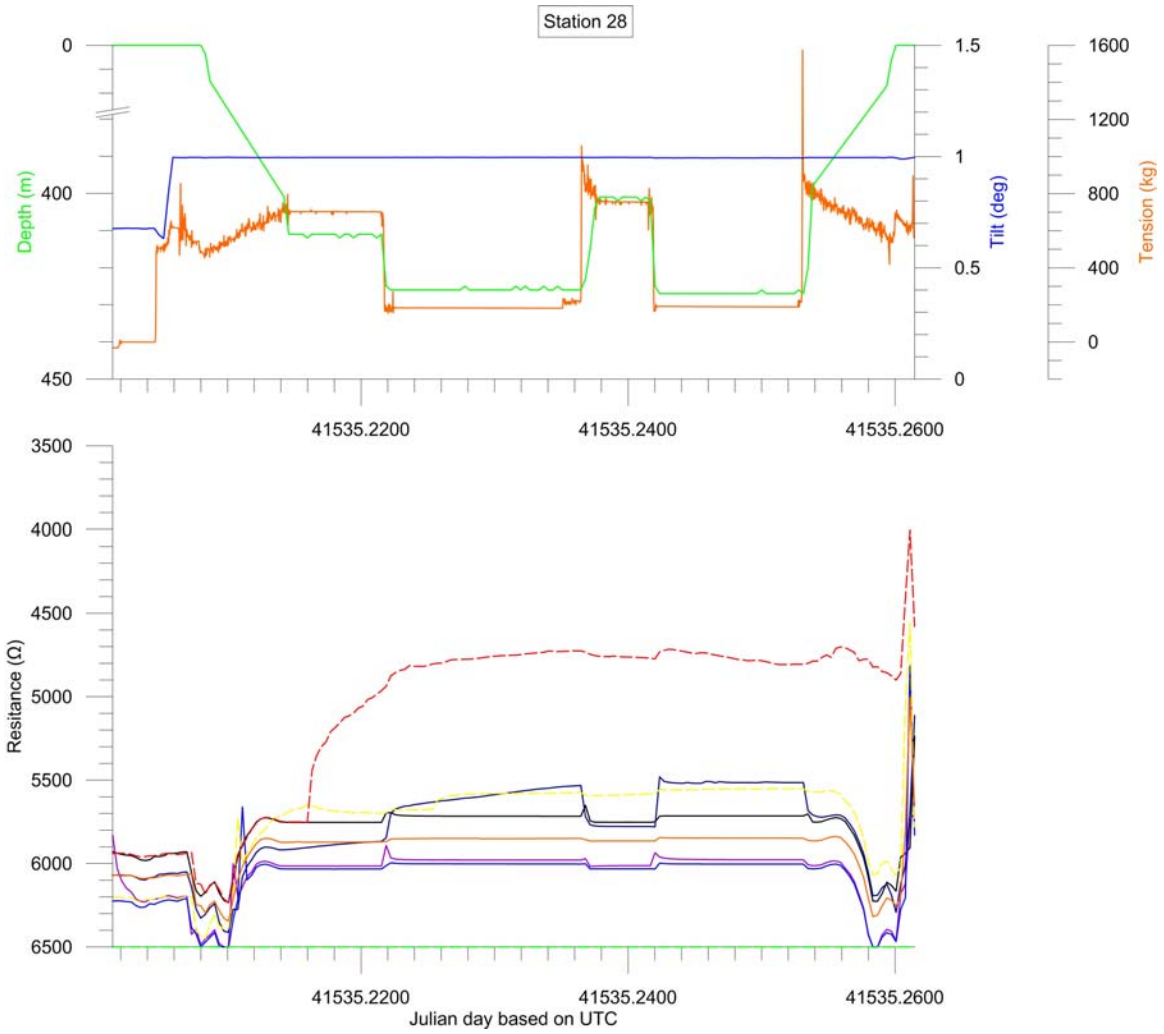
Station 28
Depth (m)
0
400
450
Tilt (deg)
1.5
1
0.5
0
Tension (kg)
1600
1200
800
400
0
41535.2200
41535.2400
41535.2600
Resitance (Ω)
3500
4000
4500
5000
5500
6000
6500
41535.2200
41535.2400
41535.2600
Julian day based on UTC

(c)

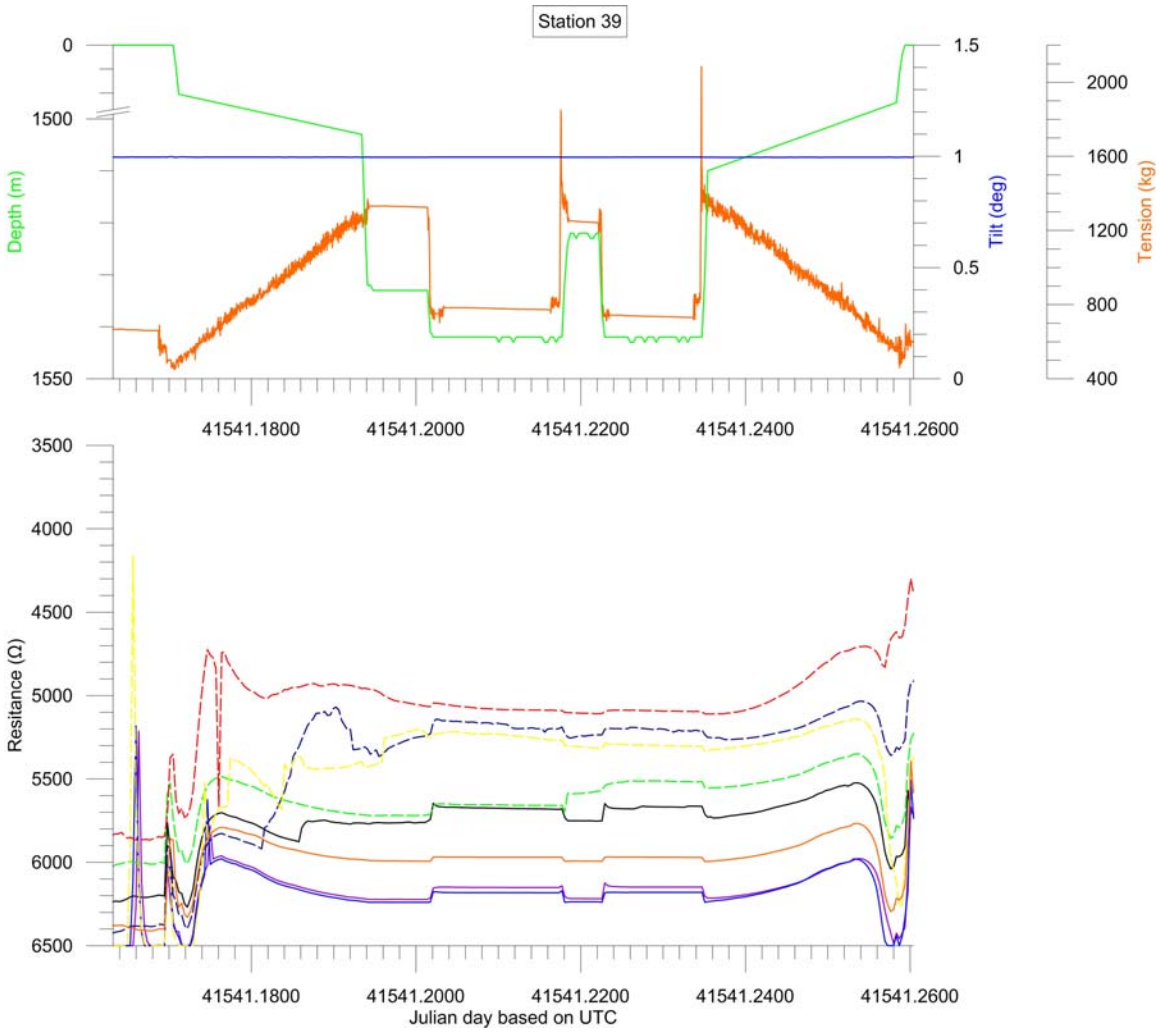

Figure 7.3 Raw data of three stations: (a) Station 12, (b) Station 28, and (c) Station 39. In each subfigure, the upper panel shows depth and tilt of the data logger during the measurements. Note that the axis of depth is irregular to account for the strongly different water depths of these three stations. Resistance with time is displayed in the lower panel. Total eight thermistors are attached to the heat probe: topmost thermistor (red), 2nd (orange), 3rd (yellow), 4th (green), 5th (blue), 6th (navy), 7th (purple), and 8th (black). Usable data are represented as solid line, likely unusable data are plotted as dashed lines. At this stage, exact temperature at depth and geothermal gradient cannot be determined because the calibration functions are not available onboard. The difference in the equivalent temperature distribution between the three stations with and without upward fluid flow (i.e. Station 12 vs. Station 23 and the background Station 39) is clearly visible.

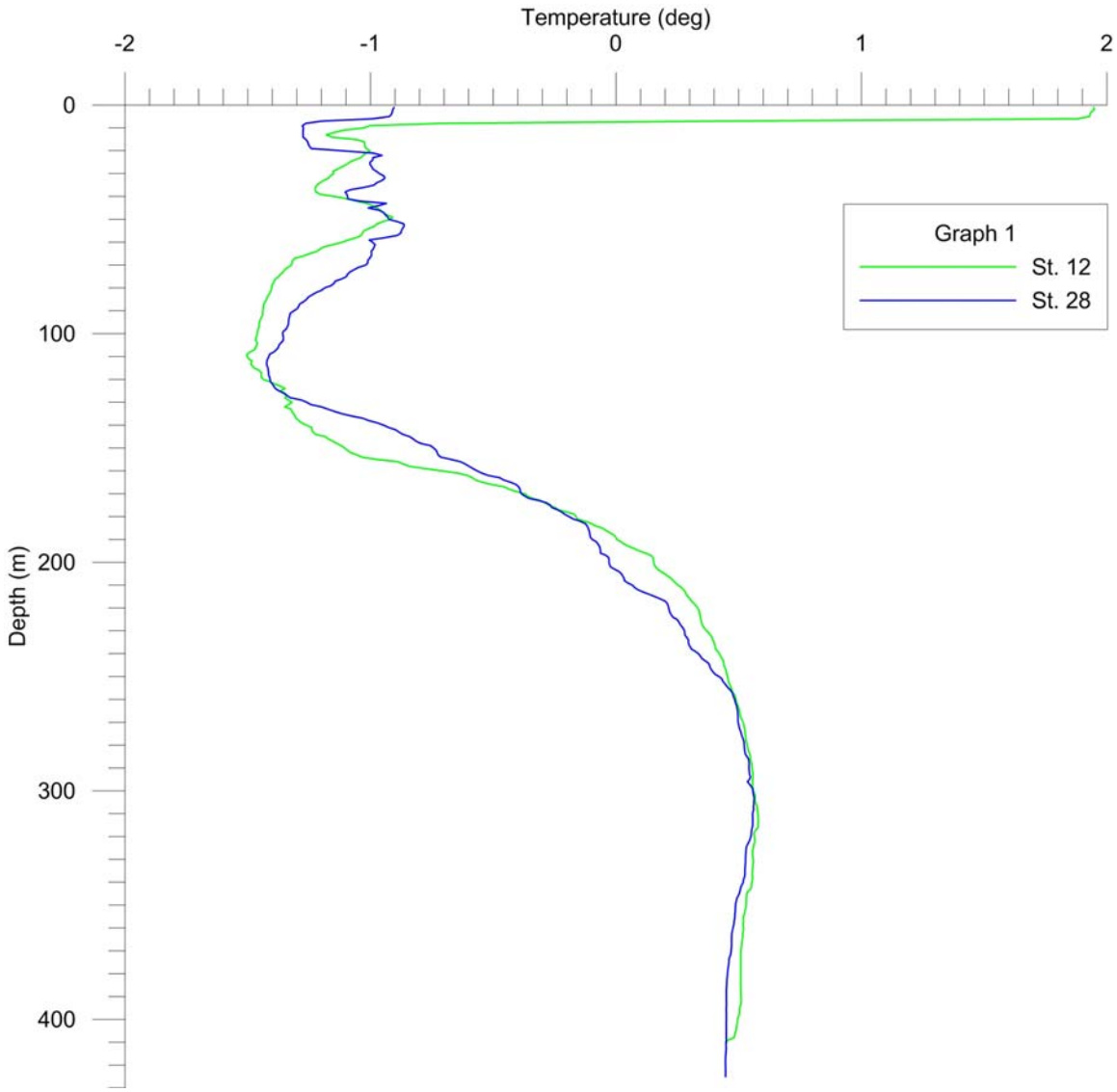

Figure 7.4 Comparison of temperatures measured at Station 12 and Station 28 with the CTD tool.

Chapter 8 Sediment coring and geochemistry

S.I. Nam, Kim W. Conway, S.Y. Kim, B.R. Lee, Y.S. Sim, M. Schreck, A.H. Quantmann-Hense, C.H. Han, Y.J. Lee, E.J. Byun

8.1 Introduction

The marine geology program was conducted in combination with geophysics and geochemistry onboard ARAON during the second leg of the fourth Arctic expedition (ARA04C) in 2013. The overall goal of the marine geology program for this second leg is to take new and undisturbed sediment cores from the selected research target areas, including the northern Alaskan continental margin and the Mackenzie Trough, related to the IODP proposal 753 and the Beaufort Sea continental margin for an improved understanding of the stratigraphy, glacial history, geohazards and gas hydrate occurrence (Figure 8.1).

Within this context, the marine geology program was divided into three parts based on the following scientific targets: 1) recovery of sediment cores for reconstructing late Quaternary glacial history and paleoceanographic changes from the northern Alaskan continental margin; 2) sediment coring and acquisition of sub-bottom profile (SBP) and multibeam data in support of IODP proposal 753 for drilling in the Beaufort Sea; and 3) recovery of sediment cores from the selected core sites looking for potential gas hydrate evidences from the Beaufort Sea.

To select sediment core sites, sub-bottom acoustic profiling has been carried out along the whole cruise track in a 24-hour operation using SBP technique. Bottom and sub-bottom reflection patterns obtained by SBP characterize the uppermost sediments of the western Arctic Ocean in terms of their acoustic behavior down to about 100 m below the sea floor. This can be used to investigate depositional environments of unexplored areas on larger scales in terms of space and time, retrieving the uppermost sediments. The objectives of sediment echo sounding during this cruise are: 1) to contribute to the database for an acoustic facies interpretation indicative of different sedimentary environments; 2) to obtain different patterns of high resolution acoustic stratigraphy

useful for lateral correlation over shorter and longer distances thereby aiding correlation of sediment cores retrieved during the whole cruise; 3) to select coring stations based on acoustic pattern and backscatter; and 4) to provide a high-resolution supplement for the uppermost sections of seismic profiles recorded during the whole cruise. The bathymetric survey will be performed using a Multi-Beam Echo Sounder (MBES), which is hull-mounted.

8.2 Strategic Selection of Coring Sites

8.2.1 Northern Alaskan margin

The main objectives of the marine geology program in the northern Alaska margin were: 1) the reconstruction of paleoceanographic conditions during warm periods of the Holocene along the northern Alaskan margin; 2) the investigation of the glacial history in the western Arctic including the extent and timing of glaciations during the late Quaternary; 3) the improvement of the understanding of sedimentation systems in the front of the Barrow canyon mouth (eastern side); and 4) the identification of potential sites for future ocean drilling.

The Alaska Beaufort margin (east of Barrow Canyon) was selected as the target area for mapping glacial and sedimentary features along the shelf break and upper slope. Barrow Canyon was targeted for the mapping of sediment accumulation to better understand its glacial history and potential for ocean drilling along the front of the major canyon which transports water and sediment across the Chukchi shelf.

To achieve the study objectives we employed the following geological/geophysical methods:

- Multi-beam bathymetric mapping for seafloor morphology combined with sub-bottom reflection profiling for geometry of sedimentary bodies and seismo-stratigraphic correlations;
- Coring seafloor sediment with a gravity corer for sediment composition and stratigraphy (up to ~5 m deep);
- Coring with a multiple corer for modern/recent seafloor processes;

- Logging recovered cores with the Multi-Sensor Core Logger and ITRAX geochemical core scanner along with describing the split cores and taking various samples for further analyses.

8.2.2 Mackenzie Trough, Beaufort Sea

Dr. M. O'Regan (Stockholm University, Sweden) and his Canadian colleagues submitted IODP pre-proposal for drilling in the Mackenzie Trough (MT) region of the Beaufort Sea (IODP Pre-753, Late Quaternary Paleoceanography and Glacial Dynamics in the Beaufort Sea). It is hypothesized that the region has a number of strategic advantages in terms of high sedimentation rates which provide high-resolution time series and the preservation of mixed marine and terrestrial flora/fauna in Holocene and deglacial hemipelagic sediments (Schell et al., 2008). In January of 2012, PEP (new Proposal Evaluation Panel) of IODP encouraged the development of Pre-753 into a full drilling proposal. However, a major challenge in the development of the full proposal is the need to identify drilling targets where continuous recovery of sediments from at least MIS (Marine Isotope Stage) 5, and preferably a complete mid- to late Pleistocene sequence, is well preserved.

O'Regan et al. proposed that KOPRI use the coring and geophysical surveying capabilities of the Araon to acquire jumbo piston cores from the two most prominent ridges, and investigate the seafloor topography and acoustic stratigraphy of sediments surrounding these features. The main questions that need to be addressed in regard to the IODP drilling proposal are:

1) Do sediments from these deeper water settings preserve organic-walled, calcareous and siliceous microfossils needed for paleoenvironmental reconstructions?

2) Is there seismic evidence for continuous sediment deposition at one or both of these sites?

3) Can we date the sediments with radio-isotopic and paleomagnetic approaches?

Within this context, during the Araon cruise ARA04C/Leg 2, we retrieved two sediment cores from the topographic highs (ridges) located above the abyssal plains and one core from the slope of the Mackenzie Trough using the gravity corer and multiple corer, respectively (Figure 8.1).

8.2.3 Beaufort Continental Margin

Sediment coring was undertaken during the Araon cruise ARA04C to address issues of marine geohazards as well as fundamental questions about the Quaternary development of the Beaufort margin. There also is an interest to study the late glacial history and paleoclimatic/oceanographic regime of the Beaufort Sea. The Mackenzie Trough is an area of particular interest as shallow areas of the Trough (<150 m) may contain a record of past glaciations and deeper water areas (>750 m) may contain a near continuous record of marine deposition. It was thus proposed that the Araon carry out a short geological reconnaissance of this area during the first several days that it was in the Canadian Beaufort Sea. An initial survey consisted of sea floor bathymetric mapping and bottom sediment imaging using hull mounted sounders. Coring and heat flow measurements were undertaken on an opportunity basis to characterize the surficial sediments.

Previous works (CCGS Sir Wilfred Laurier surveys in 2010 and 2012) have described a tentative seismostratigraphic framework for the upper portion (top 100 m) of the Quaternary shelf edge and upper slope section (Figure 8.2). In addition, the understanding of the surfical geology of the western Beaufort shelf is advancing with the collection of a large number of sub-bottom profile lines collected during surveys aboard the CCGS Amundsen under the auspices of the ArcticNet Program (Thomson et al., 2010). Integration of sub-bottom data collected to date yields the interpretation shown in Figure 8.2. Only some of the units shown have been properly sampled. These include the cyan unit, which is deforming into pingo-like features (Figure 8.2) and the draping orange unit which appears to post date the deformation.

The units described are key elements involved in large mass wasting processes in the western part of the study area (see Chapter 1- Introduction). The identified units require sampling to better describe the lithology and chronology with the goal of developing a robust and testable late Quaternary lithostratigraphy for the area. In addition physical properties measurements will assist in geotechnical investigations of slope stability. The advantage of the Araon is the excellent station-keeping capacity with a dynamic positioning system being used so very accurate coring targets may be cored.

In addition to the above targets, several mud volcanoes occur in the study area at a variety of depths. While no hydrate has been observed during previous explorations of these features they are of a large scale and appear to vent significant volumes of methane into the water column. Heat flow and water column methane measurements at these sites are of great interest to determine flow pathways of fluids and gas.

8.3 Methods

8.3.1 Gravity Corer

A gravity corer of 10 cm diameter was employed with a 1.5 tons headstand and using 3 m length core barrels with assemblies allowing recovery of cores of up 9 m in length. Cores were extracted from the corer and sectioned into 1.5 m lengths and then scanned with a GeoTek multisensor core logger after temperature equilibration overnight. Rhizon samplers were employed to collect pore waters from selected cores at 20 cm intervals.

8.3.2 Multiple corer

A multiple corer constructed by Denmark was utilized to recover up to 8 identical cores at selected sites where sediments were relatively soft. Multiple cores with 8 inner plastic tubes (diameter of ca. 10cm and a length of 80 cm) were used at 12 stations to obtain undisturbed subsurface sediments and overlying bottom waters. In general, two surface sediment cores collected with the multiple corer were sub-sampled in slices of 1 cm intervals and freeze-dried for further investigation.

8.4 Results

A total of three multiple cores were taken from the northern Alaskan margin in water depths of 235 to 282 m, and 4 sediment cores were recovered. The recovered core lengths ranged from 415 to 503 cm (Tables 8.1 and 8.2). Three multiple cores were collected offshore of the Mackenzie Trough in water depths of 331 to 1190 m, and a total of 3 sediment cores were retrieved for IODP proposal 753. The length of recovered core sediments ranges from 470 to 647.5 cm. Once retrieved on deck, gravity cores were cut up in lengths of 1.5 m and labeled. The labeled core segments were transported to the laboratory for logging using MSCL. All sediment cores were logged on the Geotek

Multi-Sensor Core Logger (see example of MSCL data in Figure 8.3) and then preserved in core storage.

Six multiple cores were retrieved from the eastern Beaufort shelf and 16 sediment cores were collected over the region, focused on three areas which included the Mackenzie Trough inshore and offshore sequences in water depths of 55 to 1540 m. The recovered core lengths range from 26 to 496 cm. Cores recovered for this general inner trough location included stations 5, 6, 7, 41 and 42 (Tables 8.1 and 8.2). Five coring stations were occupied along a transect on the eastern edge of the Mackenzie Trough. Three of these were in the first few days of operations and two during the last sampling day (Table 8.1 and 8.2).

8.4.1 Pingo-Like-Features (PLFs)

A prominent shelf edge PLF was selected (Figure 8.4) for coring because of apparent thin surficial cover over the mound and the relative width of the PLF. Careful positioning of the ship was required because of the small target size, even with the dynamic positioning system engaged. The first core (26GC-01) was collected on the flank of the feature and recovered a 30 cm core consisting of loose brown mud overlying stiff grey silt. The core catcher sample (retained) provided a good hand sample of the lowermost unit which is most likely to be the PLF material. MSCL data confirm the dense nature of the lower unit. A second attempt at a longer recovery cored a small depression, identified on the multibeam, near the apex of the mound. This core recovered 39 cm of grey to brown loose mud overlying a stiff gravelly, sandy mud below. Again the catcher sample (retained) provides a very good hand sample of what are probably the PLF sediments. Physical properties indicate dense and relatively high magnetic susceptibility of these lower units in both cores (Fig. 8.9 – upper left).

8.4.2 Deepwater Expulsion Feature (mud volcano)

The prominent expulsion feature at 420 m on the continental slope was cored using a 6 m assembly (Figure 8.5). The core was very gassy, and the corer was noted to over penetrate into the soft surface. The top 1.5 m section was opened for initial examination and gassy texture similar to chocolate mousse was noted.

8.4.3 Seismostratigraphic Units

Cyan Unit – The cyan unit is a widely distributed, relatively thick (up to 40 m) acoustically massive interval (Figure 8. 6). There are few sites where the unit comes close to the seabed as an outcrop, being normally covered by younger sediments. Station 25 was occupied four times in an attempt to recover core from this critical target (Table 8.3). The first attempts, which were 6 m two barrel core assemblies, are thought to have fallen over during impact resulting in poor recovery (26 and 52 cm) of what may only be the surficial, recent sediments. A third attempt using a 3 m (one barrel assembly) resulted in recovery of an 81 cm core that showed soft sediments overlying a stiff unit at the base of the core, which is probably the cyan unit recovered in place. Physical properties data indicate a much denser material underlying 30 cm of soft mud.

Orange Unit – The orange unit is the uppermost unit in the deeper water sequence and it drapes the deformed and broken underlying units. The unit may date from the most recent lowstand(s) of sea level as it is deposited below 160 m which is just below the presumed lowstand of late Quaternary sea level (Blasco et al., 2011). The underlying yellow unit is considered to be a glaciomarine sediment package that is subject to normal faulting along much of the shelf edge as the underlying cyan unit deforms. Dating the orange unit would thus help date the most recent deformation of the underlying sediments.

Mackenzie Trough – Three gravity cores (Station 36 – 38) were taken in the outer Mackenzie Trough region (Figure 8.1). Steep topographic ridges dominate the site locations and a short SBP survey was conducted to define optimum core location with laminated sediment sequence (Figure 8.8). A first interpretation of the MSCL data is given in Chapter 9.

8.5 Future plans for post-cruise work

Detailed analyses such as stable isotopes of planktonic and benthic foraminifera, organic geochemistry, biogenic opal contents, microfossils (e.g., foraminifera, pollen and spores, dinoflagellate cysts) will be performed at KOPRI and/or GSC. Pore water analysis will be performed at the Monterey Bay Aquarium Research Institute (MBARI) after this expedition, whereas head-space gases and void gases taken from the selected sediment cores will be measured using ICP-Mass at KIGAM.

Elemental analysis (total carbon, inorganic carbon and nitrogen) will be measured using CHN-Analyzer and/or IR Mass, and then calculated TOC and CaCO3 contents (wt. %) and C/N ratio. Stable carbon and nitrogen isotopes of bulk sediment and organic matter will be determined using a Delta Plus V Mass spectrometer (Thermofishers, Germany) at KOPRI. Biomarkers will be analyzed by Prof. Dr. R. Stein at AWI, Germany. For benthic foraminifera analysis, multiple core sediments were sub-sampled at 1 cm intervals and stained with a 70 % ethanol solution of Rose Bengal.

Core will be split, described, photographed, and then scanned using an ITRAX XRF core scanner. Sediment cores will be sub-sampled both at KOPRI and GSC.

For further stable isotope analysis and AMS 14C dating, sliced core subsamples will be wet-sieved with a 63 μm mesh and dried in an oven at about 60℃. The dried sand fraction will be estimated with a binocular microscope to hand-pick the planktonic and benthic foraminifers, sinistral and dextral coiling species of N. pachyderma and C. wuellerstorfi, respectively. Stable oxygen and carbon isotopes will be measured on N. pachyderma sin. and dex., and C. wuellerstorfi with Finnigan MAT 253 at the Alfred-Wegener-Institute for Polar and Marine Research, Germany and/or at Hokkaido University, Japan. AMS 14C dating of N. pachyderma sin. will be performed at Georgia University, USA.

8.6 Gas-geochemistry

8.6.1 Introduction

Eighty three samples were taken for headspace gases and 15 for void gases from sediments in the gravity cores collected, as well as 14 samples for headspace gases in sediments from multi cores. These samples will be analyzed in the lab onshore using gas chromatography and GC-IR-MS. We can garner information about quantity and quality of hydrocarbon and other gases from both headspace and void gas samples. Stable isotope ratios of carbon and hydrogen in the hydrocarbon gases will be analyzed on the selected samples. The analysis data can provide the characteristics of hydrocarbon and other gases in the study area. In addition, origin of the hydrocarbon gases will be assessed.

We are also interested in organic geochemical analysis of the sediments from selected gravity core samples. TOC (total organic carbon content), type and level of thermal maturation of organic matter will be determined using various geochemical analyses. The analyses focus mainly on understanding the organic geochemical characteristics of the sediments from core samples.

8.6.2 Methods

8.6.2.1. Headspace gas

Three millilitre sediment samples were taken from gravity and multi cores immediately after cutting and extruded into a 20 ml glass vial. We took 5-6 samples over a 1.5 m interval including top and bottom from gravity cores and every 10 cm for multi cores.

8.6.2.2. Void gas and headspace gas

Void gases were taken if core sediments contained voids due to expansion of gases in the liner. Void gases were sampled by piercing the core liner and then stored in a 60 ml glass vial filled with saturated NaCl solution**.**

References

Blasco, S., Bennett, R. Brent, T., Campbell, C., Carr, R., Covill, S., Dallimore, S.R., Davies, E., Hughes-Clarke, J., Issler, D., MacKillop, K., Mazzotti, S., Patton, E., Shearer, J., White, M., 2011. 2010 Status of knowledge Geological Survey of Canada, Open File Report, 6989. 335 pp.

O'Regan, M., de Vernal, A., St-Onge, G., Hillaire-Marcel, C., Rochon, A., 2013. Coring and seismic surveying seaward of the Mackenzie Trough in support of IODP proposal 753 for drilling in the Beaufort Sea. (3 pp. Proposal to SI Nam).

Paull, C. K., Ussler, W., Dallimore, S. R,. Blasco, S. M., Lorenson, T. D., Melling, H.., Medioli B. E, Nixon, F. M., McLaughlin, F. A., 2007. Origin of pingo-like features on the Beaufort Sea shelf and their possible relationship to decomposing methane gas hydrates. Geophysical Research Letters, v. 34, no. 1, doi: 10.1029/ 2006GL02797.

Paull, C. K., Dallimore, S.R., Hughes-Clarke, J., Blasco, S. M., Lundsten, E., Ussler, W. III, Graves, D., Sherman, A., Conway, K., Melling, H., Vagle, S., Collett, T.S., 2011. Proceedings of the 7th International Conference on Gas Hydrates, Edinburg, Scotland, July 2011.

Schell, T.M., Scott, D.B., Rochon, A., Blasco, S.M., 2008. Late Quaternary paleoceanographic and paleo-sea ice conditions in the Mackenzie Trough and Canyon, Beaufort Sea. Canadian Journal of Earth Science, 45, 1399-1415.

Thomson, J., Dingler, J., Blasco, S., Hughes-Clarke, J., 2010. Integration of multiple data types for geohazard survey planning, Canadian Beaufort Sea. ArcticNet Annual Science Meeting 2010, Ottawa, Ontario, 14-17, 2010.

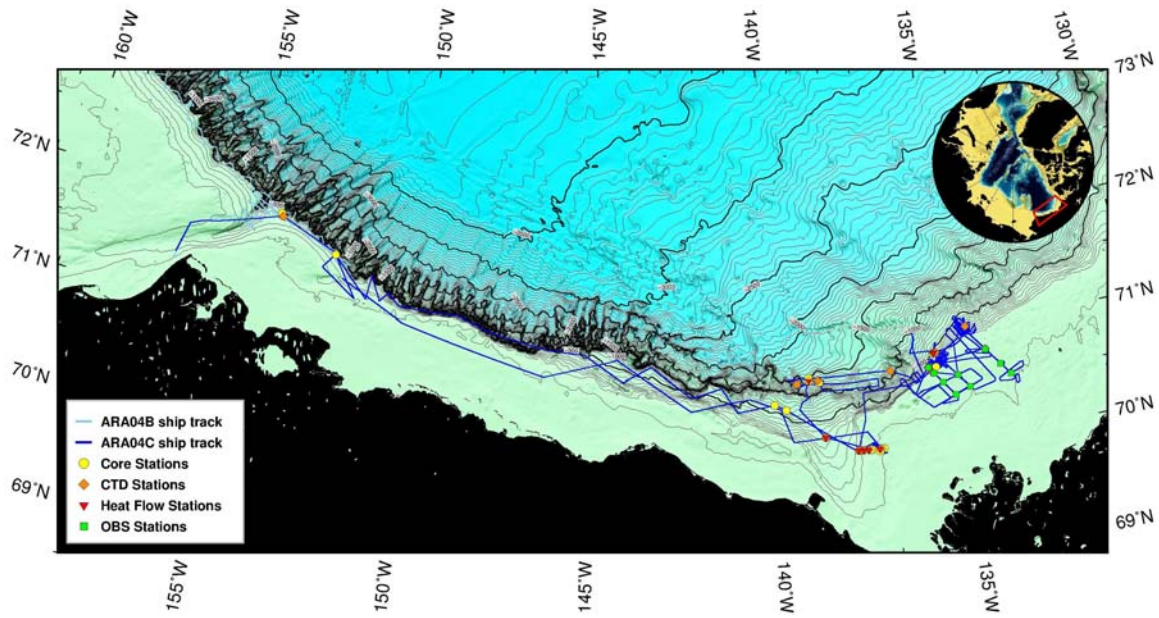

Figure 8.1 Research area map with survey lines for SBP, MB and core sites.

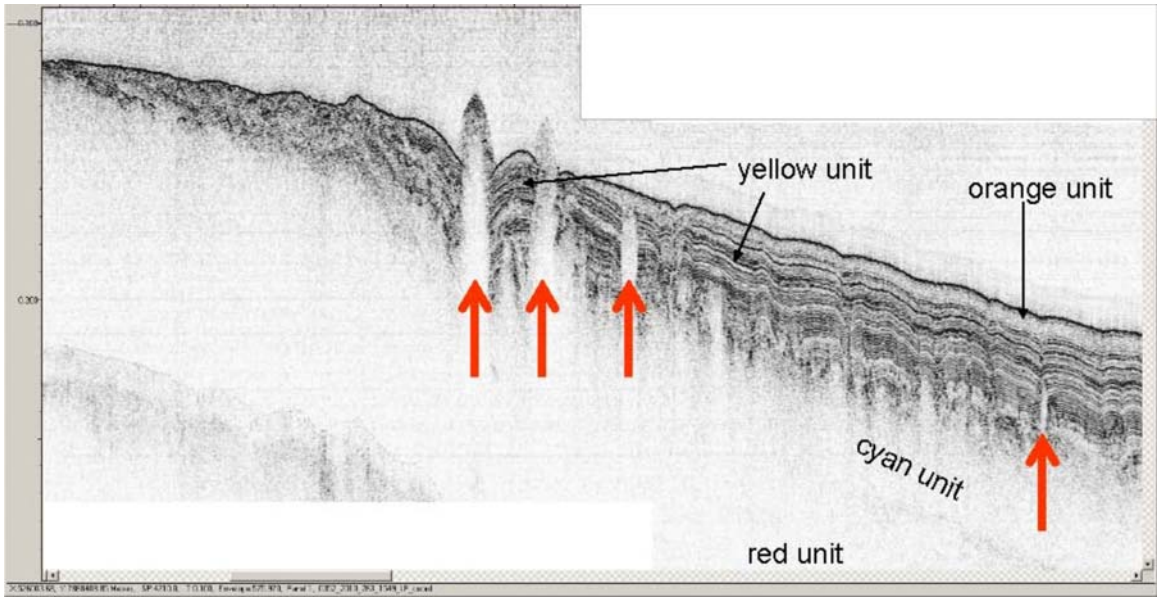

Figure 8.2 Shelf Edge Stratigraphy – tentative seismostratigraphic units have been mapped in much of the study area. Pingo-like features (PLFs) are identified with red arrows.

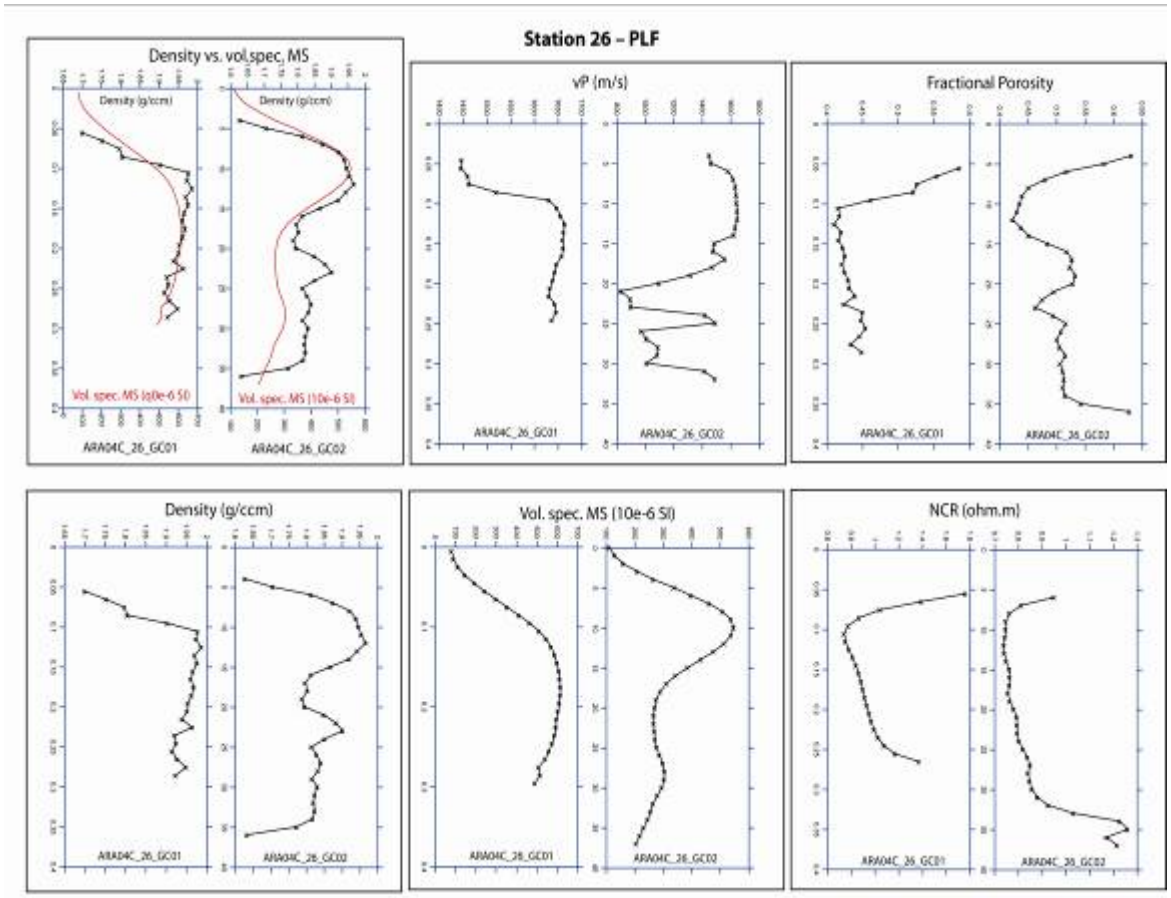

Figure 8.3 Physical properties data from the PLF sampled at Station 26. For a complete explanation and methods see Chapter 9.

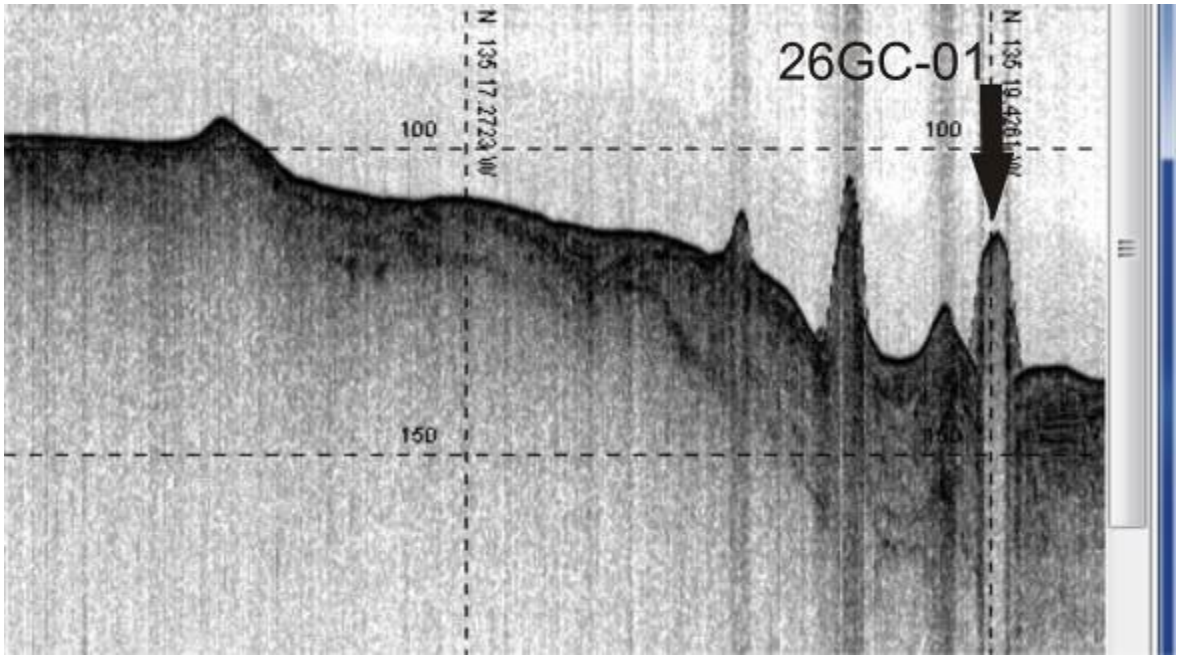

Figure 8.4 PLF core site at the shelf edge.

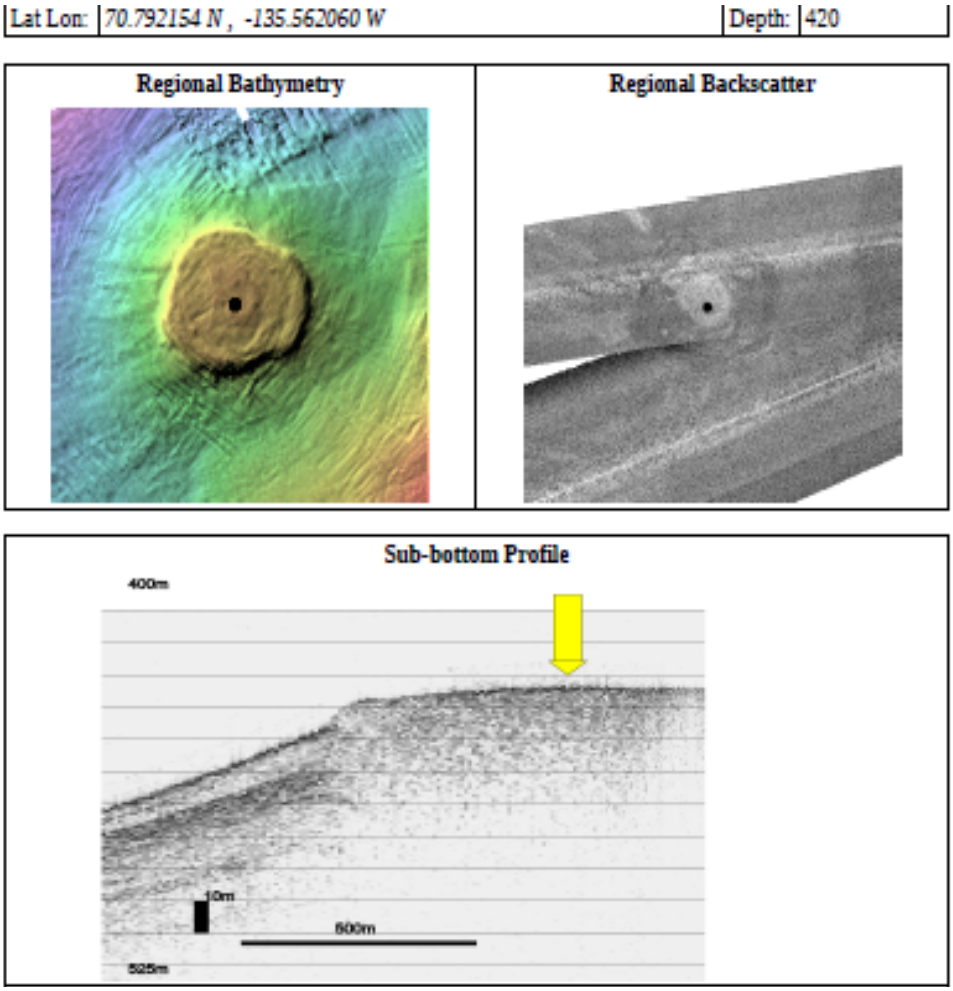

Figure 8.5 The 420 m depth mud volcano was cored, and heat flow data were gathered.

(a)

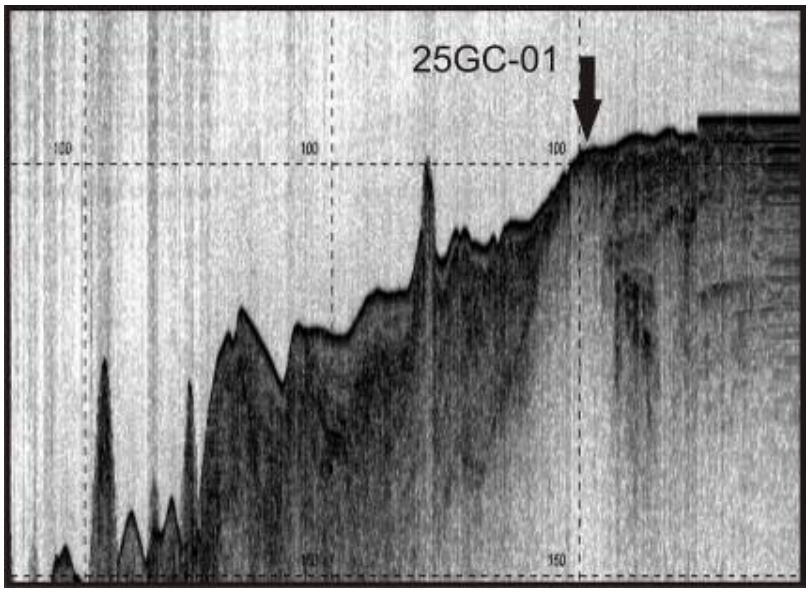

(b)

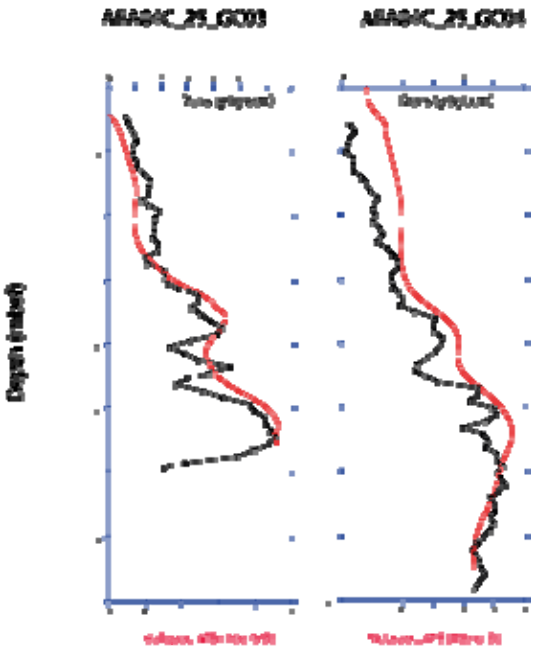

Figure 8.6 (a) The cyan unit was cored at the shelf edge. (b) Density and magnetic susceptibility MSCL data indicate a stiff unit forms the massive white unit in the sub bottom profile (below). Three cores, 26GC-01, 26GC-03 and 26GC-04, were collected at this site.

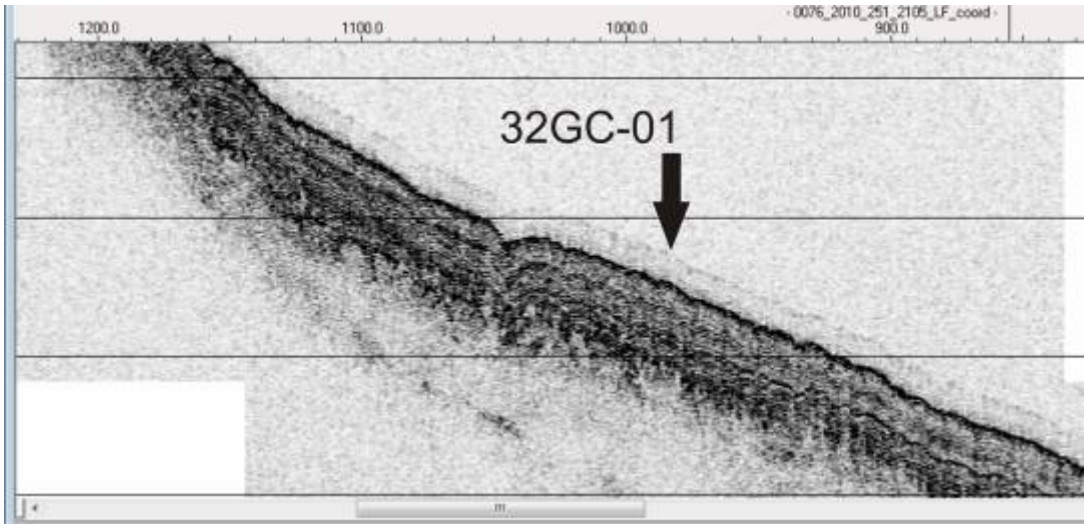

Figure 8.7 The orange unit, which post dates cyan unit deformation, was cored.

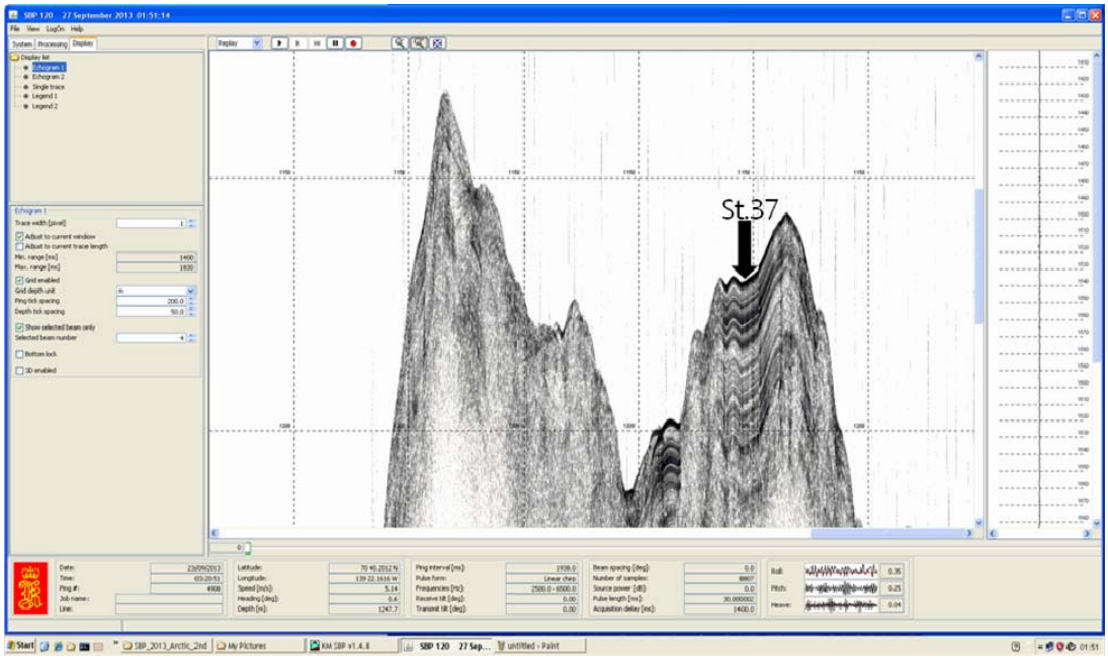

Figure 8.8 Example of SBP records from the topographic highs above abyssal plains of the Mackenzie Trough in 1150 m water depth (geological station for coring site ARA04C-37GC02). This site was selected to support an IODP proposal to recover sediment core for creating a high-resolution time series back to MIS 5.

Table 8.1 Multiple core sampling list and recovery of sediments.

Core	Water depth (m)	Recovery (cm)	Number of sediment cores
01MUC-01	257	ca. 68	8
02MUC-02	235	ca. 43	8
04MUC-01	282	ca. 47	8
07MUC-02	127	ca. 51	8
25MUC-02	75	ca. 28	8
26MUC-03	97	ca. 18	8
27MUC-01	419	ca. 58	8
32MUC-01	260	ca. 47	8
37MUC-01	1173	ca. 57.5	8
38MUC-01	1194	ca. 57.5	8
40MUC-01	331	ca. 59.5	8
43MUC-02	57	ca. 55.5	6

Table 8.2 Recovery of sediments retrieved with gravity corer.

Gravity Cores	Water depth (m)	Recovery (cm)
01GC-02	257	495
02GC-01	235	477
03GC-01	270	415
04GC-02	282	503
05GC-01	87	367
06GC-01	110	371
07GC-01	127	413.5
25aGC-01	76	27.5
25bGC-03	75	59.5
25cGC-04	75	77
26aGC-01	90	26
26bGC-02	107	36
27GC-02	419	281
32GC-02	260	426
37GC-02	1150	595
38GC-02	1190	647.5
39GC-01	1540	357
40GC-02	331	470.5
41GC-01	70	363
42GC-01	55	300
43GC-01	57	496

Table 8.3 Location and suggested unit or area of cores collected during Expedition ARA04C.

	Date UTC	Time UTC	Station number	Latitude North	Longitude West	Station	Comment
1	251	6:35	ARA04C_01MUC001	71°53.9204	154°05.6323	MUC	Barrow
	251	7:35	ARA04C_01GC001	71°53.9198	154°05.6331	GC	Barrow
2	251	9:04	ARA04C_02GC001	71°53.8200	154°05.9600	GC	Barrow
	251	10:05	ARA04C_02MUC001	71°53.8201	154°04.9589	MUC	Barrow
3	251	11:27	ARA04C_03GC001	71°55.3392	154°07.8769	GC	Barrow
4	251	23:14	ARA04C_04MUC001	71°38.0876	152°24.0282	MUC	Barrow
	251	23:57	ARA04C_04GC001	71°38.0880	152°24.0287	GC	Barrow
5	253	18:02	ARA04C_05GC001	69°59.4162	137°44.1724	GC	Mac Trough
6	253	21:48	ARA04C_06GC001	69°59.4699	137°49.0777	GC	Mac Trough
7	254	0:02	ARA04C_07GC001	69°59.002	137°52.0533	GC	Mac Trough
	254	0:43	ARA04C_07MC001	69°59.5002	137°52.0527	MUC	Mac Trough
25	260	15:38	ARA04C_25GC001	70°36.8839	135°38.7390	GC	Cyan Unit
	260	16:20	ARA04C_25MUC001	70°36.8838	135°38.7395	MUC	Cyan Unit
	260	16:48	ARA04C_25GC002	70°36.8840	135°38.7390	GC	Cyan Unit
	260	17:28	ARA04C_25GC003	70°36.8840	135°38.7395	GC	Cyan Unit
26	260	19:05	ARA04C_26GC001	70°39.5936	135°32.8190	GC	PLF
	260	19:57	ARA04C_26GC002	70°39.6012	135°32.7665	GC	PLF
	260	20:41	ARA04C_26MUC001	70°39.5988	135°32.7685	MUC	PLF
27	261	1:44	ARA04C_27MC001	70°47.3696	135°33.9699	MUC	Mud Volcano
	261	2:49	ARA04C_27GC001	70°47.4027	135°33.9012	GC	Mud Volcano
32	263	2:18	ARA04C_32MUC001	70°59.0949	134°36.2802	MUC	Orange Unit
	263	2:56	ARA04C_32GC001	70°59.0951	134°36.2798	GC	Orange Unit
37	266	6:43	ARA04C_37MUC001	70°38.0250	139°22.0587	MUC	IODP/Nam
	266	8:01	ARA04C_37GC001	70°38.0212	139°22.0745	GC	IODP/Nam

	Date UTC	Time UTC	Station number	Latitude North	Longitude West	Station	Comment
38	266	22:25	ARA04C_38MC001	70°39.2052	138°47.4753	MUC	IODP/Nam
	266	23:30	ARA04C_38GC001	70°39.2042	138°47.4775	GC	IODP/Nam
39	267	2:53	ARA04C_39GC001	70°39.3770	139°02.3373	GC	Chevron
40	267	15:52	ARA04C_40MC001	70°08.0316	138°42.0011	MUC	Mac Trough
	267	16:35	ARA04C_40GC001	70°08.032	138°42.001	GC	Mac Trough
41	267	20:24	ARA04C_41GC001	69°59.3243	137°32.7338	GC	Furrows
42	267	22:15	ARA04C_42GC001	69°59.2752	137°16.1569	GC	Unconformity
43	267	23:24	ARA04C_43GC001	69°58.2598	137°13.7940	GC	Garry Knolls
	268	0:06	ARA04C_43MUC001	69°58.2600	137°13.7935	MUC	Garry Knolls

Table 8.4 Headspace and void gas samples

HS: sediment sample for headspace method (3 ml sediment + 2 ml NaCl)

VG: void gas from gravity core

01GC-02 **HS**	
Label	Depth (cm)
01GC-02 (T)	0
01GC-02 (1)	45
01GC-02 (2)	195
01GC-02 (3)	345
01GC-02 (B)	495

01GC-02 **VG**	
Label	Depth (cm)
01GC-02 (A)	260
01GC-02 (B)	307
01GC-02 (C)	365
01GC-02 (D)	445

02GC-01 **HS**	
Label	Depth (cm)
02GC-01 (T)	0
02GC-01 (1)	28
02GC-01 (2)	178
02GC-01 (3)	328
02GC-01 (B)	478

02GC-01 **VG**	
Label	Depth (cm)
02GC-01 (A)	347
02GC-01 (B)	419
02GC-01 (C)	449

02MUC-02 **HS**	
Label	Depth (cm)
02MUC-02 0	0
02MUC-02 10	10
02MUC-02 20	20
02MUC-02 30	30
02MUC-02 40	40

03GC-01 **HS**	
Label	Depth (cm)
03GC-01 (T)	0
03GC-01 (1)	65
03GC-01 (2)	215
03GC-01 (3)	365
03GC-01 (B)	515

03GC-01 **VG**	
Label	Depth (cm)
03GC-01 (E)	245
03GC-01 (D)	309
03GC-01 (C)	372
03GC-01 (B)	451
03GC-01 (A)	495

04GC-02 **HS**	
Label	Depth (cm)
04GC-02 (T)	0
04GC-02 (1)	53
04GC-02 (2)	203
04GC-02 (3)	353
04GC-02 (B)	503

04GC-02 **VG**	
Label	Depth (cm)
04GC-02 (A)	331
04GC-02 (B)	398
04GC-02 (C)	466

04MUC-01 **HS**	
Label	Depth (cm)
04MUC-01 (1)	10
04MUC-01 (2)	20
04MUC-01 (3)	30
04MUC-01 (4)	40

05GC-01 **HS**	
Label	Depth (cm)
05GC-01 (T)	0
05GC-01 (2)	72
05GC-01 (3)	222
05GC-01 (B)	367

06GC-01 **HS**	
Label	Depth (cm)
06GC-01 (T)	0
06GC-01 (2)	77
06GC-01 (3)	227
06GC-01 (B)	371

07GC-01 **HS**	
Label	Depth (cm)
07GC-01 (T)	0
07GC-01 (2)	123
07GC-01 (3)	273
07GC-01 (B)	415

07MUC-02 **HS**	
Label	Depth (cm)
07MUC-02 (1)	0
07MUC-02 (2)	10
07MUC-02 (3)	20
07MUC-02 (4)	30
07MUC-02 (5)	40

25GC-01 **HS**	
Label	Depth (cm)
25GC-01 (B)	25

25GC-03 **HS**	
Label	Depth (cm)
25GC-03 (T)	0
25GC-03 (B)	61

25GC-04 **HS**	
Label	Depth (cm)
25GC-04 (T)	0
25GC-04 (B)	82

26GC-01 **HS**	
Label	Depth (cm)
26GC-01 (B)	26

26C-02 **HS**	
Label	Depth (cm)
26GC-02 (T)	0
26GC-02 (B)	35

27GC-02 **HS**	
Label	Depth (cm)
27GC-02 (2)	140
27GC-02 (3)	145
27GC-02 (4)	170
27GC-02 (5)	195
27GC-02 (6)	220
27GC-02 (7)	245
27GC-02 (8)	260
27GC-02 (B)	283

32GC-02 **HS**	
Label	Depth (cm)
32GC-02 (T)	0
32GC-02 (2)	129
32GC-02 (3)	279
32GC-02 (B)	426

37GC-02 **HS**	
Label	Depth (cm)
37GC-02 (T)	0
37GC-02 (1)	145
37GC-02 (2)	295
37GC-02 (3)	445
37GC-02 (B)	595

38GC-02 **HS**	
Label	Depth (cm)
38GC-02 (T)	0
38GC-02 (2)	47.5
38GC-02 (3)	197.5
38GC-02 (4)	347.5
38GC-02 (5)	497.5
38GC-02 (B)	647.5

39GC-01 **HS**	
Label	Depth (cm)
39GC-01 (T)	0
39GC-01 (2)	87
39GC-01 (3)	237
39GC-01 (B)	387

40GC-02 **HS**	
Label	Depth (cm)
40GC-02 (T)	0

40GC-02 (1)	20.5
40GC-02 (2)	170.5
40GC-02 (3)	320.5
40GC-02 (B)	470.5

41GC-01 **HS**

Label	Depth (cm)
41GC-01 (T)	0
41GC-01 (2)	69
41GC-01 (3)	219
41GC-01 (B)	363

42GC-01 **HS**

Label	Depth (cm)
42GC-01 (T)	0
42GC-01 (1)	150
42GC-01 (B)	300

43GC-01 **HS**

Label	Depth (cm)
43GC-01 (T)	0
43GC-01 (1)	57
43GC-01 (2)	196
43GC-01 (3)	346
43GC-01 (B)	496

Chapter 9 Multi-Sensor Core Logging

M. Schreck , A.H. Quatmann-Hense

9.1 Introduction

Physical properties provide initial core characterization with a very high vertical resolution, and can be used to define and interpret stratigraphic patterns, including a comparison with lithology and other properties such as data obtained from sediment color or XRF scanning. In combination with high-resolution echo sounder profiles obtained by Single-Beam-Profiling (SBP) systems, such as the SBP 120 on the IBRV Araon, down-core pattern of physical properties provide a powerful tool for lateral core correlation.

During Expedition ARA04C, a Multi Sensor Core Logger (MSCL) manufactured by Geotek (UK) was used for high-resolution measurements of density, sonic velocity, magnetic susceptibility and electrical resistivity on whole cores. In the area of investigation, these data allow to physically characterize the sedimentary units of interest, in particular with respect to their role in submarine permafrost degradation, mass wasting processes, and associated sea floor morphology, as well as their potential contribution to geohazards in the Canadian Beaufort. In addition, the physical properties obtained will improve the stratigraphic framework on the Beaufort shelf and slope, respectively, in order to access its complex glacial history.

This chapter briefly describes the acquisition of the data and provides a few examples based on preliminary results. For a more detailed description of the data acquisition the reader is referred to the cruise report of the expedition ARA03B (Kang, 2012) as logging device and procedure were identical with the exception of calibrated resistivity logging during Expedition ARA04C.

9.2 Method and Data Acquisition

Onboard measurements included non-destructive, continuous determinations of core geometry (diameter), temperature, P-wave travel time, gamma-ray attenuation,

magnetic susceptibility and electrical conduction at 10 mm intervals using a standard MSCL track (GEOTEK Ltd., UK, Ser. No. 25). These are then used to calculate the secondary physical properties such as wet bulk density (WBD in g/cm^3), P-wave velocity (Vp in m/s), volume-specific magnetic susceptibility (MS in 10^{-6} SI) and non-contact electrical resistivity (NCR in Ωm). The technical specifications of the MSCL system are summarized in Table 9.1. The principle of core logging is described in more detail in the GEOTEK manual "Multi-Sensor Core Logging", which can be downloaded from the web (www.geotek.co.uk). Gravity cores (GC) were measured in coring liners of up to 1500 mm nominal section length including end caps. In the following, we summarize the data acquisition of the different sensors, data conversion to standard parameters and the calculation of secondary physical properties.

- Geometry: The diameter of the core is measured as the distance between the faces of the Vp-transducers by using rectilinear displacement transducers coupled to the Vp transducers. The core thickness is measured as the deviation from a reference similar in length as the core diameter. The reference (industrial) outside diameter of the KOPRI GC liner is 115 mm. The median wall thickness of KOPRI liners was determined empirically as 2.8 mm (Kang, 2012) resulting in a total wall thickness of 5.6 mm. Three plastic cylinders were used to calibrate the core-diameter logging: 110 mm, 114.95 mm (close to reference), 120.02 mm. Using the Geotek Utility Software A/D readings were obtained from the test panel for each of these cylinders and plotted as a function of the deviation from the reference (-5 mm, -0.05 mm, +5.02 mm). The resulting linear regression is put into the logger settings (www.geotek.co.uk) to log core-thickness deviation in mm saved in the raw data.

- Density: Wet Bulk Density (WBD) was determined from attenuation of a gamma-ray beam transmitted from a radioactive source (^{137}Cs). A collimator was used to focus the radiation through the core-centre into a gamma detector (Table 9.1). To calculate density from gamma counts, Geotek-MSCL software was used (www.geotek.co.uk), which applies a 2nd order polynomial function to describe the relationship between the natural logarithm of gamma counts per second and the product of density and thickness of the measured material. For calibration the three constants of the equation are determined empirically for each day by logging a standard core

consisting of different proportions of aluminum and water as described in Best and Gunn (1999). The data of the standard stair-shaped block of aluminum logged in a liner filled with water are given in Table 9.2.

- Porosity: Fractional Porosity (FP) is the ratio of the total volume over the volume of the pores filled with water. FP determined by MSCL-logging is not an independent data-acquisition parameter but can be calculated from the WBD as follows:

$FP = (\rho_g - WBD) / (\rho_g - \rho_w)$

where ρ_g = grain density ($2.7 g/cm^3$)

ρ_w = pore-water density ($1.03 g/cm^3$).

This approach makes the assumption that grain density and pore-water density are constant.

- Temperature: Temperature (T) was measured as core-surface temperature. The sensor was calibrated using water samples of known temperatures ranging from 17°C to 37°C in a similar way as described for displacement transducers above. Temperature is measured to monitor equilibration of core-temperature with laboratory temperature because some sensors are temperature sensitive.

- Velocity: Sonic Compressional Velocity (Vp) was calculated from the core diameter and travel time after subtraction of the P-wave travel time through the core liner wall (see geometry above), transducer, electronic delay, and detection offset between the first arrival and second zero-crossing of the received waveform (see GEOTEK Manual for details), where the travel time can be best detected. This travel-time offset was determined using a GC-liner filled with freshwater (Vp = 1481 m/s).

- Magnetic Susceptibility (MS): Sensor specifications are summarized in Table 9.1. The meter was set to zero, 100 mm before the core reached the MS sensor. The sensor was checked for possible drift above the top and below the bottom of the core by logging a 250 mm long liner filled with water as initial and final calibration pieces, respectively. In most cases the observed drift was below 1 and remained uncorrected. However, in cores ARA04_25_GC01, ARA04_25_GC03, and ARA04_38_GC02 the drift exceeded this threshold value and a drift correction has been conducted. To calculate volume-specific magnetic susceptibility, data are corrected for loop-sensor and core diameter as follows:

Vol. spec. MS (10^{-6} SI) = measured MS value (10^{-5} SI) / K-rel * 10

with K-rel empirically determined by Geotek (www.geotec.co.uk):

K-rel = $4.8566(d/D)^2 - 3.0163(d/D) + 0.6448$

D is the diameter of the MS-2 meter core loop (140 mm) and d is the reference diameter of the core (109.4 mm, see geometry above). The resulting K-rel used is 1.2532.

- Electrical Resistivity (non-contact, NCR): The NCR technique operates by inducing a high frequency magnetic field from a transmitter coil into the core. In turn, this magnetic field induces electrical currents in the core, which are inversely proportional to the resistivity. Very small magnetic fields regenerated by the electrical current are measured by a receiver coil using a difference technique, which compares the readings generated from the measuring coils to the readings from an identical set of coils operating in air. For calibration after each core-logging run, we logged five 150 mm long containers made from KOPRI GC liners. These containers were filled with water of known salinities (0.35%, 0.7%, 3.5%, 17.5% and 35%, Figure 9.1). The sensor response to these different salinities is expressed in mV. In order to convert sensor response to NCR (Ωm), the measured values are plotted versus known resistivity values for different salinities as outlined in Figure 9.1. The power-law curve fitted to the data reveal a numerical function, which is used to convert the sensor response measured in the sediments to NCR (Ωm). The NCR sensor is zeroed 300 mm before the core reaches the sensor. In a few cases, and for reasons unknown, the NCR sensor responded with strongly negative values in the initial calibration container filled with freshwater. In addition, for some runs, a drift was observed between the calibration values at top and bottom of the core. In these cases we have applied offset and drift corrections to the entire data set so that the conduction in freshwater in the calibration pieces were set to zero (or near zero).

Data acquisition and processing went through several steps:

1. MSCL raw-data acquisition of whole cores using GEOTEK software.

2. First processing of whole-core data using GEOTEK software. This includes the calculation of core thickness, Vp, and WBD. MS and NRC sensor response remained in raw-data state (10^{-5} SI and mV, respectively).

3. Second processing of whole-core data using Kaleidagraph ™ software. This includes a data quality control on calibration sections logged on top and below the bottom of the core (250 mm liner filled with water) and a removal of these data from the core. It also includes the removal of the liner caps from the depth scale and data cleaning for effects caused by liner caps on Vp, WBD and NCR. In addition, MS is converted to volume-specific MS, and the fractional porosity is calculated from the WBD data.

4. Plotting of core data using Kaleidagraph ™ and Adobe Illustrator™.

9.3 Preliminary Results and Conclusions

MS and WBD logs provide nearly complete records in all cores. Thus these parameters offer a good database for core correlation. Minor gaps of data are at or near the end caps of the liner sections. NCR data are largely affected by the end of core sections and were deleted where sensor data drop exponentially to zero. Vp data have gaps of up to 10% mostly because sound propagation was not always possible through the core for reasons not yet known. For cores from Station ARA04C-01 to ARA04C-04, no reasonable Vp data could be obtained due development of abundant expansion (gas) cracks immediately after retrieval from the sea floor. However, in most cases cross-correlations of data pairs of FP and Vp exhibit a negative correlation suggesting the relationship of second order polynomial function. This is similar to results from cores analyzed during the cruise ARA03B last year (Kang 2012). If determined for each individual core these functions may be used to calculate missing Vp data from porosity.

We have selected one core as an example for the definition of different units (PP=physical property units 1 to 3) based on varying behavior of physical properties (Figure 9.2). In unit PP-1 WBD is strongly decreased (and FP increased) compared to the lower units, whereas the MS increases continuously throughout. In unit PP-2, all properties except MS show similar fluctuations towards maximum (minimum) values at

the base of unit PP-2, and exhibit either a negative or positive correlation. While MS remains rather constant at low values throughout most of this unit it increases in the lower part as well. The transition into unit PP-3 is marked by a drastic decrease in WBD, Vp and NCR, whereas the decrease in MS appears to be more continuous across the PP-2/PP-3 boundary. Subsequently, the general pattern of all properties is similar to that observed in PP-2. However, the fluctuations are of higher frequency but lower amplitude in unit PP-3 when compared to the latter. Finally, strongly increasing WBD, Vp and MS (and decreasing FP) characterize lowermost unit PP-4 while NCR is somewhat constant at elevated level.

In order to briefly illustrate how different cores from a particular area can be correlated using physical properties, three cores from the Mackenzie Trough were selected (Figure 9.3). While cores ARA04C-37 and ARA04-38 are located on small ridges to the east and the west of the Trough respectively, ARA04C-39 is located downslope in the trough itself. WBD and MS logs provide almost continuous records in all three cores, thus the combination of both has been used to identify and correlate different pattern laterally. In particular, high WBD associated with spikes in MS or without an increase of MS are good correlation tools as well as a significant deviation of MS and WBD such as observed in the lower parts of cores ARA04-37 and -38.

References

Best, A. I., Gunn, D.E., 1999. Calibration of marine sediment core loggers for quantitative acoustic impedance studies. Marine Geology 160, 137-146.

Kang, S.H., 2012. Cruise Report: RV Araon ARA03B, August 1 – September 10, 2012. Chukchi Borderland and Mendeleyev Ridge. pp. 1–174.

Weber, M.E., Niessen, F., Kuhn, G., Wiedecke, M., 1999. Calibration and application of marine sedimentary physical properties using a multi-sensor core logger, Marine Geology 136, 151-172.

Table 9.1 Technical specifications of the GEOTEK MSCL-25 used during Expedition ARA04C.

P-wave velocity and core diameter Displacement transducer orientation: horizontal Plate-transducer diameter: 40 mm Transmitter pulse frequency: 500 kHz Pulse repetition rate: 1 kHz Received pulse resolution: 50 ns Gate: 5000 Delay: 0 s
Density Radiation beam orientation: horizontal Gamma ray source: Cs-137 (1983) Activity: 356 Mbq (1983) Energy: 0.662 MeV Collimator diameter: 5.0 mm Gamma detector: Gammasearch2, Model SD302D, Ser. Nr. 3043 , John Count Scientific Ltd., 15 s counting time
Temperature Infrared Sensor: MICRON M50-1C-06-L Range: -20° - 300° C Output Voltage: 10 mV
Electrical Resistivity Sensor Type: Geotek Principle: Magnetic Induction Detection Range: 0.1-10 Ωm Resolution: approx. 20 mm
Magnetic susceptibility Loop sensor: BARTINGTON MS-2C Loop sensor diameter: 14 cm Alternating field frequency: 565 Hz, counting time 10 s, precision 0.1 * 10-5 (SI) Magnetic field intensity: ca. 80 A/m RMS Counting time: 10 s

Table 9.2 Thickness and density of Gamma Attenuation calibration liner filled with stair-shaped block of aluminium in water. Density of aluminium: 2.71 g/cm^3, density of water: 0.998 g/cm^3, internal liner thickness along gamma ray: 106.4 mm.

Aluminum Thickness (cm)	**Average Density (g/cm^3)**	**Average Density Thickness (g/cm^2)**
6.58	2.027	22.17
5.76	1.899	20.77
4.93	1.769	19.35
4.12	1.642	17.96
3.29	1.512	16.54
2.48	1.386	15.16
1.65	1.256	13.74
0.93	1.144	12.51
0.00	0.998	10.92

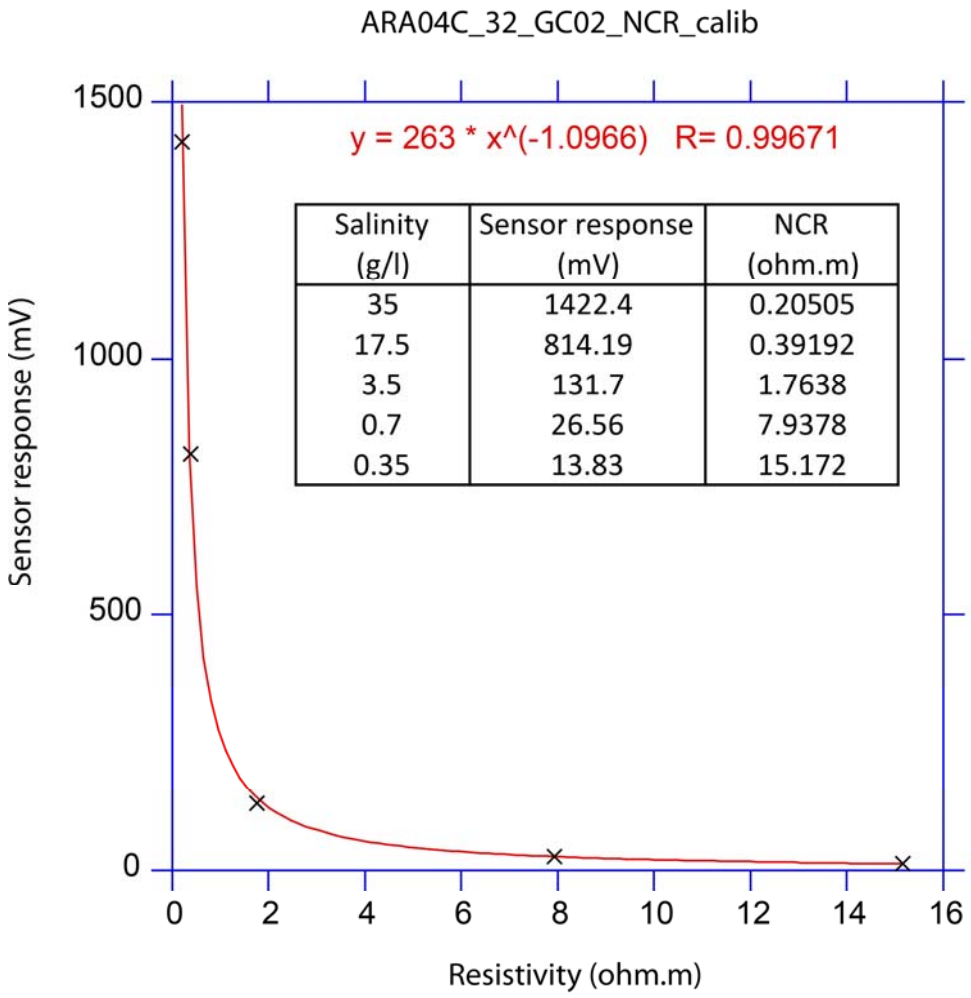

Figure 9.1 Calibration example of non-contact resistivity. Values in the inset table refer to cross symbols in the graph.

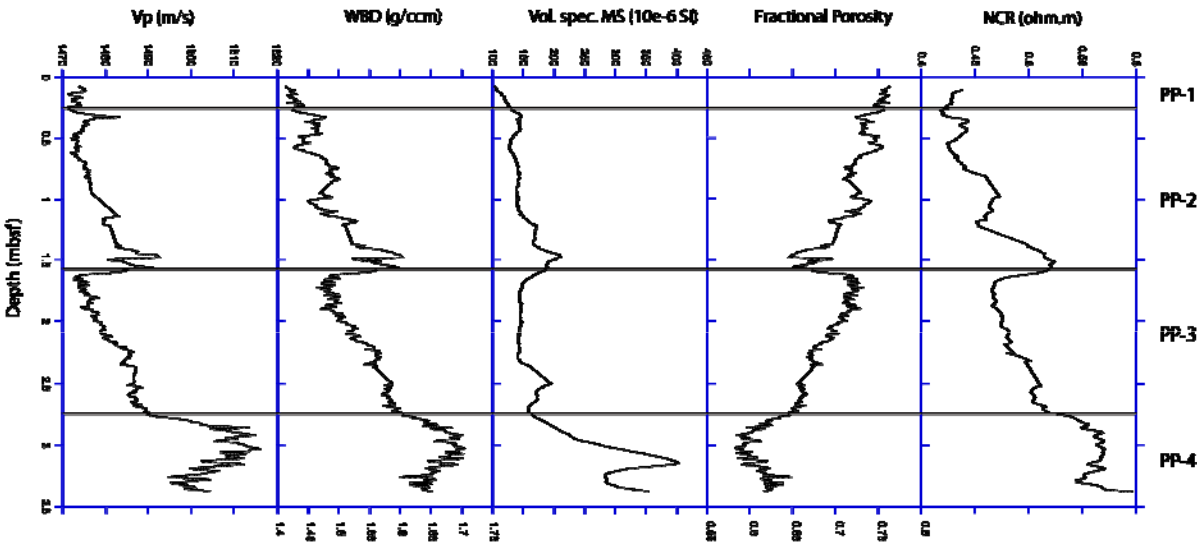

Figure 9.2 Physical property units of core ARA04C-39 from the Mackenzie Trough.

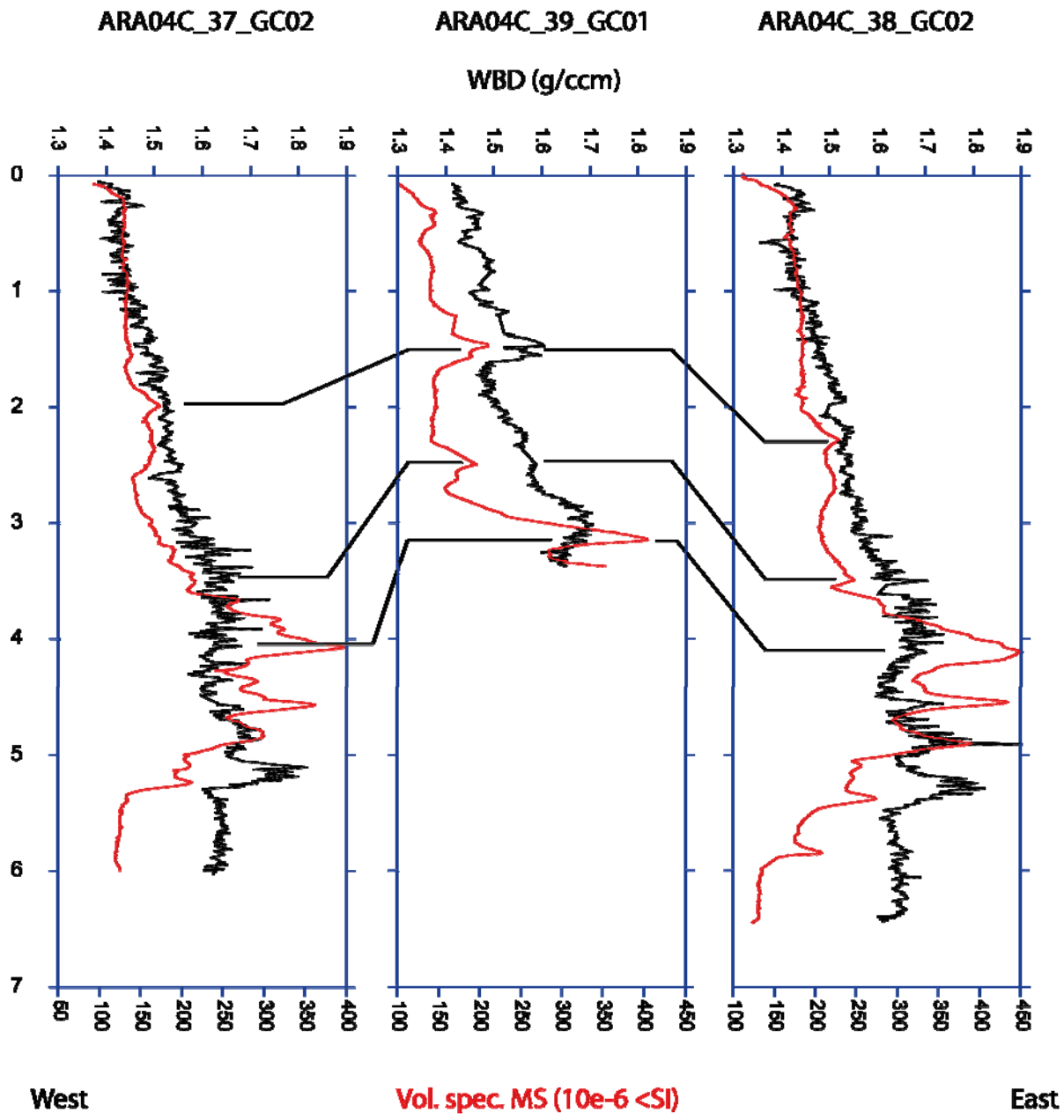

Figure 9.3 Example of core-to-core correlation using magnetic susceptibility and density (preliminary results) for stations 37, 38, and 39 in the Mackenzie Trough.

Chapter 10 Chemical oceanographic study

J. Y. Jung, S. Y. Ha, J. Y. Lee

10.1 Introduction

The Arctic Ocean is currently experiencing rapid environmental change due to natural and anthropogenic factors that include warming temperatures, sea-ice loss, and other physical changes that may result in biological and ecosystem structural changes (Bates and Mathis, 2009). These changes and feedbacks may have profound impacts on the Arctic Ocean marine carbon cycle and alter the global carbon cycle and the balance of carbon dioxide (CO_2) sinks and sources.

Atmospheric CO_2 is absorbed by the ocean or emitted from the ocean to the atmosphere by physical and biological processes. The absorbed CO_2 exists as dissolved inorganic carbon (DIC) in the ocean and is converted by phytoplankton into particulate organic carbon (POC) through photosynthesis. The POC is remineralized by bacteria into dissolved organic carbon (DOC) and/or CO_2. The Arctic Ocean has great potential for uptake of atmospheric CO_2 because of high biological production and low temperature. According to Bate and Mathis (2009), the Arctic Ocean accounts for 5 to 14% of the total ocean CO_2 uptake. However, knowledge about the distribution of CO_2, air-sea CO_2 fluxes and the carbon cycle in the Arctic Ocean is uncertain due to relatively few observations and rapid climate changes. Although the Arctic Ocean takes up atmospheric CO2, other greenhouse gases, such as nitrous oxide (N2O) and methane (CH4), can be released into the atmosphere through nitrification, denitrification, decay of detritus and thawing Arctic permafrost. These processes are also likely positive feedback mechanisms for climate warming. It is unclear whether the decrease in radiative forcing from CO2 uptake is offset by other greenhouse gases or not.

On the Chukchi Sea Shelf, one of the major shelf seas in the Arctic Ocean, particulate production rate is 208 mmol C m–2 d–1 due to the inflow of nutrient-rich North Pacific water through the Bering Strait (Cota et al., 1996; Wheeler et al., 1996) whereas DOC exhibits only minor seasonal variations. Concentration of DOC does not

show a significant seasonal change in surface waters of the Canada Basin (Davis and Bener, 2005) but POC concentration is strongly correlated with chlorophyll-a, indicating a plankton source of freshly produced organic matter. The central Arctic Ocean is a notably low productive area, but DOC concentrations in the surface waters are among the highest in the marine world (Anderson et al., 1998; Bussman and Kattner, 2000). On the other hand, the wide shelves of the Arctic Ocean receive large riverine input, suggesting that terrigenous organic carbon is one of major sources of organic matter, together with autochthonous production. The amount of terrestrial dissolved organic matter exported may increase with enhanced coastal erosion and thawing of permafrost due to global climate change (Serreze et al., 2000). However, the distribution pattern and role of DOC and POC in response to the regional extreme environmental conditions in the Arctic Ocean are rarely defined.

To improve our understanding of biogeochemical cycles of carbon and nitrogen between the ocean and the atmosphere in the Arctic Ocean, the following measurements are acquired during ARA04C: DIC, total alkalinity (TA), partial pressure of CO_2 (pCO_2), DOC, pH of seawater, CH_4, N_2O, and nutrients.

10.2 Method

10.2.1 Seawater sampling

Seawater sampling was carried out at 16 stations over the Beaufort Sea using a CTD/rosette sampler holding 24-10L Niskin bottles (OceanTest Equipment Inc., FL, USA) during the Korean research ice breaker R/V Araon expedition (ARA04C, September 7–September 28, 2013) (Fig. 9.1).

10.2.2 Dissolved inorganic carbon and total alkalinity

Seawater samples for DIC and TA measurements were drawn from the Niskin bottles of the CTD/rosette system into pre-cleaned 500 ml borosilicate bottles. DIC and TA samples were subsequently poisoned with 200 μl of $HgCl_2$ to halt biological activity, sealed, and returned to the Korea Polar Research Institute for analysis. DIC and TA samples will be analyzed using a VINDTA (Versatile INstrument for the Determination of Total Alkalinity) system.

10.2.3 pH of seawater

Seawater samples for pH measurements were drawn from the Niskin bottles into pre-cleaned 150 ml polyethylene bottles. The samples were delivered to the Analytical Chemistry Lab in R/V Araon where the pH of seawater was measured on board using a pH measurement system (Fig. 9.2).

10.2.4 Nutrients

Samples for nutrients (NH_4^+, NO_2^-, NO_3^-, PO_4^{3-}, SiO_4^{2-}) were collected from the Niskin rosette into 50 ml conical tubes and immediately stored in a freezer at −24°C prior to chemical analyses. The samples will be analyzed with standard colorimetric methods using a Quatro Auto Analyzer at the Korea Polar Research Institute.

10.2.5 Underway pCO_2 measurement

The flux of CO_2 across the sea surface is directly proportional to the difference in the fugacity of CO_2 between the atmosphere and the seawater. The fugacity is obtained by correcting the partial pressure of CO_2 (pCO_2) for non-ideality of the gas with respect to molecular interactions between CO_2 and other gases in the air, thus making pCO_2 an important parameter to measure (Pierrot et al., 2009).

To investigate the air-sea exchange rate of CO_2, pCO_2 was monitored in real-time using an automated flowing pCO_2 measuring system (Model 8050, General Oceanics Inc., USA) (Fig. 9.3). The system is compact and operates by directing seawater flow through a chamber (the equilibrator) where the CO_2 contained in the water equilibrates with the gas present in the chamber (the headspace gas). To determine the CO_2 in the headspace gas, it was pumped through a non-dispersive infrared analyzer (LICOR), which measured its CO_2 mole fraction instantaneously, and then returned to the equilibrator thus forming a closed loop. Periodically, atmospheric air was also pumped through the analyzer and its CO_2 mole fraction was measured. The analyzer was calibrated with four CO_2 standard gases at regular intervals.

10.2.6 CH_4 and N_2O measurements

Seawater samples for CH_4 and N_2O measurements were drawn from the Niskin bottles of the CTD/rosette system into glass bottles. 50 ml of N_2 gas was subsequently injected into the glass bottles using a glass syringe to make a headspace. The glass bottles were then put into a water bath (25°C) for more than one hour. To minimize underway data loss, measurements of CH_4 and N_2O concentrations in water column were carried out when the R/V Araon stopped at stations for other work (e.g., core work). 40 ml of the headspace gas was drawn from the glass bottles using a glass syringe, and then injected into a gas chromatograph equipped with a flame ionization detector (FID) and an electron capture detector (ECD) to measure CH_4 and N_2O concentrations in the water column.
During the cruise, underway measurements of CH_4 and N_2O were also carried out along the cruise track. Seawater was pumped into the equilibrator and the headspace gas in the equilibrator was drawn into the gas chromatography system (Fig. 10.4). For one cycle, it takes 40 minutes to analyze CH_4 and N_2O in ambient air and seawater, including calibration gases.

10.2.7 DOC and POC measurements

During the cruise, seawater sampling for DOC and POC was carried out at 11 stations in the Beaufort Sea using a CTD/rosette sampler holding 24-10L Niskin bottles (Fig. 10.5). Water column samples for analysis of DOC and POC were drained from the Niskin bottles into amber polyethylene bottles. DOC samples were collected with pre-combusted (6 hrs. at 450°C) GF/F filters using a nitrogen gas purging system under low (<1.0 atm) pressure (Fig. 10.6). After 20 ml of DOC samples were collected into a pre-combusted amber glass vial, 0.1 ml of $HgCl_2$ was added to the samples to halt biological activity. POC samples were collected using the same procedure as the DOC samples by filtration of known seawater volume. Both DOC and POC samples were stored frozen at –20°C for analysis in the home laboratory.

10.3 Results

The samples for DIC/TA, nutrients, DOC and POC measurements will be analyzed aat the Korea Polar Research Institute. Most dataset require substantial post-processing (e.g. pH of seawater, underway data of pCO_2, CH_4, and N_2O). Therefore, only CH_4 concentration measured at stations 5–9 and 12 will be reported on in this cruise report.

10.3.1 Depth profile of CH_4 concentration

Figure 10.7 shows depth profiles of CH_4 concentration collected at stations 5–9 and 12. CH_4 concentrations increased slightly by 2 ppm from sea surface to about 50 m, and decreased to near zero at 300 m. Although the depth profile of CH_4 concentration showed similar distributions in the upper 300 m of all stations, CH_4 concentration sharply increased by 7 ppm at 410 m at station 12 where a mud volcano was forming. This result suggests that CH_4 gas is being released at this station and possibly at other similar features in the region.

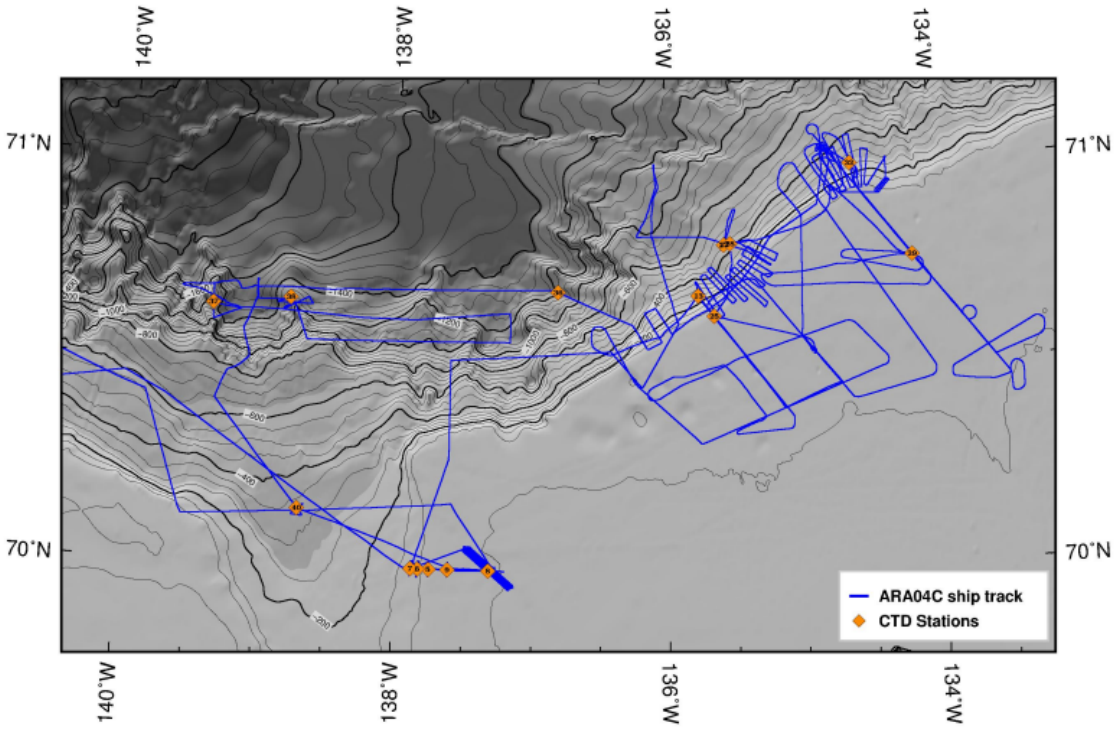

Figure 10.1 Seawater sampling stations and cruise track during the cruise.

Figure 10.2 pH measurement system.

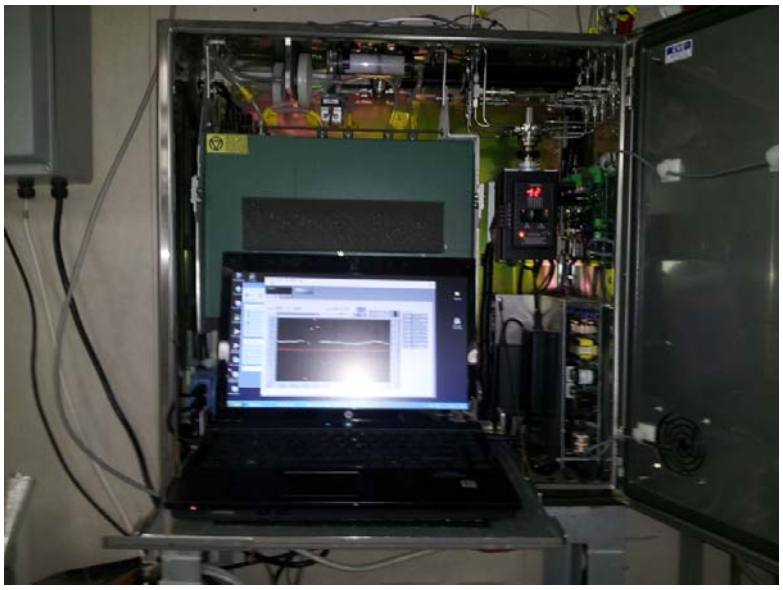

Figure 10.3 Automated flowing pCO_2 measuring system.

Figure 10.4 Gas chromatography system for measurements of CH_4 and N_2O.

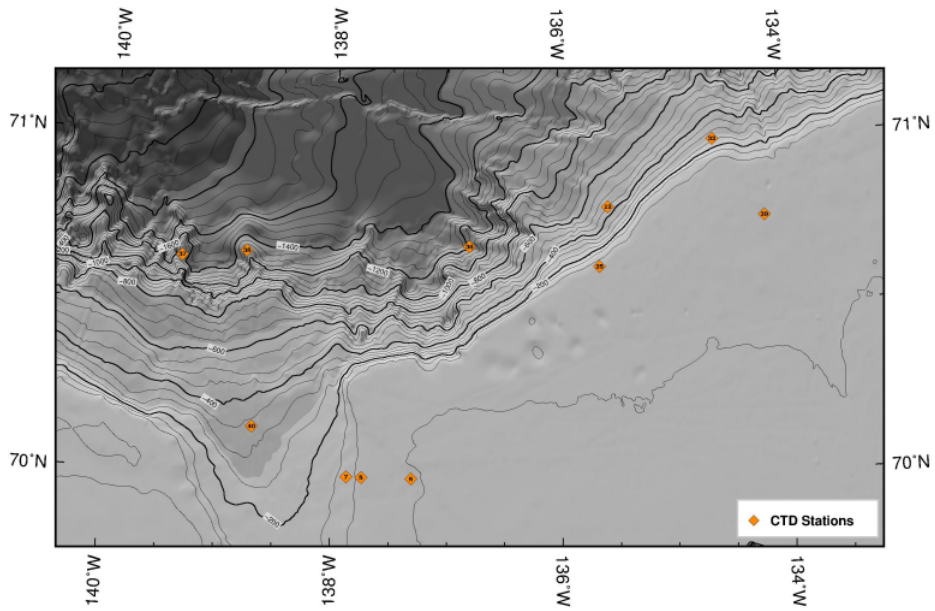

Figure 10.5 DOC and POC sampling stations during the cruise.

Figure 10.6 Nitrogen gas purging system for collecting DOC and POC.

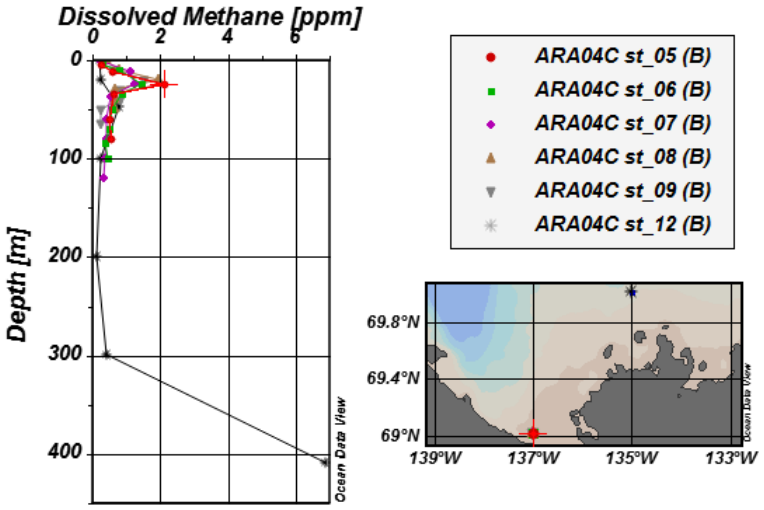

Figure 10.7 Depth profiles of CH_4 concentrations at stations 5–9 and 12.

References

Anderson, L, G., Olsson, K., Chierici, M., 1998. A carbon budget for the Arctic Ocean. Global Biogeochem. Cy., 12(3): 455–465.

Bates, N. R., Mathis, J. T., 2009. The Arctic Ocean marine carbon cycle: evaluation of air-sea CO2 exchanges, ocean acidification impacts and potential feedbacks. Biogeoscience, 6, 2433–2459.

Bussman, I., Kattner, G., 2000. Distribution of dissolved organic carbon in the central Arctic Ocean: the influence of physical and biological properties. J. of Marine System, 27:209–219.

Cota, G, F., Pomeroy, L. R., Harison. W. G., Jones, E. P., Peters, F., Sheldon Jr., W. M. Weingartner, T. R., 1996. Nutrients, primary production and microbial heterotrophy in the southeastern Chukchi Sea; arctic summer nutrient depletion and heterotriphy. Mar. Ecol. Pro. Ser., 135:247–258.

Davis, J., Benner, R., 2005. Seasonal trends in the abundance, composition and bioavailability of particulate and dissolved organic matter in the Chukchi/Beaufort Seas and western Canada Basin. Deep-Sea Res., 52:3396–3410.

Pierrot, D., Neill, C., Sullivan, K., Castle, R., Wanninkhof, R., Luger, H., Johannessen, T., Olsen, A., Feely, R. A., Cosca, C. E., 2009. Recommendations for autonomous underway pCO2 measuring systems and data-reduction routines. Deep-Sea Res., 56:512–522.

Serreze, M., Walsh, J. E., Chapin, F. S., Osterkamp, T., Dyurgerov, M., Romanovsky, V., Oechel, W. C., Morison, J., Zhang, T., Barry, R. G., 2000. Observational evidence of recent change in the northern high-latitude environment. Clim. Change. 46: 159-207.

Wheeler, P. A., Gosselin, M., Sherr, E., Thibault, D., Kirchman, D. L., Benner, R., Whitledge, T. E., 1996. Active cycling of organic carbon in the central Arctic Ocean. Nature 380:697–699.

Chapter 11 Atmospheric observations

J. Yoo, G. Kim

11.1 Introduction

The Arctic is a critical region of the Earth, highly sensitive to small environmental changes in the Earth's climate and having a complex feedback system (Behrenfeldt et al., 2008). The highest increase of annual mean temperature was observed in the Arctic, and the warming rate in the Arctic during the last century is almost two times higher compared to the rest of the world (ref). The warming trend may be explained by a global increase in greenhouse gas concentrations or changes in the Arctic carbon budget. Kort et al. (2012) reported high methane concentrations over open regions with partial sea-ice cover obtained by airborne measurements in the Arctic Ocean. This observation suggests that a significant decrease in ice cover of the Arctic Ocean may induce augmented emissions of methane. Semiletov et al. (2007) also suggested that sea-ice melting ponds and open channels may change the dynamics of carbon cycling between the atmosphere and the ocean. Summer sea ice coverage in the Arctic Ocean has been steadily decreasing since 1997, with the lowest ice coverage recorded in 2012 (reference needed). However, the impact of the reduced ice cover on the global climate through the modification of the energy and carbon cycles is not yet fully understood And highlights the need for continuous, on-site observations of atmospheric parameters in the Arctic Ocean.

The transport of anthropogenic light absorbing carbonaceous particles from lower latitudes may also be responsible for the Arctic warming trends seen in recent years. Typically, aerosols play a decisive role in the radiation balance by scattering or absorbing incoming solar light and influence cloud formation by acting as cloud condensation nuclei (CCN). For instance, black carbon (BC), which absorbs solar radiation, has the second largest influence on global warming following greenhouse gases (Jacobson, 2002).

Ship-based atmospheric observations provide important records and contribute to the global database of gas concentrations in the Arctic Ocean. The IBRV Araon has various atmospheric observation instruments on board. Atmospheric observations

onboard the Araon include monitoring basic meteorological parameters such as wind, air temperature, and pressure, as well as observations of greenhouse gases (carbon dioxide, water vapor, and methane), and aerosols. In addition, the vessel also is equipped with an eddy covariance system to calculate scalar fluxes at the sea-air interface during the vessel's voyage. For aerosol observations, measurements of hygroscopicity, volatility, and particle size distribution were conducted. Light scattering coefficient, number concentration, and mass of the Arctic aerosols were also measured including concentration of black carbon. In addition, aerosols smaller than 2.5 μm were sampled for off-line morphological and elemental analyses (transmission electron microscopy (TEM)/energy dispersive spectroscopy (EDS)) to better understand morphology and mixing state of particles. An overview of the atmospheric observations made during Expedition ARA04C are shown in Figure 11.1.

11.2 Materials and methods

11.2.1 Observations made from Radar Mast

Observations made from the radar mast of the ship include air temperature and relative humidity (HMP45D, Vaisala, the Netherlands), air pressure (PTB100, Vaisala) and downward short-wave (PSP, Eppley, USA) and long-wave radiation (PIR, Eppley) (Figure 11.2). Measurements are taken at an average height of 38 m from the water surface. The data logger (CR3000, Campbell Scientific, Inc., USA) scans each sensor every 10 seconds and saves average values of each scan every 10 minutes. The computer in the Atmospheric Sciences Laboratory retrieves the data from the data logger on a regular basis. These data are shared through an onboard webpage (Figure 11.3).

11.2.2 Observations on Foremast and Bow

On the foremast, a windmill anemometer (05103-L, RMYoung, USA) measures wind speed and direction at an average height of 29.8 m from the water surface (Figure 11.4). The data logger (CR3000, Campbell Scientific) in the CRDS container (on Deck 2) collects wind data from wind vane anemometer every 10 seconds to calculate half-hourly average wind speed and relative wind direction values. The relative wind regime is corrected to true value considering ship’s course and speed.

At the bow of the ship, the eddy covariance system was deployed to measure heat and scalar fluxes of carbon dioxide and methane during the cruise (Figure 11.5). The eddy covariance method is used to calculate scalar fluxes through turbulent transport at a reference plane using observation of vertical wind motion and scalar's fluctuation. The Araon's eddy covariance system consists of a sonic anemometer (CSAT3, Campbell Scientific, Inc.) and two gas analyzers. The first instrumentis an infra-red gas analyzer (LI7500, Li-cor, USA) measuring molar density of carbon dioxide and water vapor at high sampling rate. This instrument is installed next to the sonic anemometer. The other instrument is a wave-scanned cavity ring-down spectroscopy analyzer (CRDS, G2301-f, Picarro Inc., USA) (Figure 11.6). CRDS is placed in the shelter on the 2nd deck. Air samples taken at the measurement point of sonic anemometer travel through a tube (3/8 inch) to the CRDS. Flow rate of sampled air in the tube is maintained to ensure turbulent flow (Hong *et al*., 2000). The CRDS was operated in CH_4-H_2O mode. In order to capture chaotic motion of the eddy, these instruments measure each component at high sampling rate of 10 Hz. These data were collected in the data logger of CRDS shelter then sequentially transferred to the computer in the Atmospheric Sciences Laboratory. The instruments are mounted on the movable platform at the bow. The platform was moved ~3 m away from the vessel on September 7, 2013, at the beginning of the cruise (Figure 11.7). Figure 11.8 shows the overview of the signal flow of the eddy covariance system on Araon. To acquire the final product, the dataset goes through several correction steps including density correction, frequency-response correction, and motion correction as post-processes. Details on the post-processes are not included since it is beyond the scope of this report.

As a component of the eddy covariance system, two motion sensors (MotionPakII, BEI, USA) are deployed (one motion sensor in CRDS shelter is not updated in Figure 11.8). One is next to sonic anemometer to monitor the motion of the platform as well as sensors itself. The other is placed in the CRDS shelter to monitor vibration of the ship as a reference. Motion data will be used to correct apparent wind regime due to movement and vibration of the ship using the navigation data. Along with the eddy covariance system, a net radiometer (CNR1, Kipp and Zonen, the Netherlands) is installed at the bow. CNR1 measures four components of radiation, incoming and out-going, short- and

long-wave radiation (Figure 11.5). Radiation data were saved in the data logger in the CRDS shelter with other meteorological data.

11.2.3 LIDAR

Atmospheric boundary layer processes, aerosol, and cloud cover are important factors in polar climate processes. An on board elastic LIDAR system was operated to measure the profile of aerosol (Figure 11.9). The LIDAR tool is located at the middle of the vessel on the 4th Deck. It operates for 120 seconds per data-point on a half-hourly basis.

11.2.4 Aerosol Observations

The aethalometer (AE, Magee Scientific, USA) collects a sample (flow rate of 5 LPM) on a quartz fiber filter tape, and performs a continuous optical analysis for the quantification of black carbon emitted from the combustion from which the mass concentration (ng/m^3) of black carbon can be calculated (Figure 11.10a). When the optical particle counter is collecting data (OPC, #365, GRIMM Aerosol Technik, Germany), the sample passes through the measuring cell, past the laser diode detector and is collected onto a filter (Figure 11.10b). During the measurement process all particles are categorized in their proper size. The measurements are determined as mass concentration (μg/m^3). These measurements are reported for the various size distribution channels. In addition, the number concentrations (#/cm^3) of aerosols were determined in real-time by using two condensation particle counters (CPC, CPC 3772 and CPC 3776, TSI, USA, figure 11.10(C)). The nephelometer (3563, TSI, USA) measures the angular integral of light scattering that yields the quantity called the scattering coefficient, used in the Beer-Lambert Law to calculate total light extinction (Figure 11.10d). Also, continuous measurements of size distributions were measured using differential mobility particle sizer (DMPS), which consists of a differential mobility analyzer (DMA) and a condensation particle counter (CPC). The hygroscopicity and volatility tandem differential mobility analyzer (HVTDMA) technique was employed to measure hygroscopicity and volatility of aerosols (Figure 11.11). The HVTDMA system consists of two DMAs, a heated tube, a humidifier, and a CPC (TSI 3010, USA). Particles of a

certain size were selected by the first DMA, and were directed into a heated tube or humidifier, subsequently being routed to the second DMA and CPC to determine particle size change under increased temperature (~100℃) or elevated relative humidity (RH) (~85%). This provides the hygroscopic growth factor (GF) and shrinkage factor (SF) at a given RH and heater temperature, respectively. The GF represents a ratio of particle mobility diameter at elevated RH to that at dry condition (10~15% RH), while the SF is a ratio of particle mobility diameter at an increased temperature (100℃) relative to room temperature (~25℃). Lastly, aerosols smaller than 2.5 μm were collected on the TEM grid by using the impactor (cutoff diameter of 2.5 μm). All these observations were conducted on a daily basis according to the schedule (Table 11.1)

11.3 Expected result

11.3.1 Meteorological condition

Figure 11.12 shows meteorological conditions during the expedition (from the top panel, air temperature, air pressure, relative humidity, apparent wind speed and relative wind direction). Air temperature (*Ta*) during the cruise ranged from -5.6°C to 7.4°C with average of 0.0°C. Due to the location of sensor, some data may be affected by direction. Since the funnel of the ship is located at 210 degrees relative to the temperature sensor, caution should be used with temperatures data recorded during wind direction of around 210°. Air pressure (*P*) ranged from 98.0kPa to 102.2kPa with average of 100.5kPa. The lowest P values were recorded on September 22, 2013, and strong wind and high swell were observed. Relative humidity (*RH*) ranged from 74.5% to 97.8% with average of 94.1%, which is generally drier than during the previous Arctic expedition (ARA03B). During the previous expedition some sensors suffered from frequent freezing, especially the open-path gas analyzer and sonic anemometer. However, the frequency of blockage of sensor paths by ice dropped significantly during Expedition ARA04C. Due to bad weather usually accompanying rain and snow, many data points may have to be filtered out in the quality control process. Interference with combustion gas is suspected and extra caution has to be paid when using temperature and relative humidity data. Maximum wind speed (*WS*) of 17.5 m/s was recorded on September 10, 2013. However, overall

wind speed was around 9.1 m/s with a standard deviation of 3.7 m/s. Due to ship's movement, relative wind directions (*WD*) plotted within 330° to 030°. True wind direction and speed will be calculated considering the ship's course and speed after the expedition.

11.3.2 Methane, carbon dioxide and water vapour measurements

During the transit from Barrow to Nome, the CRDS was operated in CH_4-H_2O mode in the CRDS shelter as a part of eddy covariance system (Crosson, 2008; Figure 11.13). The methane concentration level was relatively steady during the expedition, except at the beginning and on September 21, 2013 (Figure 11.14). A peak, CRDS value of 2.13 ppm was recorded on September 21, 2013. Further investigation on the peak on that day is in progress, but it is hypothesized that the peak value is a result of some terrestrial influence as the vessel was close to land. The average methane concentration during the cruise was 1.88ppm (±0.04ppm). Water vapor concentration measured by CRDS ranged from 3.6mmol/mol to 9.9mmol/mol and the average during the expedition was 5.6mmol/mol (±1.04mmol/mol), while water vapor concentrations by LI7500 ranged from 1.6mmol/mol to 10.0mmol/mol. The agreement of the two water vapor concentrations is poor ($R^2 = 0.68$). The disagreement can be explained by the fact that the LI7500 is more susceptible for environmental condition because sensor detector is exposed to the environment. Carbon dioxide concentration by LI7500 also suffered from interference of environmental condition like water vapor. Retrieval rate of LI7500 data was 38% due to frequent precipitation and cold air temperature conditions. It was lower than the value obtained by CRDS, which was 95%. The average carbon dioxide concentration during the cruise was 388.4ppm (±15.9ppm)

11.3.3 Eddy covariance system

Eddy covariance is a direct measurement system of the air-sea turbulent fluxes of momentum and sensible and latent heat. The two main aims of the present deployment were 1) to continuously measure a suite of key meteorological variables (such as wind speed and direction, air temperature, and humidity, radiation and air pressure) and 2) to

measure directly the air-sea fluxes of CO_2 and CH_4, sensible heat, latent heat and momentum. The new platform for eddy covariance system was installed at the bow in June 2013A motion sensor, measuring three accelerations and three angular rates, is needed for on board eddy covariance flux measurement due to the ship motion. A motion sensor is installed near the sonic anemometer to capture the motion of the anemometer. Motion correction will be applied through a MatLab code every 30 minutes (Miller et al., 2008), and motion corrected data will be saved for further onshore analysis. However, more than 50% of the data are expected to be filtered out during quality control.

Figure 11.15 shows wind speeds measured by the sonic anemometer (CSAT) at the bow and by the windmill anemometer (RMY) at the foremast. Wind speeds are binned against relative wind direction and error bars indicate standard deviation of wind speed within each bin. These two instruments are installed at different heights and flow distortion effects from the ship's body may affect the data. However, as noted previously, more than 70% of the wind records from sonic anemometer were filtered out because of bad weather conditions, and the remaining data may not be sufficient to draw a significant conclusion. The calculation of the eddy flux is a time-consuming process incorporating the integration of eddy covariance measurements (such, wind, scalar fluctuation), motion information (3-axis acceleration and angular rates) and navigation data (course and speed of the ship), therefore it will be processed post-cruise.

11.3.4 LIDAR

Atmospheric boundary layer processes, aerosol, and clouds are important factors in polar climate processes. On board, an elastic LIDAR was operated to measure the profile of aerosols. Figure 11.16 shows one example of the measurements (range-corrected backscatter signal) of the LIDAR during the expedition. Further analysis on the data will be carried out post-cruise.

11.4 Summary and conclusions

During Expedition ARA04C, most of meteorological instruments operated stably. However, the open-path analyzer and sonic anemometer were suffering from poor weather condition (rain, fog), resulting in low retrieval rates. The CRDS operated stably in CH_4-H_2O flux mode to quantify methane flux. Further analysis including motion correction is required to acquire flux values. Despite the importance of direct atmospheric observation at sea, many challenges still exist to acquire good quality, continuous data, including ship motion, low temperatures, and sea spray. Aerosol measurements will continue until October 14, 2013, on the voyage to Korea crossing the Pacific.

References

Behrenfeldt, U., Krejci, R., Ström, J., Stohl, A., 2008. Chemical properties of Arctic aerosol particles collected at the Zeppelin station during the aerosol transition period in May and June of 2004. Tellus, Series B: Chemical and Physical Meteorology 60 B:405-415.

Crosson, E.R., 2008. A cavity ring-down analyzer for measuring atmospheric levels of methane, carbon dioxide, and water vapor, Applied Physics B, 92, 403–408.

Hong, J, Kim, J., Choi, T., Yun, J., Tanner, B., 2000. On the effect of tube attenuation on measuring water vapor flux using a closed-path hygrometer, Korean Journal of Agricultural and Forest Meteorology, 2(3), pp. 80–86.

Jacobson, M. Z., 2002. Control of fossil-fuel particulate black carbon and organic matter, possibly the most effective method of slowing global warming, Journal of Geophysical Research D: Atmospheres 107(19).

Kort, E. A., Wofsy, S. C., Daube, B. C., Diao, M., Elkins, J. W., Gao, R. S., Hintsa, E. J., Hurst, D. F., Jimenez, R., Moore, F. L., Spackman, J. R., Zondlo, M. A., 2012. Atmospheric observations of Arctic Ocean methane emissions up to 82° north, Nature Geoscience, 5,318–321.

Miller, S.D., Hristov, T.S., Edson, J. B., Friehe, C. A., 2008. Platform motion effects on measurements of turbulence and air-sea exchange over the open ocean, Journal of Atmospheric & Oceanic Technology, 25(9), 1683–1694.

Semiletov, I. P., Pipko, I. I., Repina, I., Shakhova, N. E., 2007. Carbonate chemistry dynamics and carbon dioxide fluxes across the atmosphere–ice–water interfaces in the Arctic Ocean: Pacific sector of the Arctic, Journal of Marine Systems, 66, 204–226.

Table 11.1 Time interval for daily measurement

Time	Measurement	Time	Measurement
08:00-09:00	DMPS	13:00-16:00	HVTDMA
09:00-11:00	HVTDMA	16:00-17:00	DMPS
09:00-12:00	TEM/EDS sampling	19:00-20:00	DMPS
11:00-12:00	DMPS	20:00-21:00	HVTDMA
12:00-13:00	DMPS	21:00-22:00	DMPS

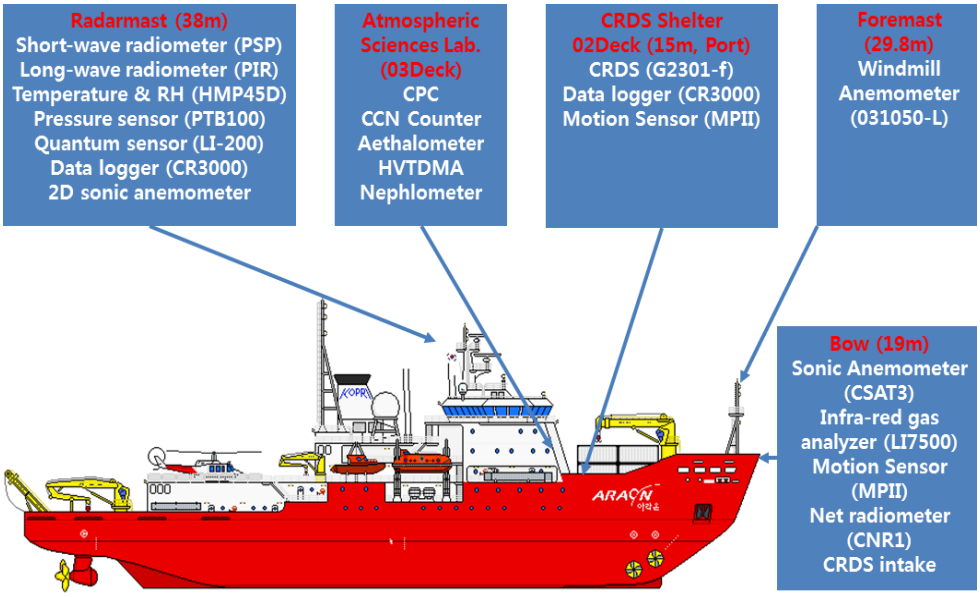

Figure 11.1 Overview of atmospheric observations on the IBRV Araon.

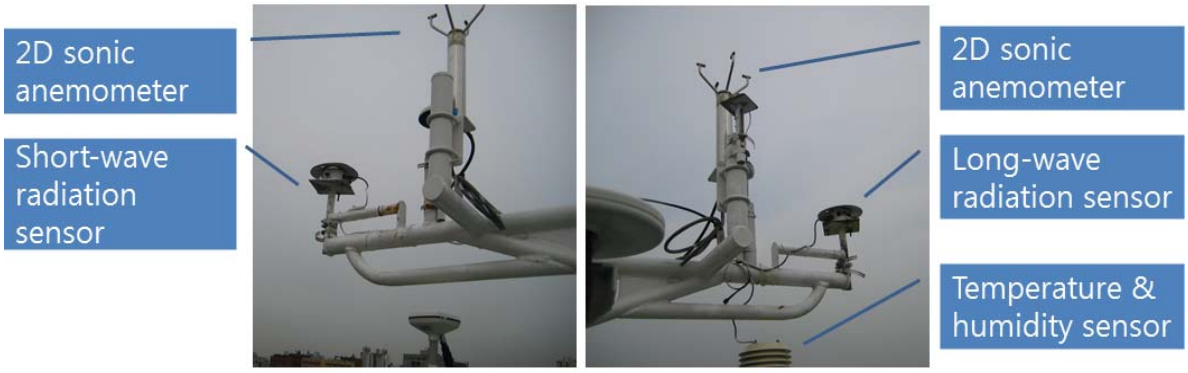

Figure 11.2 Instruments located on the radar mast of the Araon. Note that 2D sonic anemometers provide wind information for the cruise only.

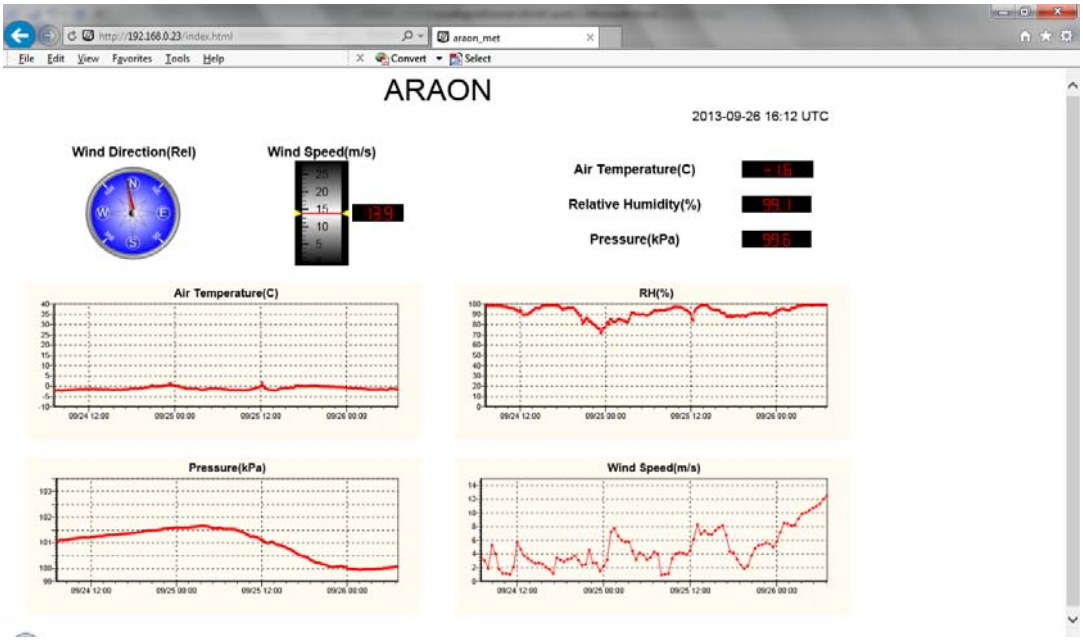

Figure 11.3 Webpage to announce meteorological data

Figure 11.4 Windmill anemometer at the foremast of Araon

Figure 11.5 Instruments at the bow of Araon.

Figure 11.6 Cavity ring-down spectroscopy analyzer in the shelter.

Figure 11.7 Movable platform of instruments at the bow.

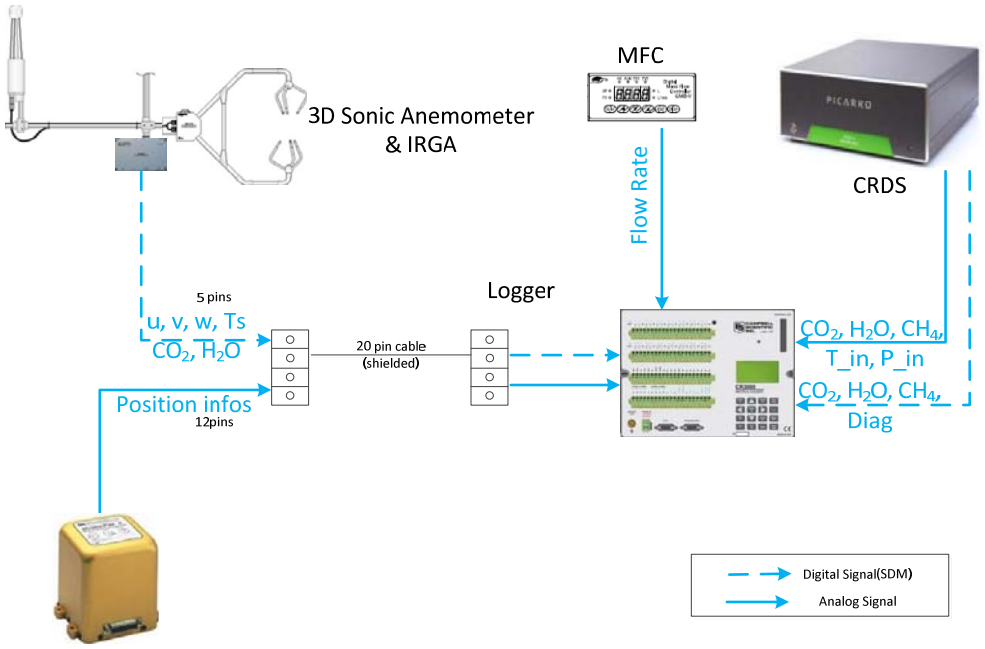

Figure 11.8 Overview of signal flow in Araon eddy covariance system.

Figure 11.9 LIDAR system.

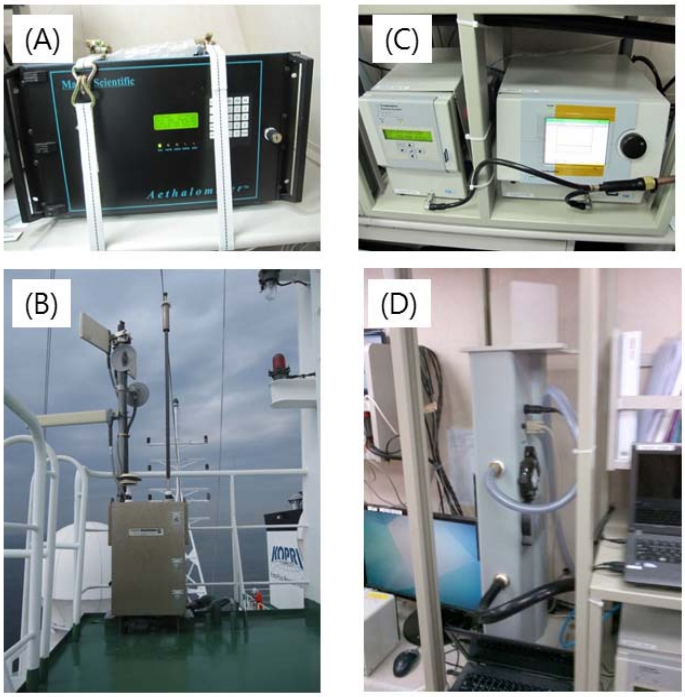

Figure 11.10 Aerosol measurement instrumentation on the Araon: (a) Aethalometer, (b) Optical Particle Counter (OPC), (c) Condensation Particle Counters (CPC3772 and CPC3776), and (d) Nephelometer.

Figure 11.11 HVTDMA system operated on the Araon.

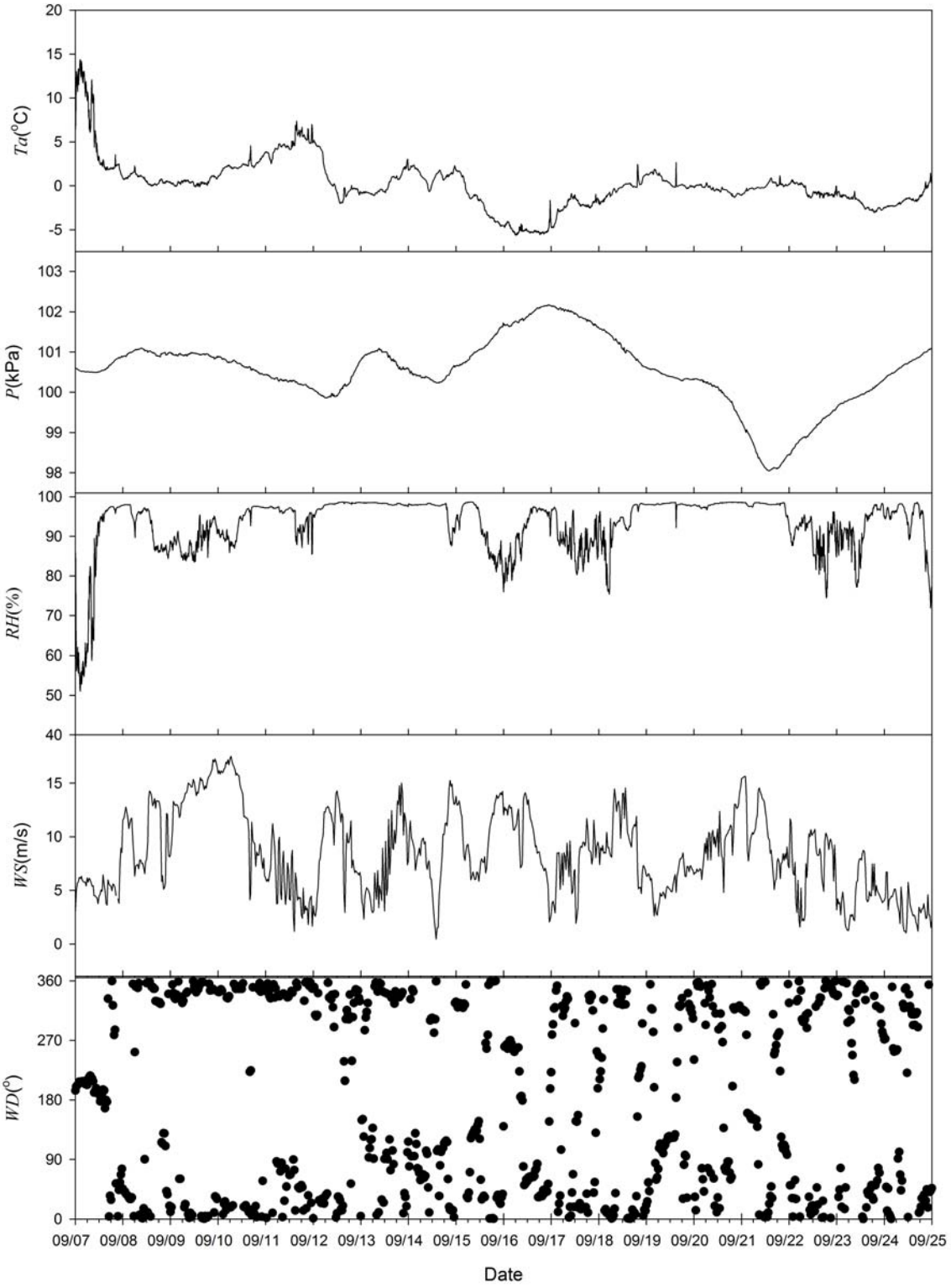

Figure 11.12 Meteorological variables acquired during Expedition ARA04C.

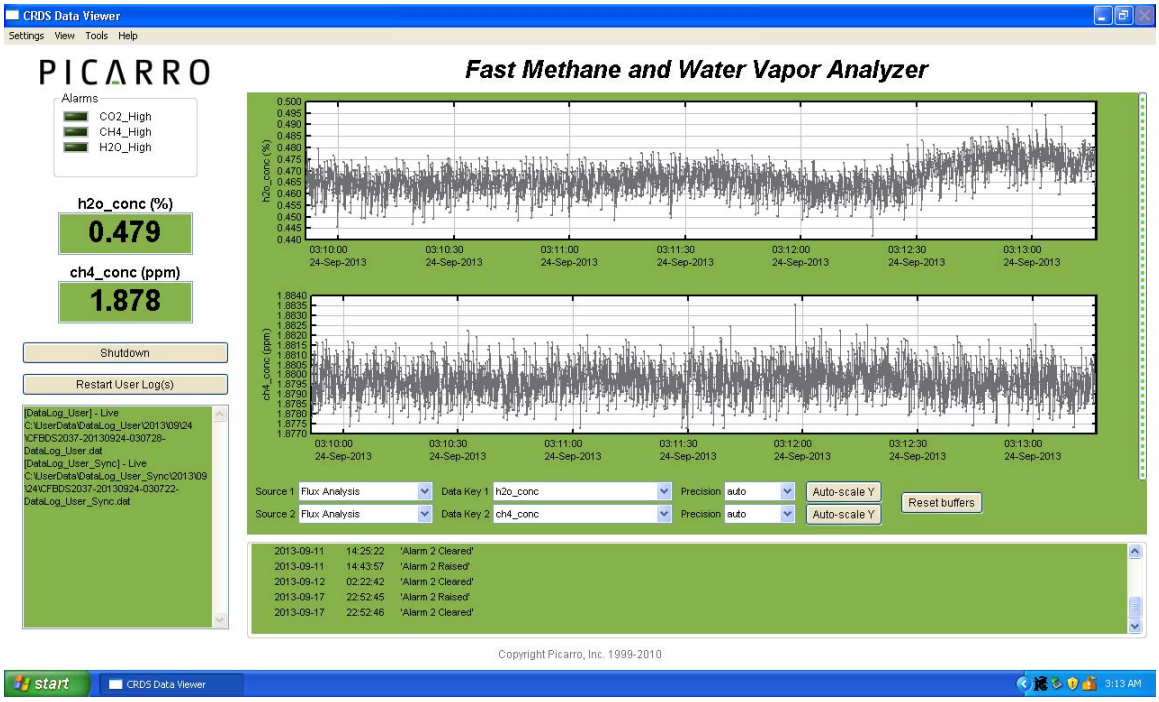

Figure 11.13 Real-time monitoring of CH_4 and H_2O in flux mode.

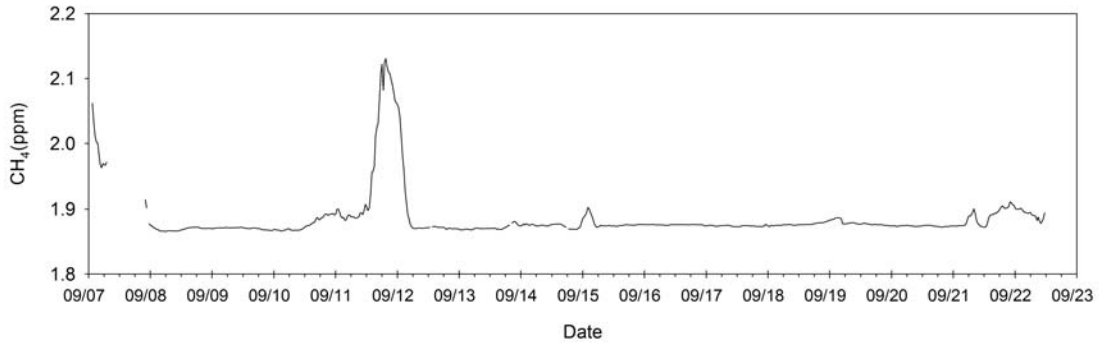

Figure 11.14 Variation of methane concentration during the expedition.

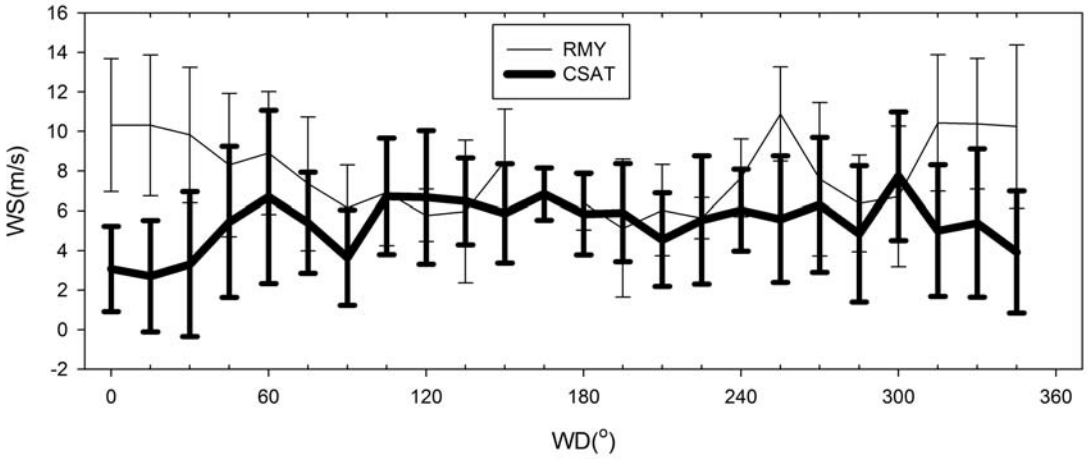

Figure 11.15 Wind speed variation during the expedition.

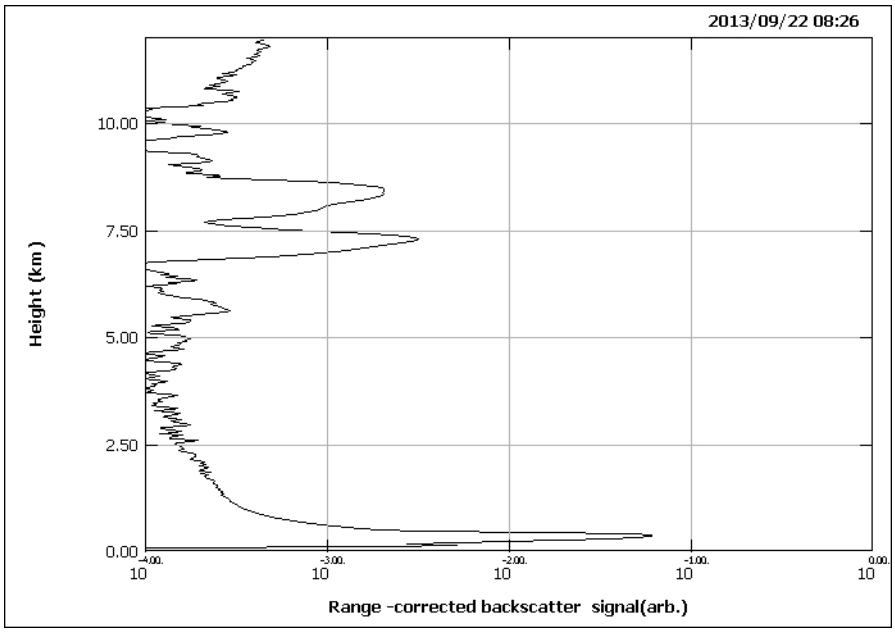

Figure 11.16 Range-correct backscatter signal on September, 22, 2013.